INVESTIGATING THE COMBINED EFFECT OF BRCA1 LOSS AND ESTRADIOL INCREASE ON OVARIAN TUMOURIGENESIS

By

Sara Rafferty

This thesis is submitted to the Faculty of Graduate and Postdoctoral Studies at the University of Ottawa in partial fulfillment of the requirements for the degree of

Master of Science (Cellular and Molecular Medicine)

Department of Cellular and Molecular Medicine
Faculty of Medicine
Ottawa, Canada

June 2011

TABLE OF CONTENTS

ACKNOWLEDGEMENTS

I have many people to thank for support and assistance throughout the work and writing that has gone into the successful completion of this thesis. My first and largest thank you goes to my supervisor Dr. Barbara Vanderhyden for giving me the opportunity to work in her lab, where guidance, encouragement, and passion for science make for a valuable graduate school experience. Barb was always available for support and advice, but provided me with enough independence to make decisions about my project and therefore further appreciate successes and learn from mistakes. I also want to thank the staff of the Vanderhyden lab, Colleen Crane, Ken Garson, Olga Collins, and especially Elizabeth MacDonald for their advice and assistance with many technical parts of my project. Thanks to my fellow Vanderhyden graduate students for making the lab such an enjoyable workplace. Along with our post-doc François Paradis, I could always count on them for support and learned a lot from each one of them. I must also thank Rhea Ferguson for stepping up at the last minute to help with statistical analyses. I am proud to call all of these people my colleagues and friends. All of the students, scientists, and staff of the 3rd floor of the Cancer Centre must be thanked for contributing to such a great work environment. Finally, I must thank my closest family and friends for their constant support and encouragement. Thanks to Colin for being understanding of my work load, taking care of me when I needed him most, and reminding me to take time to relax. Thanks to my parents, Dan and Therese Rafferty, and sister and best friend Kelly for always believing in me and being there for my highs and lows throughout this project. I am proud of the work I have accomplished in this thesis, but it truly would not have been the same without any one of these people.

ABSTRACT

The mechanism of how *BRCA1* mutation exclusively increases susceptibility to breast and ovarian cancer is unknown, however evidence suggests that Brca1 loss upregulates aromatase, the enzyme that produces estradiol, and that increased estradiol promotes tumourigenesis. To investigate these processes, *Brca1* was inactivated in the ovarian surface epithelium (OSE) of mice that were then exposed to placebo or estradiol for 60 days. Ovaries were examined histologically at time points up to one year. Estradiol did not induce tumourigenesis of the OSE, but did increase preneoplastic morphological changes. Inactivation of *Brca1* in OSE and granulosa cells (GCs) *in vitro* did not upregulate aromatase or increase estradiol production. An *in vivo* model of *Brca1* inactivation in GCs and OSE that enables monitoring of aromatase, estradiol levels and tumourigenesis remains desirable, as elucidation of the relationship between Brca1 and aromatase could impact understanding of the pathways responsible for ovarian tumour initiation and early progression.

LIST OF FIGURES

LIST OF ABBREVIATIONS

ºC	degrees Celsius
α	alpha
β	beta
AdCre	adenovirus expressing Cre recombinase
AdGFP	adenovirus expressing GFP
AMHR2	anti-Müllerian hormone type II receptor
ANOVA	analysis of variance
bp	base pair
BRCA1	breast cancer type 1 susceptibility protein
BRCA2	breast cancer type 2 susceptibility protein
BRCC	BRCA1-BRCA2-containing complex
BrdUrd	bromodeoxyuridine
CA-125	cancer antigen 125
cAMP	cyclic adenosine monophosphate
cDNA	complimentary DNA
cm	centimetre(s)
CL	corpus luteum
CLS	cAMP-responsiveness element-like sequence
CO_2	carbon dioxide
CREB	cAMP response element-binding
DAB	diaminobenzidine
Dab2	Disabled-2
DES	diethylstilbestrol
DMEM/F12	Dulbecco's Modified Eagle's Medium Nutrient Mixture F-12 Ham
DMSO	dimethylsulfoxide
DNA	deoxyribonucleic acid
dNTP	deoxyribonucleotide triphosphate
DSB	double strand break
E2	17β-estradiol
EDTA	ethylenediaminetetraacetic acid
EOC	epithelial ovarian cancer
ER	estrogen receptor
ERE	estrogen-responsive enhancer element
FBS	fetal bovine serum
FSH	follicle stimulating hormone
GC	granulosa cell
GFP	green fluorescent protein

GnRH	gonadotropin-releasing hormone
HBOC	hereditary breast and ovarian cancer
HCl	hydrochloric acid
H&E	stained with Harris Modified Haematoxylin and eosin
HER2/neu	human epidermal growth factor receptor 2
HR	homologous recombination
IgG	immunoglobulin G
ITSS	insulin-transferrin-sodium-selenite solution
KCl	potassium chloride
kDa	kiloDalton
LCM	laser capture microdissection
LH	luteinizing hormone
loxP	locus of X over P1
µg	microgram(s)
µl	microlitre(s)
µm	micrometre(s)
µM	micromolar
M	molar
mg	milligram(s)
$MgCl_2$	magnesium chloride
ml	millilitre(s)
min	minute(s)
mM	millimolar
MOSE	mouse OSE
mRNA	messenger RNA
MRN complex	complex containing MRE11, RAD50, and NBS1
NaCl	sodium chloride
ng	nanogram(s)
NHEJ	non-homologous end joining
nM	nanomolar
NRE	nuclear receptor 5a transcription
OSE	ovarian surface epithelium or ovarian surface epithelial
p53	tumour protein 53
PARP	poly(ADP-ribose) polymerase
PBS	phosphate buffered saline
PCOS	polycystic ovarian syndrome
PCR	polymerase chain reaction
pfu	plaque forming unit

PGE2	prostagladin E2
PKA	protein kinase A
pmol	picomole
RB	retinoblastoma
RIA	radioimmunoassay
RNA	ribonucleic acid
rpm	rotations per minute
RT	reverse transcriptase
SEM	standard error of the mean
sec	second(s)
siRNA	small interfering RNA
SSA	single strand annealing
SF-1	steroidogenic factor-1
S-PBS	Stockholm PBS
TAE	tris acetate EDTA
TAg	large and small Simian virus 40 T antigens
Taq	thermophilic DNA polymerase
TIC	tubal intraepithelial carcinoma
TVS	transvaginal sonography
U	units
V	volts

CHAPTER 1: INTRODUCTION

1.1 Ovarian Cancer: General Overview

One out of seventy women develops ovarian cancer, the sixth leading cause of cancer death and the most lethal gynaecological malignancy in women (Canadian Cancer Society's Steering Committee, 2010; Murdoch and McDonnel, 2002). The low survival rate, about 30% (Canadian Cancer Society's Steering Committee, 2010), is attributed to two main factors. Firstly, symptoms of ovarian cancer, such as abdominal distension, postmenopausal bleeding, altered bowel function, and early satiety, are easily mistaken for normal aspects of aging or gastrointestinal conditions (Bankhead et al., 2008; Bast et al., 2009). Secondly, there is no effective screening method to detect early stage ovarian cancer. Cancer antigen 125 (CA-125) monitoring and transvaginal sonography (TVS) are available, but are only used to diagnose advanced cases or recurrent disease (Auersperg et al., 1997; Bast et al., 2009; Murdoch and McDonnel, 2002). These factors result in most cases being diagnosed after metastasis has occurred, when the disease is difficult to treat successfully. Investigations of ovarian cancer initiation and early progression strive to improve early detection and successful treatment to increase survival rates.

1.2 Ovarian Cancer: Classification

1.2.1 Staging

Ovarian cancer can be diagnosed at four stages: confined to a single ovary (stage I), spread but confined to the peritoneal cavity (stage II), metastasized outside of the pelvic region, mainly in lymph nodes (stage III), or metastasized to distant sites outside of the pelvic region, commonly bowel, omentum and liver (stage IV) (Bast et al., 2009; Murdoch and McDonnel, 2002).

1.2.2 Subtypes

Numerous cell types give rise to cancer of the ovary, each resulting in a different subtype. A small portion of ovarian cancers originate from primitive germ cells, forming germ cell tumours, and from stromal, granulosa, or thecal cells, forming sex cord-stromal tumours. The majority (90%) of ovarian cancers derive from epithelial cells and are called epithelial ovarian cancer (EOC) (Bast et al., 2009; Ji et al., 2008). Unlike most cancers, EOC becomes more differentiated as it progresses; this results in four main subtypes that each resembles a well-differentiated cell type of the female reproductive tract: serous resembles fallopian tube epithelium, mucinous resembles cervical epithelium, endometrioid resembles the endometrium, and clear cell resembles cells of the vagina (Auersperg et al., 2001; Bast et al., 2009; Bell, 2005; Bowtell, 2010; Kobel et al., 2008). Each subtype of EOC differs in its risk factors, gene expression, and response to therapy (Bast et al., 2009; Kobel et al., 2008).

1.2.3 Grading of Serous EOC

Serous EOC, the most common subtype, is subdivided into two grades associated with the pathway taken to malignancy (Shih and Kurman, 2004; Vang et al., 2009). Type I progresses slowly and step-wise from a benign cystadenoma or adenofibroma to an atypical proliferative serous tumour to a non-invasive micropapillary serous carcinoma before transitioning into an invasive low grade serous tumour (Shih and Kurman, 2004). Type II progresses rapidly and results in high grade tumours. Characterizing its preneoplastic lesions has been difficult, although at least a subset are presumed to originate from the ovarian surface epithelium (OSE). Type I is characterized by mutated *KRAS*, *BRAF*, or *ERBB2*. These mutations are rare in Type II, but high DNA copy

number changes, *TP53* mutations, and *BRCA1* dysfunction are common (Bowtell, 2010; Shih and Kurman, 2004; Vang et al., 2009). The two grades of serous EOC differ in age at diagnosis and response to chemotherapy (Vang et al., 2009) and high grade is nine times more common than low grade (Seidman et al., 2006). The wide range of features exhibited by subtypes of ovarian cancer, even within serous EOC, argues for considering ovarian cancer a general term for a wide range of diseases (Bowtell, 2010).

1.3 Treatment of Ovarian Cancer

In nearly all cases of ovarian cancer, initial control is accomplished by surgical removal of as much tumour as possible. In stage I ovarian cancer, surgery alone cures 90% of patients. In any later stage, chemotherapy consisting of carboplatin usually in combination with paclitaxel is used after surgery. This treatment regimen confers response in 65% of patients, increasing overall survival from 32 to 57 months. Unfortunately it is common for ovarian cancer or its metastases to reoccur as unresponsive to previously-used therapeutics (Bast et al., 2009; Pignata et al., 2011).

1.4 Ovary: Cell Types, Structures, and Functions

1.4.1 General Overview

In order to understand ovarian cancer, it is important to understand cell types and structures of the ovary as well as ovarian functions, which include generating and housing oocytes and producing steroid hormones. During reproductive years, the ovary contains many follicles, each consisting of an oocyte surrounded by layers of granulosa cells (GCs) which themselves are bordered by a basement membrane surrounded by thecal cells. The ovary also contains stromal and corpus luteal (CL) cells, the latter being short-lived remnants of ovulated follicles. Covering the outside of the ovary is the OSE, a

single layer of epithelial cells which are separated from ovarian stroma by a basement membrane and a collagen-based layer, the tunica albuginea. At any given time the ovary contains follicles in different stages: primordial, primary, secondary, and antral (the stage at which the oocyte is ready to be ovulated) as well as atretic (degenerating) follicles and post-ovulatory CLs (Nussey and Whitehead, 2001; Oktem and Oktay, 2008) (**Figure 1**).

Follicular development and ovulation are hormonally regulated. Gonadotropin-releasing hormone (GnRH) stimulates the pituitary to secrete luteinizing hormone (LH) and follicle stimulating hormone (FSH). FSH causes the growth of secondary and antral follicles, with one follicle eventually becoming dominant and the others undergoing atresia. The GCs of the dominant follicle secrete high levels of estradiol (E2) that cause a spike in LH secretion which then leads to ovulation. GCs of the follicle remaining in the ovary differentiate to form the CL, which produces high levels of both progesterone and estradiol. If fertilization and implantation of the ovulated oocyte do not occur, the CL degrades and estradiol and progesterone levels decrease; FSH secretion then increases and the cycle begins again (Nussey and Whitehead, 2001; Oktem and Oktay, 2008).

1.4.2 Ovarian Surface Epithelium

Particular attention must be paid to OSE cells because they are thought to be the cell of origin of EOC. The OSE is a single layer of flat-to-cuboidal epithelial cells loosely attached to the surface of the ovary (Auersperg et al., 2001; Murdoch and McDonnel, 2002). OSE cells are also found lining epithelial invaginations and inclusion cysts within the ovary (Auersperg et al., 2001; Scully, 1995). OSE cells are derived from the mesoderm, specifically epithelial cells that line the coelom of the embryo (Auersperg et al., 2001; Murdoch and McDonnel, 2002). In their role of repairing ovulatory wounds,

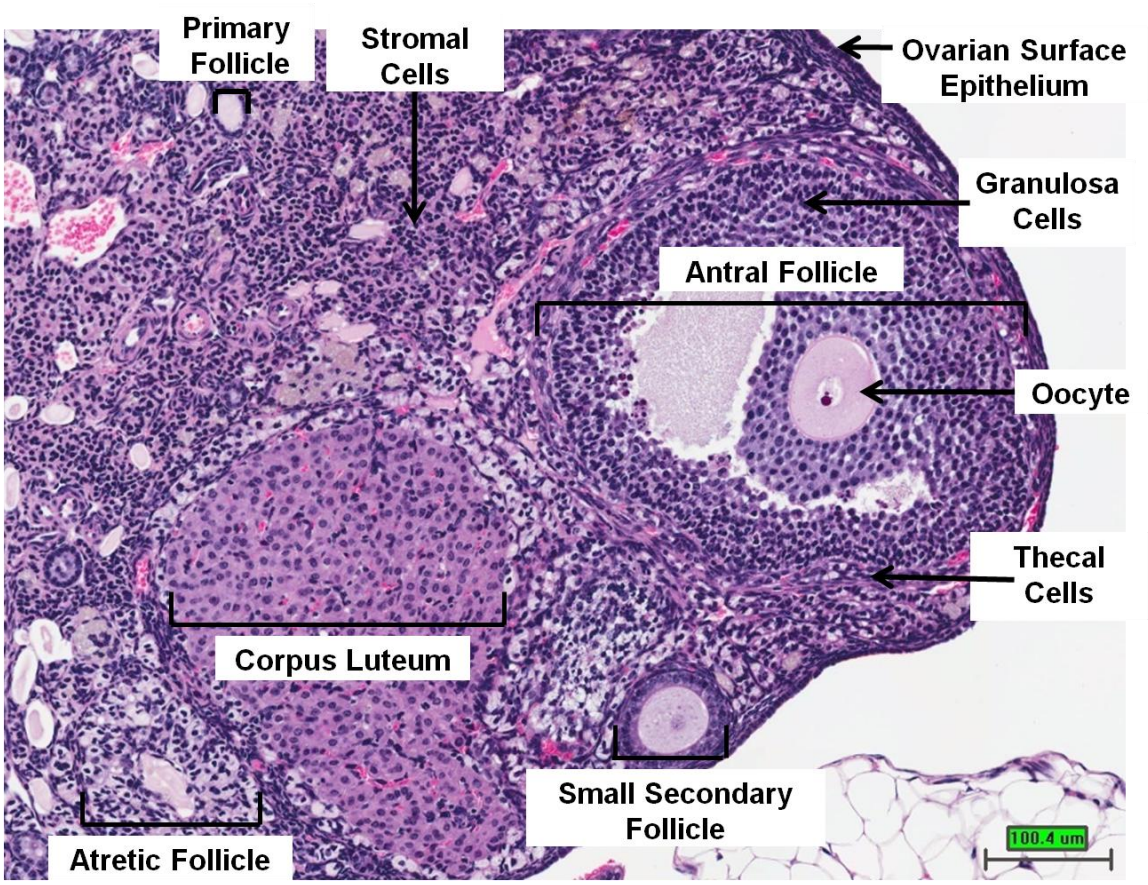

Figure 1. Representative mouse ovarian section with cell types and structures indicated. Ovarian section stained with haematoxylin and eosin shows ovarian cell types, including oocytes, granulosa cells, thecal cells, stromal cells, and ovarian surface epithelial cells. Ovarian structures are also indicated, including primary, small secondary, antral, and atretic follicles as well as a corpus luteum.

OSE cells are mobile and modify extracellular matrix, abilities reminiscent of mesenchymal cells; however, during tumourigenesis, OSE cells acquire characteristics of well-differentiated epithelium. Furthermore, OSE cells express markers of both mesenchymal and epithelial cells (Auersperg et al., 2001), indicating they are poorly differentiated epithelial cells with phenotypic plasticity.

Evidence supports a function of the OSE in ovulation. Although debated, OSE cells may secrete enzymes that assist in expulsion of the oocyte from antral follicles (Bjersing and Cajander, 1975). OSE cells also proliferate to cover the wound created during ovulation; OSE cells of rhesus macaques proliferated in response to a wound created by brushing the ovarian surface (Wright et al., 2008) and OSE cells of mice proliferated in response to superovulation induced by gonadotropins (Burdette et al., 2006). The OSE also secretes extracellular matrix components and proteases (Kruk et al., 1994) needed to remodel the ovarian stroma near the ovulation site back to its previous state (Auersperg et al., 2001). Transporting substances between the ovary and the peritoneal cavity may be another function of the OSE (Auersperg et al., 2001).

1.5 Aetiology of Ovarian Cancer

1.5.1 Cell of Origin

Progression through preneoplastic to neoplastic states is well established in some cancers, such as cervical and colon (Fearon and Vogelstein, 1990; Pinto and Crum, 2000) and evidence suggests a stepwise process also occurs as OSE cells transform (Schlosshauer et al., 2003). Morphological changes, specifically invaginations of surface OSE cells into the stroma of the ovary and inclusion cysts, as well as nuclear changes, are putative preneoplastic lesions of EOC. OSE cells within invaginations and inclusion cysts

tend to be columnar in shape, suggesting a higher degree of differentiation (Auersperg et al., 2001; Scully, 1995). OSE lining inclusion cysts, as well as OSE cells exhibiting hyperplasia or forming invaginations in some cases, have also been found expressing proteins found in epithelial ovarian tumours, but not in OSE cells on the ovarian surface, including CA-125, c-KIT, E-cadherin, and HOXA7 (Kabawat et al., 1983; Maines-Badniera and Auersperg, 1997; Naora et al., 2001; Sundfeldt et al., 1997; Tonary et al., 2000). OSE cells within inclusion cysts may be more likely to undergo transformation because they are exposed to higher concentrations of growth factors and hormones than OSE cells on the ovarian surface (Auersperg et al., 2001). Ovaries removed from healthy women have been found to contain microscopic tumours occurring within OSE cells on the surface or within invaginations and inclusion cysts, with OSE cells showing cytologic atypia, features of malignant but not normal cells (Bell and Scully, 1994) and ovarian tumours arising from the surface have been found to be contiguous with OSE of normal morphology through an area of histological transition (Cai et al., 2009).

Further substantiating OSE hyperplasia, invaginations, inclusion cysts, and nuclear abnormalities as precursors to ovarian cancer is the existing correlation between their occurrence and circumstances in which ovarian tumours are likely to develop. Such changes were found significantly more often in ovaries from women with stage I ovarian cancer, endometrial cancer, or polycystic ovarian syndrome (PCOS) compared to ovaries from control women as well as in tumourigenic ovaries compared to their contralateral counterparts (Mittal et al., 1993; Plaxe et al., 1990; Resta et al., 1993). Also, application of a carcinogen to rat ovaries significantly induced hyperplasia, papillae, inclusion cysts, and epithelial ovarian tumours compared to vehicle treatment (Stewart et al., 2004).

Recent evidence suggests that some EOCs originate from tubal intraepithelial carcinomas (TICs) of the distal fallopian tube (Mehrad et al., 2010). Since most ovarian cancers are discovered in late stages, with involvement of the fallopian tube, it has been suggested that TICs that developed into large tumours involving the ovary have long been misdiagnosed as ovarian cancer. Alternatively, malignant cells of TICs could spread to and form large tumours in the ovary, resulting in a diagnosis of ovarian cancer despite extraovarian origin (Mehrad et al., 2010; Vang et al., 2009). The relatively new finding of fallopian tube epithelial cells as originators of some ovarian cancer cases proves that the earliest stages of this disease are in desperate need of further understanding.

1.5.2 Incessant Ovulation

The hypothesis that increased ovulations elevate ovarian cancer risk was originally based on the fact that humans develop ovarian cancer much more frequently and also likely undergo a higher number of ovulations than any other mammal (Fathalla, 1971). This idea has gained much support, as events that increase lifetime number of ovulatory cycles, including early onset of menses and late menopause, increase ovarian cancer risk (Bast et al., 2009; Tung et al., 2003) while events that decrease ovulatory cycles, including pregnancy and use of oral contraceptives, decrease ovarian cancer risk (Anonymous, 1987; Bast et al., 2009; Bosetti et al., 2002; Modugno et al., 2001; Ness et al., 2000; Purdie et al., 2003; Tung et al., 2003). Experimental evidence also supports the idea. Women who experienced more ovulations, by undergoing treatments causing superovulation, exhibited more preneoplastic atypia in OSE cells than controls (Nieto et al., 2001) and ovaries from young mice induced to undergo a higher than normal number of ovulations contained more invaginations and inclusion cysts than controls (Clow et al.,

2002). It is hypothesized that invaginations of the OSE form during ovulation and then pinch off, creating inclusion cysts from which ovarian cancer is more likely to form.

1.5.3 Gonadotropins

Because most ovarian cancers present after menopause and the hormonal milieu in post-reproductive years is characterized by high gonadotropins and low steroid hormones, it has been suggested that the gonadotropins FSH and LH promote ovarian cancer development (Bast et al., 2009). OSE cells express receptors for FSH (Zheng et al., 1996) and FSH-induced OSE cell proliferation *in vivo* has been observed (Davies et al., 1999). Furthermore, women with PCOS, which involves elevated LH levels, have an increased risk of developing ovarian cancer (Schildkraut et al., 1996) and the decrease in ovarian cancer risk associated with pregnancy and oral contraceptives may not only be related to decreased ovulations, but also decreased gonadotropin secretion resulting from negative feedback by elevated steroid hormones acting on the pituitary (Risch, 1998). Gonadotropin promotion of OSE transformation has not been proven, but evidence suggests elevated gonadotropins do play a role in ovarian tumourigenesis.

1.5.4 Genetics

Most ovarian cancers develop sporadically, but about 10% are associated with an inherited germline mutation (Bast et al., 2009; Miki et al., 1994). To date there appears to be three distinct modes of hereditary ovarian cancer. In hereditary site-specific ovarian cancer, although the genetic mutation responsible is not yet known, ovarian cancer risk is increased by having a family history of the disease (Auersperg et al., 2001). In hereditary nonpolyposis colon cancer, mutations in mismatch repair genes *hMSH1*, *hMSH2*, *hPMS1*, and *hPMS2* confer a 7% lifetime risk of ovarian cancer. Up to 95% of hereditary ovarian

cancers are classified as hereditary breast and ovarian cancer (HBOC) syndrome, which is characterized by mutations in the tumour suppressor genes *BRCA1* or *BRCA2*, which code for the breast cancer type 1 or 2 susceptibility protein respectively (Auersperg et al., 2001; Bast et al., 2009; Petrucelli et al., 2010; Weberpals et al., 2008).

1.5.4.1 Hereditary Breast and Ovarian Cancer Syndrome

One in every 300 to 800 people carries either a germline *BRCA1* or *BRCA2* mutation, although the frequency is much higher in certain populations (Chen and Parmigiani, 2007; Petrucelli et al., 2010). Breast and ovarian cancer risk by age 70 in *BRCA1* mutation carriers is 57 % and 40 % respectively and in *BRCA2* mutation carriers is 49 % and 18 % respectively, which is significantly higher than the general population (13 % and 1.5 % respectively) (Chen and Parmigiani, 2007; Petrucelli et al., 2010; Pruthi et al., 2010). BRCA1 and BRCA2 do not have similar protein structure; it has been suggested that their shared association with breast and ovarian cancer may be due to functional similarity, such as participating in DNA damage repair (Petrucelli et al., 2010).

Genetic testing is used to identify mutation carriers and assess cancer risk. More than 1,600 and 1,800 mutations have been identified in *BRCA1* and *BRCA2* respectively, consisting of both changes in a few base pairs and large deletions. Most known mutations lead to non-functional proteins, however many have unknown consequences. Furthermore, cancer risk can vary between carriers of the same mutation. Both of these factors complicate the assessment of cancer risk. The location of the mutation can also impact the likelihood of cancer development. For example, mutations in a segment of exon 11 of *BRCA2* called the ovarian cancer cluster region are more likely to be associated with ovarian than breast cancer (Petrucelli et al., 2010). Women found to have

increased susceptibility for developing ovarian cancer have limited options for managing their risk. Close surveillance has not been shown to detect early stage ovarian cancer (Oei et al., 2006; Olivier et al., 2006), oral contraceptives decrease but do not fully eliminate ovarian cancer risk (Narod et al., 1998; Whittemore et al., 2004), and surgical removal of the ovaries and fallopian tubes, although very effective, is invasive and can have mental and physical side effects (Pruthi et al., 2010; Rebbeck et al., 2002).

The focus of the current study is *BRCA1* inactivation because it is the strongest risk factor for ovarian cancer development. *BRCA1* is mutated in up to 90% of hereditary ovarian cancer cases (Berchuck et al., 1998; Pal et al., 2005) and 7% to 9% of sporadic ovarian cancers (Berchuck et al., 1998; Geisler et al., 2002; Merajver et al., 1995). *BRCA1* is found inactivated by epigenetic mechanisms such as methylation in 5% to 40% of sporadic ovarian cancers (Senturk et al., 2010) and BRCA1 protein is faint to absent in 65% of stage III sporadic ovarian cancers (Thrall et al., 2006). The consequences of *BRCA1* and *BRCA2* mutations provide an opportunity to study the cellular and molecular events responsible for initiation and early progression of ovarian cancer.

1.6 BRCA1

1.6.1 Structure

BRCA1 is found on human chromosome 17 and contains 24 exons, with exon 11 encoding 60% of the protein (Deng, 2006; Schrock et al., 1996; Weberpals et al., 2008). BRCA1 protein is 220 kDa and contains 1,863 amino acids (Deng, 2006; Weberpals et al., 2008). At the N terminus, BRCA1 has a RING finger domain that binds BARD1, resulting in a BRCA1-BARD1 complex that has E3 ubiquitin ligase activity, BRCA1's only enzymatic capability. BRCA1 also contains two nuclear localization signals and two

transcriptional activation domains that are important for interaction with other proteins (Deng, 2006; Rosen et al., 2006) (**Figure 2**). The mouse homolog of the human *BRCA1* is found on chromosome 11D (Lane et al., 1995; Schrock et al., 1996; Sharan et al., 1995). Mouse Brca1 consists of 1,812 amino acids and is 60% identical to the human version (Lane et al., 1995; Sharan et al., 1995)

1.6.2 Expression

BRCA1 is widely expressed in both humans and mice. Up to day 7.5 of mouse embryonic development, Brca1 is ubiquitously expressed (Blackshear et al., 1998). In adult mice, Brca1 protein is low or not found in cells of the liver, lung, and skeletal muscle, but otherwise is thought to be ubiquitous and is most strongly expressed in the spleen, thymus, and lymph nodes (Blackshear et al., 1998; Lane et al., 1995). Within the ovary, Brca1 is expressed in GCs, thecal cells, oocytes, CLs, and OSE cells (Blackshear et al., 1998). Expression in humans appears to be similar (Miki et al., 1994).

1.6.3 Function

1.6.3.1 DNA Damage Response

The most well established role of BRCA1 is promoting the repair of double strand breaks (DSBs). DNA damage, including DSBs, is detected by protein kinases ATM and ATR, which then phosphorylate targets that cause cell cycle arrest and DNA damage repair (**Figure 3**). BRCA1 is one target and the site that becomes phosphorylated dictates the response elicited (Gudmundsdottir and Ashworth, 2006; Venkitaraman, 2009).

Repair of DSBs occurs through one of three processes, from least to most error prone: homologous recombination (HR), single-strand annealing (SSA), or non-homologous end joining (NHEJ) (Coleman and Greenberg, 2011; Gudmundsdottir and Ashworth, 2006).

Figure 2. Structure of the BRCA1 protein. Functional domains of BRCA1 include a highly conserved RING finger domain at its N-terminus from amino acid 20 to 64, two nuclear localization signals in exon 11, and two transcriptional activation domains at its C-terminus from amino acid 1,293 to 1,863.

Evidence supports a role of BRCA1 in HR and SSA. Therefore, when BRCA1 is not functional, the cell only has error-prone mechanisms of repair available, resulting in increased mutations (Gudmundsdottir and Ashworth, 2006; Venkitaraman, 2009). A cell that recognizes increased DNA damage and mutations will stop dividing or apoptose. However, if mutations occur in genes responsible for inducing cell cycle arrest and apoptosis, the cell can survive and continue gaining DNA damage; this is thought to be a major mechanism of BRCA1-associated tumourigenesis (Venkitaraman, 2009).

BRCA1 fulfills multiple roles during HR. BRCA1 is in a complex with CtIP which is physically associated with the MRN complex containing MRE11, RAD50, and NBS1. This complex binds to and trims back the 5'end of both strands of DNA at the break site, resulting in 3' overhangs that can then invade a sister chromatid to use as a template for DNA repair (Coleman and Greenberg, 2011; Gudmundsdottir and Ashworth, 2006). BRCA1 loss therefore interferes with end resection and the entire process of HR cannot proceed. BRCA1 is also found in a complex with RAP80 that is brought to sites of DSBs through γH2AX and MDC1-directed recruitment and is thought to help promote HR being used over NHEJ (Coleman and Greenberg, 2011; Venkitaraman, 2009). BRCA1 is also found in the BRCA1-BRCA2-containing complex (BRCC) that also contains RAD51 and BARD1 (Gudmundsdottir and Ashworth, 2006) and is thought to contribute to DNA repair through its ubiquitin ligase activity (Dong et al., 2003) (**Figure 3**).

The inability of HR to occur without functional BRCA1 is exemplified by the success of poly(ADP-ribose) polymerase (PARP) inhibitors in clinical trials for treatment of BRCA1-associated ovarian cancer. PARP is required to repair single strand breaks of DNA and therefore PARP inhibitors cause single stand breaks to be left unrepaired.

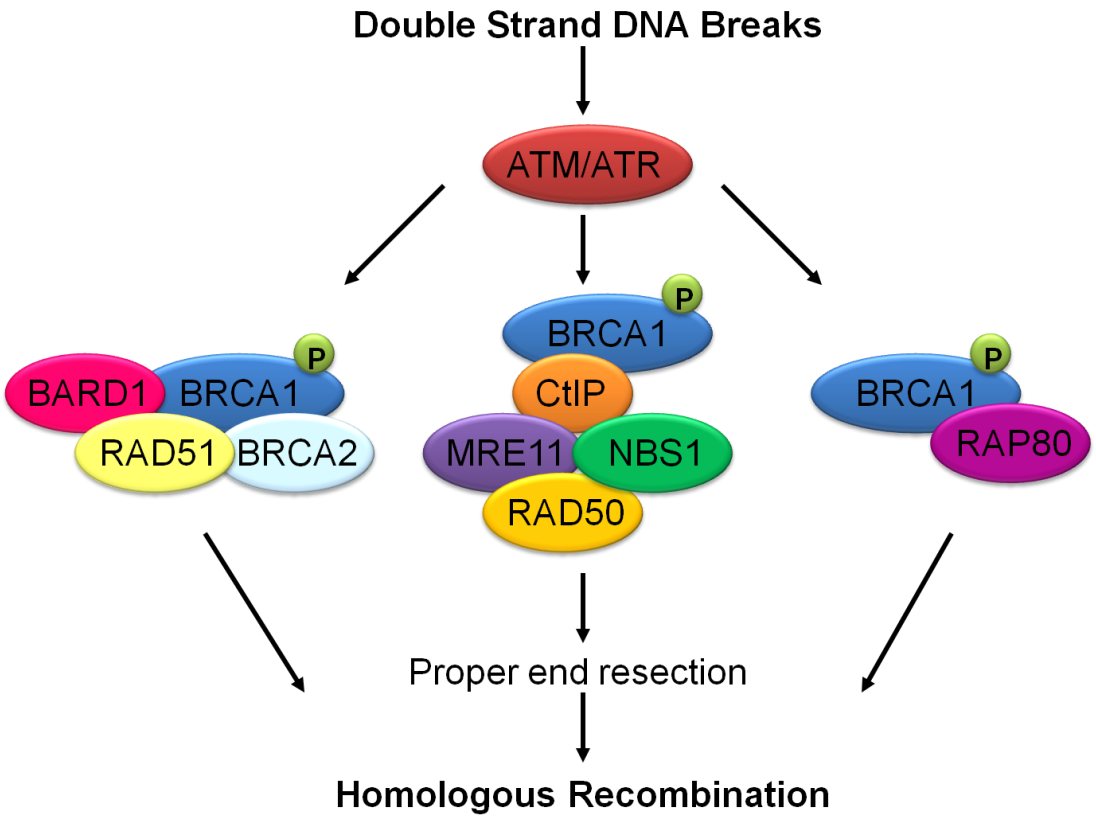

Figure 3. Complexes involving BRCA1 that participate in homologous recombination repair of double strand DNA breaks. DNA damage causing double strand breaks (DSBs) is detected by protein kinases ATM and ATR. BRCA1 is one target of subsequent ATM/ATR phosphorylation. Phosphorylated BRCA1 interacts with numerous protein complexes required for the error-free DNA damage repair process of homologous recombination. BRCA1 is found in the BRCA1-BRCA2-containing complex that also contains RAD51 and BARD1, which is thought to contribute to DNA repair through its ubiquitin ligase activity. Through interaction with CtIP, which is physically associated with the MRN complex containing MRE11, RAD50, and NBS1, BRCA1 allows proper end resection required during homologous recombination. The complex of BRCA1 and RAP80 is thought to help promote use of homologous recombination over more error-prone DNA repair mechanisms.

Single strand breaks often become DSBs which are then repaired by HR. However, in cells lacking functional BRCA1, the DSBs can also not be repaired and the cell dies due to synthetic lethality. The effectiveness of PARP inhibitors in killing cells with mutated *BRCA1* highlights the necessity of BRCA1 function in HR (Calvert and Azzariti, 2011).

1.6.3.2 Cell Cycle Control

As mentioned previously, BRCA1 phosphorylation by ATM and ATR in response to DNA damage can affect the cell cycle (Gudmundsdottir and Ashworth, 2006; Venkitaraman, 2009). In the transition from G1 to S phase, BRCA1 helps RB protein remain hyperphosphorylated and upregulates p21, both of which lead to cell cycle arrest. BRCA1 is also required for the S phase checkpoint, which prevents DNA replication occurring in the presence of DNA damage, although the mechanisms remain unknown (Deng, 2006), and BRCA1 helps to control the G2 to M transition by regulating proteins required for mitosis initiation including Chk1 (Deng, 2006; Gudmundsdottir and Ashworth, 2006). Aneuploidy commonly observed in BRCA1-deficient cells and BRCA1 transcriptionally increasing expression of Mad2, a protein required for preventing chromosome missegregation, implicates BRCA1 in the spindle checkpoint, which prevents cell division when chromosomes are not aligned properly during metaphase. Unrepaired DNA damage and inappropriate cell cycle progression both contribute to the genetic instability observed in BRCA1-deficient transformed cells (Deng, 2006).

1.6.3.3 Differentiation

Evidence exists to support a role for BRCA1 in regulating differentiation in mammary tissue. Because BRCA1-associated breast cancers are almost always of the basal subtype, characterized by lack of expression of estrogen receptor (ER),

progesterone receptor, and human epidermal growth factor receptor 2 (HER2/neu), and because basal-like breast cancers are thought to originate from mammary stem cells, investigations into BRCA1 control of stem cell populations have been undertaken. Both *in vitro* and *in vivo* evidence from mice and humans show that loss of BRCA1 increases the pool of mammary stem/progenitor cells; BRCA1 must be present for ER negative mammary progenitor cells to differentiate into ER positive epithelial cells and may also promote the survival of the cells once they have differentiated (Liu et al., 2008).

1.6.3.4 Transcription

Many of the consequences of BRCA1 loss may be due to its role in transcription. BRCA1 is part of the RNA polymerase II complex involved with transcription of every gene. Although BRCA1 cannot recognize specific DNA sequences, it may act as a coregulator of transcription factors that are sequence-specific in addition to its potential role in basal transcription. BRCA1 is a coactivator of p53, specifically inducing genes for DNA repair and cell cycle arrest rather than apoptosis, and also serves as a coactivator of STAT1, resulting in increased p21 and subsequent cell cycle arrest (Mullan et al., 2006; Rosen et al., 2006). BRCA1 is a negative coregulator of both c-Myc and ERα (Mullan et al., 2006; Rosen et al., 2006). BRCA1 has been observed to specifically inhibit ERα-induced transcription of genes that cause proliferation, suggesting loss of functional BRCA1 allows greater estrogen-induced proliferation (Fan et al., 1999). BRCA1 also inhibits estrogen action by transcriptionally repressing *CYP19A1*, the gene that encodes aromatase which is the enzyme responsible for estradiol synthesis (Ghosh et al., 2007; Hu et al., 2005; Lu et al., 2006). The relationship between Brca1 and aromatase will be discussed in detail in a subsequent section, as it is the focus of the current study. In

another role, BRCA1 may increase access of transcription factors to DNA by interacting with chromatin remodelling proteins, including members of SWI/SNF chromatin-remodelling complexes and histone deacetylases (Mullan et al., 2006). Some effects of BRCA1 in response to DNA damage occur too quickly to be transcriptionally regulated, but otherwise it has been difficult to tease out whether consequences of BRCA1 loss are due to transcriptional dysregulation or roles in other cellular processes. BRCA1 fulfills functions both within normal cell physiology and in response to DNA damage that contribute to its role as a tumour suppressor (Mullan et al., 2006; Rosen et al., 2006).

1.6.4 Role in Ovarian Cancer

Histological examination of ovarian and fallopian tube tissue prophylactically removed from *BRCA1* mutation carriers in comparison to tissues removed from women without a predisposition to ovarian cancer provides an opportunity to identify the disease in its earliest stages. Salazar *et al.* (1996) and Schlosshauer *et al.* (2003) both found a panel of morphological changes, such as hyperplasia, papillomatosis, invaginations, and inclusion cysts, significantly more often in ovaries from women with a *BRCA1* or *BRCA2* mutation or a family history of ovarian cancer compared to controls. Inactivation of *Brca1* in OSE cells of mice also showed these morphological changes occur significantly earlier and more frequently than in ovaries from age-matched mice containing intact *Brca1* (Clark-Knowles et al., 2007). Another study did not substantiate morphological changes as markers of premalignancy in women with a family history of ovarian cancer, but did find significant increases in nuclear atypia (Werness et al., 1999).

Other studies have not found evidence for preneoplastic lesions in ovaries from mutation carriers. In comparing the occurrence of inclusion cysts, invaginations,

columnar OSE, hyperplasia, and papillae in women with *BRCA1* and *BRCA2* mutations to women with a family history of ovarian cancer carrying intact *BRCA1* and *BRCA2*, no significant differences were found (Casey et al., 2000; Stratton et al., 1999). Similar comparisons have been performed between women with and without reported family history (Piek et al., 2003; Sherman et al., 1999), and with and without confirmed *BRCA1* mutations (Barakat et al., 2000), all showing no significant difference in any feature.

The most recent study of this kind based a dysplasia score on many characteristics examined in previous studies and is the only study to separate results of *BRCA1* and *BRCA2* mutation carriers from participants with reported family history without a confirmed mutation. A significant increase in dysplasia was found in mutation carriers versus controls and also versus those with reported family history, allowing authors to conclude that the panel of abnormalities represents preneoplastic lesions that are more frequent in mutation carriers (Chêne et al., 2009). The inconsistent findings of previous studies may be due to evaluation methods, the subtlety of the characteristics examined, and small sample sizes. Overall, OSE cell hyperplasia, invaginations, and inclusion cysts are considered morphological preneoplastic precursors of ovarian cancer.

Germline BRCA1 mutations strongly predispose to ovarian cancer development, but mouse models have shown that inactivation of *Brca1* alone is not sufficient to cause ovarian cancer. *In vivo Brca1* inactivation in OSE cells, accomplished by exposure of $Brca1^{loxP/loxP}$ OSE to adenovirus expressing Cre recombinase (AdCre) through either intrabursal injection or a cross with a $Amhr2^{Cre/+}$ mouse, did not result in tumour formation even after one year. However, inactivation of *p53* alone caused tumours in 100% of mice and the concomitant inactivation of *Brca1* significantly accelerated tumour

progression (Clark-Knowles et al., 2009; Xing et al., 2009). *In vitro* data show that downregulation of BRCA1 causes increased p53 and p21 expression, suggesting activation of DNA damage responses and cell cycle checkpoints (Reedy et al., 2001). Furthermore, inactivation of *Brca1* alone increased apoptosis, while the concomitant inactivation of *p53* allowed Brca1-deficient cells to proliferate significantly faster than controls (Clark-Knowles et al., 2007). It appears that increased genomic instability caused by the loss of BRCA1 alone triggers cell cycle arrest or apoptosis in a cell with intact checkpoints and only once these pathways are defunct, such as through *TP53* mutation, can BRCA1-deficient cells proliferate, acquire more mutations, and eventually transform (Reedy et al., 2001).

1.6.5 Tissue Specificity of BRCA1-associated Cancers

Although an association between germline *BRCA1* mutations and increased risk of prostate, uterine, cervical, pancreatic, and colon cancer has been found, by far the greatest cancer risk in women with *BRCA1* mutations is breast and ovarian (Risch et al., 2001; Thompson et al., 2002). The best characterized functions of BRCA1, error-free DNA damage repair and cell cycle control, are important in every cell type and therefore do not explain the tissue-specific nature of BRCA1-associated cancers. It has been proposed that breast and ovarian tissue are more proliferative or lack proteins that can compensate for BRCA1 loss, but high proliferation rates of other tissues and embryonic lethality due to BRCA1 loss argue against these suggestions respectively (Elledge and Amon, 2002; Monteiro, 2003). Speculation has also been made that breast and ovarian tissue experience greater DNA damage and are more likely to undergo loss of heterozygosity than other tissues, potentially induced by estrogen metabolites (Monteiro, 2003). Elledge

and Amon (2002) postulated that unique factors in the breast and ovary promote survival of BRCA1 deficient cells, giving them enough time to accumulate mutations necessary to transform, however no evidence for the identity of such factors was provided.

BRCA1's regulation of the transcription of particular genes could be tissue-specific and the occurrence of BRCA1-associated cancers in the two main estrogen producing and responsive tissues has led to investigations of BRCA1 function and estrogen regulation, particularly expression and activity of ERα and aromatase (Hu, 2009; Monteiro, 2003). BRCA1 regulation of these targets has been tested experimentally more so than most postulations about the origins of BRCA1-associated cancers and further elucidation of the relationship between BRCA1 and aromatase is the focus of the current study.

1.7 Aromatase

1.7.1 Structure

Aromatase is encoded by *CYP19A1*, located on chromosome 15. It is the sole member of family 19 of the cytochrome P450 superfamily (Hong et al., 2009; Li et al., 2008; Simpson et al., 2002). Aromatase is 503 amino acids in length, localizes to the endoplasmic reticulum, and is a heme protein (Hong et al., 2009; Simpson et al., 2002). Aromatase only functions in a complex with NADPH-cytochrome P450 reductase, which provides electrons required for aromatase activity (Hong et al., 2009).

The *CYP19A1* gene contains nine coding exons, II to X. Located upstream of exon II is a regulatory region containing multiple versions of exon I. Each exon I serves as the promoter of *CYP19A1* in a particular tissue. After activation by specific transcription factors, the newly formed messenger RNA (mRNA) of the particular exon I is spliced directly upstream of the mRNA of exon II; this results in tissue-specific mRNA

transcripts. With the translation start site located in exon II, regardless of which tissue-specific promoter is used, exon I is not translated and the aromatase protein created in all tissues is identical. The exon I named PII is used specifically in the ovary. PI.3 is also used in the ovary, as well as in adipose tissue. Although not normally used in the breast, PII and PI.3 promoters are activated in malignant and surrounding tissues of breast tumours. PI.7, PI.4, and PI.1 regulate aromatase expression in endothelium, adipose, and placenta respectively and at least five other promoters exist (Bulun et al., 2005; Simpson et al., 2002) (**Figure 4**). Humans contain the most tissue-specific aromatase promoters; the gene in the most vertebrates contains only two promoters, specific to the gonads and brain (Li et al., 2008; Simpson et al., 2002).

1.7.2 Function

Aromatase controls the rate-limiting step of estrogen synthesis, conversion of androstenedione to estrone and testosterone to estradiol (Li et al., 2008; Simpson et al., 2002). Within the ovary, GCs of antral follicles contain aromatase and are responsible for the production of most circulating estradiol, although OSE cells and luteinized GCs of the CL also express aromatase (Okubo et al., 2000; Richards et al., 1987; Simpson et al., 2002). During menopause, ovarian production of estradiol ceases and aromatase in other tissues is sufficient for local effects of estradiol (Simpson et al., 2002).

1.7.3 Regulation

The regulation of aromatase expression is different in each tissue in which the protein is expressed because transcription initiation of each promoter is controlled by different regulatory factors; it is best studied in GCs (Simpson et al., 2002). FSH induces

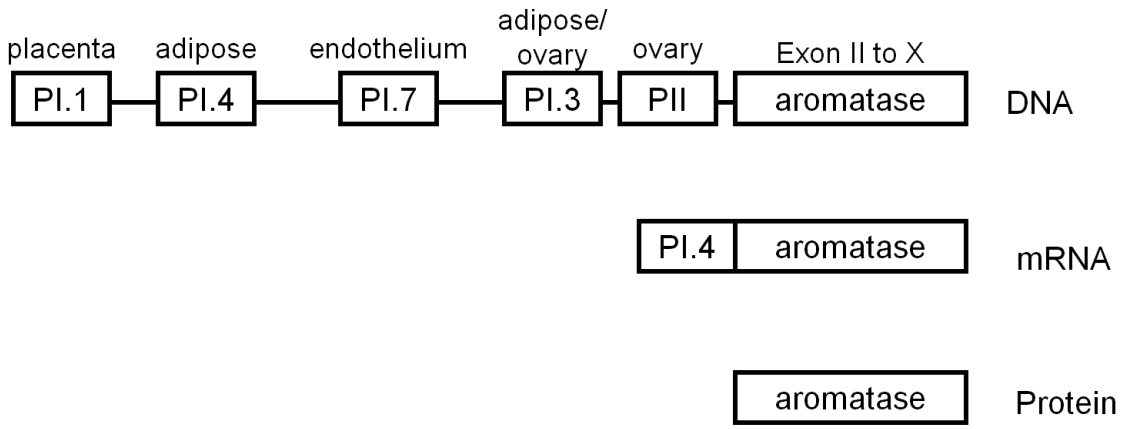

Figure 4. Structure of the *CYP19A1* gene. Exons II to X are both transcribed and translated, making up the functional protein. Upstream of exon II is a large regulatory region containing multiple exon Is (five shown here) that serve as tissue-specific promoters. The promoter names and the tissues in which they regulate aromatase expression are indicated. After transcription of a particular exon I promoter, the mRNA formed is spliced upstream of exon II mRNA, resulting in tissue-specific mRNA transcripts. The translation start site is contained within exon II, therefore regardless of which tissue-specific promoter is used, the aromatase protein created is identical is all tissues.

aromatase expression in GCs by binding its receptor, resulting in stimulation of cyclic adenosine monophosphate (cAMP) and subsequent activation of protein kinase A (PKA). These events cause recruitment of various coactivators to the *CYP19A1* promoter (Simpson et al., 2002; Stocco, 2008) (**Figure 5 B**). FSH receptor is also expressed in OSE cells and regulation of aromatase likely works in a similar manner (Okubo et al., 2000; Zheng et al., 1996). Aromatase expression is also increased by prostaglandin E2 (PGE2) in various cell types, including adipocytes, via the cAMP/PKA pathway (Subbaramaiah et al., 2008).

One transcription factor induced via FSH stimulation of GCs is cAMP response element-binding (CREB), which is phosphorylated by PKA and then binds to the cAMP-responsiveness element-like sequence (CLS) in the aromatase promoter (**Figure 5 B**) (Simpson et al., 2002; Stocco, 2008). In addition to the CLS, the PII promoter contains a GATA binding site recognized by GATA-4 and binding sites for nuclear receptor 5a transcription (NRE) factors, which are activated by steroidogenic factor-1 (SF-1) (Lu et al., 2011; Stocco, 2008). Binding of sequence-specific transcription factors to CLS, GATA, and NRE sites within the PII promoter upon FSH stimulation of GCs recruits coactivators that allow transcription of ovary-specific aromatase mRNA (Stocco, 2008).

1.8 BRCA1 and Aromatase

A connection between Brca1and aromatase was first suspected because of opposite timing of expression in developing follicles of mice (Hu et al., 2005; Phillips et al., 1997). Furthermore, cAMP-induced increases in aromatase expression in a human GC cell line (KGN) and in primary breast adipose fibroblasts and stromal cells correlated with decreased BRCA1 expression (Ghosh et al., 2007; Hu et al., 2005; Lu et al., 2006)

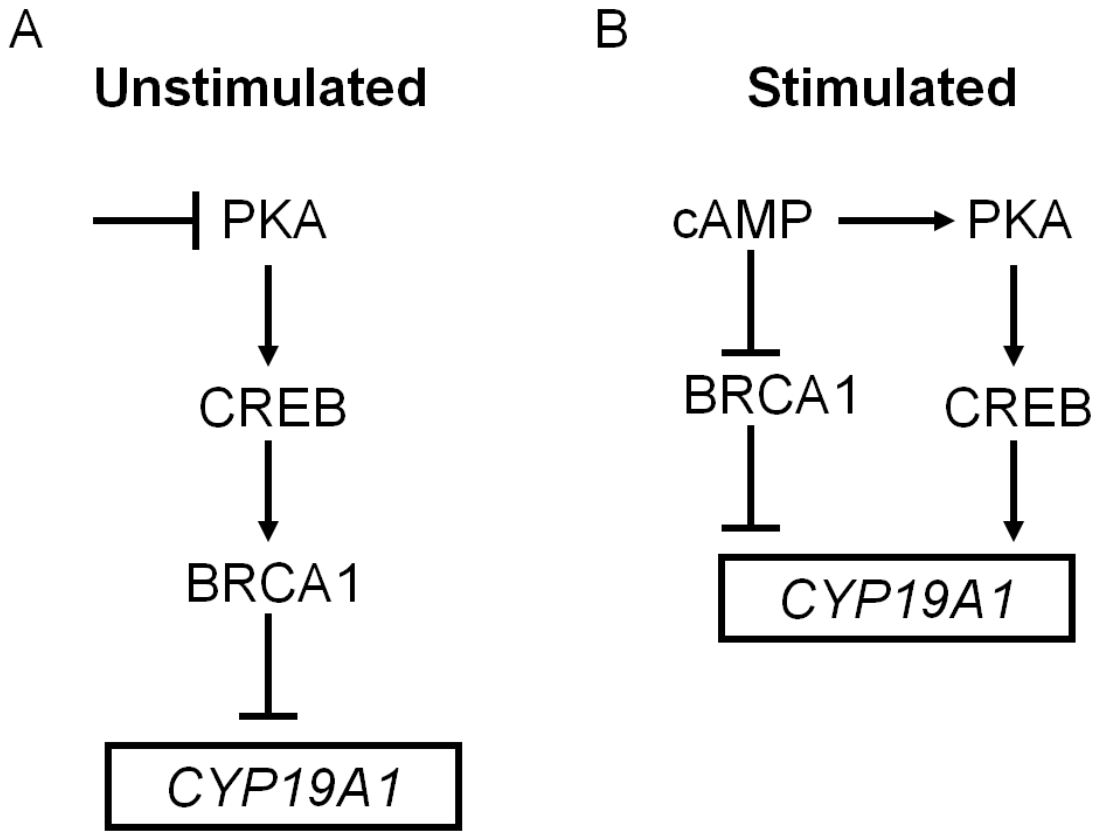

Figure 5. Regulation of *CYP19A1* transcription in granulosa cells. A) Ghosh *et al.* (2008) showed that, under basal conditions, inhibition of protein kinase A (PKA) reduced cyclic adenosine monophosphate (cAMP) response element-binding (CREB) interaction with the BRCA1 promoter, which decreased BRCA1 expression and subsequently increased aromatase expression. B) It is well established that cAMP activates PKA which then recruits coactivators, including CREB, to promoters of *CYP19A1* to stimulate its transcription. Induction of cAMP also decreases BRCA1 expression and decreased BRCA1 expression causes increased aromatase expression.

(**Figure 5 B**). This effect is specific to aromatase-expressing cells and is not a general effect of increased cAMP on BRCA1 expression (Hu et al., 2005).

The mechanism of how increased intracellular cAMP increases aromatase and decreases BRCA1 expression nearly simultaneously was investigated in one study. Ghosh *et al.* (2008) showed that, in unstimulated GCs, inhibition of PKA reduced CREB interaction with the BRCA1 promoter, which decreased BRCA1 expression and subsequently increased aromatase expression. These findings contradict the well established induction of aromatase by increased PKA and CREB via cAMP. The authors suggest PKA and CREB have different effects on aromatase expression in basal versus cAMP-stimulated cells (Ghosh et al., 2008) (**Figure 5 A**).

Further investigation of a relationship between BRCA1 and aromatase expression has been performed on human cell lines. Hu *et al*. (2005) proved that knocking down *BRCA1* expression with small interfering RNA (siRNA) specifically increased aromatase mRNA, protein, and activity levels in the KGN human GC line due to super-activation of the ovarian promoters, PII and PI.3 (**Figure 5 B**). BRCA1 knockdown also induced aromatase mRNA expression in primary human breast adipose fibroblast, mature adipocyte, and human breast cancer cell lines through activation of promoters PII and PI.3, while expression of the normal adipose tissue promoter remained stable (Ghosh et al., 2007; Lu et al., 2006). These findings suggest the ability of BRCA1 to regulate aromatase expression is tissue-specific because of the specific promoters it regulates.

The mechanism by which BRCA1 inhibits aromatase expression began to be elucidated in adipocytes and primary breast adipose fibroblasts in studies showing basal BRCA1 interaction with the PII/PI.3 region of the aromatase gene decreases once

intracellular cAMP increases, suggesting BRCA1 transcriptionally represses aromatase expression (Lu et al., 2006; Subbaramaiah et al., 2008). SF-1, previously mentioned as a transcription factor involved with the PII promoter of *CYP19A1*, is required for BRCA1 repression of PII-induced aromatase transcription in KGN cells. This appears to occur through direct interaction between SF-1 and BRCA1's binding partner BARD1, however, this interaction has only been seen in the HEK 293 T cell line, not GCs, and the mechanism of repression once BRCA1 is present at the PII promoter remains unknown (Lu et al., 2011). Different mechanisms must mediate BRCA1 repression of aromatase in adipocytes and breast tumours because SF-1 is not expressed in breast tissue. Using human adipocytes, Subbaramaiah *et al.* found that a PGE2-mediated cAMP increase reduced interaction between BRCA1 and the PII/PI.3 promoter and increased interaction between p300 and the PII/I.3. As a coactivator, p300 would be expected to promote aromatase expression (Subbaramaiah et al., 2008).

Evidence linking BRCA1 to estrogen regulation *in vivo* is limited. One mouse model accomplished *Brca1* inactivation in GCs by expressing Cre recombinase under the control of the promoter of the FSH receptor in a mouse homozygous for loxP-flanked (floxed) *Brca1*; 68% of the Brca1-deficient mice developed benign tumours of the ovary and uterine horns within 12 to 20 months of age compared to no abnormalities in Brca1-intact littermates. Tumours carried wildtype *Brca1* and therefore did not originate from the Brca1-deficient GCs. It was suggested that GCs with inactivated *Brca1* secreted an effector which promoted tumourigenesis in nearby epithelial tissue (Chodankar et al., 2005). Although the authors did not speculate what the paracrine-acting factor promoting tumour formation may be, a logical candidate is estrogen.

Later work in the same mouse model of *Brca1* inactivation revealed that mice with inactivated *Brca1* had significantly higher circulating estradiol levels and longer proestrous phases of their estrous cycle, which is the phase with the highest estrogen levels, compared to littermates with wildtype *Brca1*. Mutant *Brca1* mice with the longest proestrous phases were also more likely to develop benign tumours in their reproductive tract than mutant *Brca1* mice with shorter proestrous phases, suggesting the increased estradiol levels experienced had a functional consequence (Hong et al., 2010). A similar mouse model of *Brca1* inactivation generated by a separate group showed different results: floxed *Brca1* mice crossed with mice expressing Cre recombinase under the control of the promoter of anti-Müllerian hormone receptor II (*Amhr2*) resulted in *Brca1* inactivation within the female reproductive tract, including GCs, but none of these mice developed tumours (Xing et al., 2009). The discrepancy between the two similar models could be due to the different mouse strains used, timing of promoter activation, and the additional inactivation of *Brca1* in the pituitary of Hong *et al*'s mice. The authors did thoroughly explore the latter possibility and, despite evidence that Brca1 loss within the pituitary has a small impact, it is clear that the loss of Brca1 in GCs alone is sufficient to significantly lengthen proestrous and promote benign tumour development in their model (Hong et al., 2010).

Chand *et al.* (2009) investigated the clinical relevance of the BRCA1 regulation of aromatase. Aromatase expression was 25.8-fold higher in breast tissue and 8-fold higher in ovarian tissue from prophylactic mastectomies and oophorectomies respectively in *BRCA1* mutation carriers versus control women due to significant upregulation of PII and

PI.3 transcripts. Circulating estradiol was not measured; it therefore remains unknown if the upregulation of aromatase mRNA due to BRCA1 loss causes physiological effects.

The demonstration that BRCA1 inactivation increases aromatase expression indicates that the combination of decreased DNA damage repair and increased estradiol may be responsible for promoting tumourigenesis specifically in estrogen-responsive tissues.

1.9 Estradiol

For increased aromatase expression to affect cancer initiation in *BRCA1* mutation carriers, estradiol must be capable of promoting transformation of BRCA1-deficient cells. Estradiol exerts effects via binding to cytoplasmic ER α or β. The receptor translocates to the nucleus and dimerizes (Fan et al., 1999; Nussey and Whitehead, 2001). Through their transcriptional activation domains and a DNA binding domain, ERs cause transcription of genes containing estrogen-responsive enhancer elements (EREs) (Fan et al., 1999).

It has been suggested that proliferation induced by estradiol binding to its receptors makes mutations in oncogenes and tumour suppressor genes more likely, including loss of heterozygosity of the *BRCA1* gene (Berstein, 2008). Experimental evidence has shown that ERs are detectable in rat and human OSE (Karlan et al., 1995; Lau et al., 1999; Stewart et al., 2004) and that estradiol significantly promoted the proliferation of ERα-positive primary rabbit OSE cells *in vitro* (Bai et al., 2000).

Correlational evidence also strongly links high circulating estrogen to cancer development. Hormone replacement therapy, wherein perimenopausal women take exogenous estrogen and/or progestin to help manage symptoms of menopause, increases the risk of breast and ovarian cancer, particularly with over ten years of use (Lacey et al., 2006; Li et al., 2008; Zhou et al., 2008). Prophylactic oophorectomy reduces the risk of

developing breast cancer by at least 25% (Kauff et al., 2002; Rebbeck et al., 2002) and this is assumed to be due to decreased circulating estradiol levels preventing the proliferation of breast cancer cells (Hu, 2009).

The effects of estradiol on promoting tumourigenesis have been observed *in vivo*. In rabbits, constant estradiol stimulation for 28 days, accomplished by slow-release pellets, increased OSE proliferation and formation of papillae on the ovarian surface (Bai et al., 2000). In mice, significantly increased patches of columnar and hyperplastic OSE cells were found after as little as eight days of continuous estradiol treatment compared to placebo-treated controls (Gotfredson and Murdoch, 2007; Laviolette et al., 2010). Twice weekly treatment of guinea pigs with estradiol for two to nine months resulted in benign tumours of the ovaries (Silva et al., 1998). While prolonged exposure to estradiol clearly promotes formation of preneoplastic structures in the ovary, there is no evidence that estradiol alone is sufficient to cause the development of ovarian malignancy. The combined insult of *Brca1* inactivation and estradiol treatment did cause tumour development in the mammary gland within one year (Li et al., 2007).

Increased estradiol can also promote cancer development independent of ERs through its metabolic products, particularly in cells that are deficient in DNA damage repair such as due to BRCA1 loss (Hu, 2009). Metabolism of estradiol results in the catechol metabolites 2-, 4-, and 16-hydroxyestrogen that can form DNA adducts and undergo redox cycling with semiquinone and quinone forms, generating free radicals. Both of these processes cause DNA damage (Nussey and Whitehead, 2001; Roy et al., 2007; Tsuchiya et al., 2005). The effects of estradiol-induced DNA damage have been investigated experimentally. Treating Syrian hamster embryo cells with estradiol

increased aneuploidy and colonies formed in soft agar (Tsutsui et al., 1997). Because these cells do not express ERs, observed results are due to estradiol metabolites. Mouse OSE cells contain the enzymes responsible for estradiol metabolism and estradiol treatment of these cells induced DNA damage within 24 hours (Symonds et al., 2008). *In vivo,* daily treatment of mice with 2- and 4-hydroxyestradiol for twelve or eighteen months resulted in significantly more uterine tumours compared to 17β-estradiol-treated mice (Newbold and Liehr, 2000) and OSE preneoplastic morphological changes in sheep induced by combination treatment of a carcinogen and estradiol were significantly reduced by treatment with the anti-oxidant Vitamin E (Murdoch et al., 2008). The carcinogenic metabolites of estradiol provide a mechanism by which estradiol can promote cancer development in ER negative cells, such as those found in the vast majority of BRCA1-associated breast cancers. This idea is supported by the fact that estrogen stimulation upregulates BRCA1 expression, perhaps as a mechanism to protect against the potential DNA damaging effects of estradiol (Hu, 2009).

1.10 Project Rationale

Accumulating evidence supports the hypothesis that loss of functional BRCA1results not only in decreased genome stability, but also increased aromatase expression and estradiol production that can promote the proliferation and transformation of estrogen-responsive cell types in the breast and ovary. However, important issues remain unanswered and should be addressed using physiologically relevant models for studying a system in which secreted factors from one cell type can impact the transformation of another. Specific to ovarian cancer, a causal link between BRCA1 and aromatase has only been found in one GC cell line and the ability of estradiol to promote the

transformation of BRCA1-deficient OSE cells has not been shown. An *in vivo* model allowing monitoring of estradiol levels and their effects on Brca1-deficient OSE cell transformation is required to determine if the loss of Brca1 increases estradiol synthesis to levels that are sufficient to initiate ovarian cancer. The goal of the current study was to develop a model that could help elucidate the mechanism by which BRCA1-associated cancers develop exclusively in the breast and ovary, by which estrogen-replacement therapy increases the risk of ovarian cancer, and to provide evidence for or against aromatase inhibitors for cancer prevention in women with *BRCA1* mutations.

1.11 Hypothesis

It was hypothesized that exogenous estradiol would promote preneoplastic morphological changes and ovarian tumours in mice with Brca1-deficent OSE and that loss of Brca1 function *in vitro* would increase aromatase expression in and estradiol production from both primary GCs and OSE cells. Furthermore, inactivation of *Brca1* in both GCs and OSE cells *in vivo* was expected to increase estradiol levels and subsequently induce preneoplastic changes and tumours in Brca1-deficient OSE.

1.12 Project Objectives

1) To evaluate the effects of exogenous estradiol on the promotion of tumourigenesis in Brca1-deficient OSE *in vivo*.
2) To determine if loss of Brca1 function in OSE cells and primary granulosa cells increases aromatase activity and estradiol production *in vitro*.
3) To create a mouse model exhibiting loss of Brca1 function in both GCs and OSE cells and determine if this combined deficiency increases estradiol levels and promotes ovarian tumourigenesis.

CHAPTER 2: MATERIALS AND METHODS

2.1 Experimental Animals

All experiments involving animals were performed in accordance with the *Guidelines for the Care and Use of Animals* established by the Canadian Council on Animal Care. The conditional knockout mouse *Brca1*$^{loxP/loxP}$ [FVB;129-*Brca1*^{tm2Brn}] was obtained from the Mouse Models of Human Cancers Consortium Mouse Repository (National Cancer Institute, Rockville, MD, USA). These mice contain loxP sites in introns 4 and 13 of their *Brca1* gene. The *Amhr2-Cre* 'knock-in' mice, which express Cre recombinase in the female reproductive organs under the control of the *Amhr2* promoter, were generated by Ken Garson and Kerri Courville in the Vanderhyden lab. Homozygous floxed *Brca1* mice (*Brca1*$^{loxP/loxP}$) were crossed with homozygous *Amhr2-Cre* mice (*Amhr2*$^{Cre/Cre}$) to attain F1 pups heterozygous for both genes of interest (*Brca1*$^{loxP/+}$; *Amhr2*$^{Cre/+)}$. F1 pups were then mated and after genotyping their F2 pups, breeding pairs were set up with both mice homozygous for floxed *Brca1* (*Brca1*$^{loxP/loxP}$), one carrying the Cre transgene ("*Cre* positive"; *Amhr2*$^{Cre/Cre}$ or *Amhr2*$^{Cre/+}$), and one not carrying the Cre transgene ("*Cre* negative"; *Amhr2*$^{+/+}$). Each pup from such breeders was genotyped and found to be homozygous for floxed *Brca1*. Mice negative for *Cre* were controls, since their *Brca1* gene would remain intact and produce functional protein, and mice positive for *Cre* were experimental, since their *Brca1* gene would be recombined and inactivated in both OSE and GCs (**Figure 6**). Five experimental and five control mice were euthanized at 60, 120, and 180 days of age.

2.2 Genomic DNA Extraction

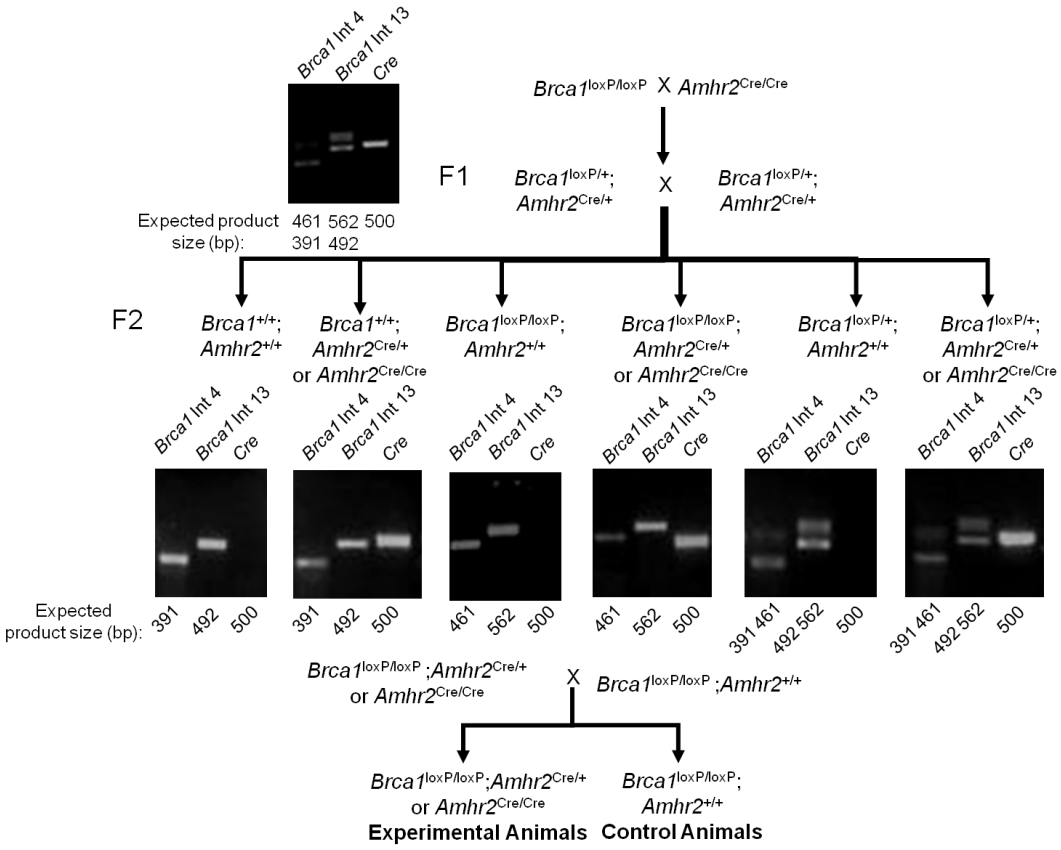

Figure 6. Breeding strategy to generate mice exhibiting loss of Brca1 function in both granulosa cells and ovarian surface epithelial cells from *Brca1*$^{loxP/loxP}$ and *Amhr2*$^{Cre/Cre}$ mice. *Brca1*$^{loxP/loxP}$ mice crossed with *Amhr2*$^{Cre/Cre}$ mice generated F1 pups heterozygous for both genes of interest. PCR of genomic DNA extracted from ear punches of F1 pups showed wildtype and floxed *Brca1* alleles in intron 4 (int 4; 391 bp and 461 bp respectively) and 13 (int 13; 492 bp and 562 bp respectively) and the presence of the *Cre* gene (500 bp). F1 pups were mated and genotyping of F2 pups showed mice with all possible genotypes. Homozygous floxed *Brca1 Cre*-positive mice (carrying the *Cre* transgene) were mated with homozygous floxed *Brca1 Cre*-negative mice (not carrying the *Cre* transgene) to obtain experimental and control animals.

Cell pellets of cultured cells or freshly isolated mouse ovarian surface epithelium (MOSE) cells and GCs, ear punches and tissue fragments from mice, and MOSE cells isolated by laser capture microdissection (LCM) (all described in subsequent sections) were incubated overnight at 56°C in 100-250 µl DNA extraction buffer (50 mM KCl, 10 mM Tris-HCl, 2 mM $MgCl_2$, 0.1 mg/ml gelatin, 0.45% Nonidet, and 0.45% Tween-20) plus 0.48-1.2 mg/ml proteinase K (Roche, Mississauga, ON). The following morning, samples were incubated at 100°C for 10 min and then stored at 4°C. Extracted DNA was quantified using the NanoDrop ND-1000 Spectrophotometer (Thermo Scientific, Waltham, MA, USA). For *in vitro* experiments, the number of cells from each treatment condition was counted with a Vi-CELL^{TM}XR Cell Viability Analyzer (Vi-CELL; Beckman Coulter Inc., Brea, CA, USA) and the same number of cells was collected and pelleted for DNA extraction.

Ethanol precipitation was performed to increase the purity of extracted DNA in some samples. Sodium acetate (3 M, pH 5.2) and ice cold 100% ethanol, one-tenth and two and a half times the volume of DNA extraction buffer used respectively, were added to the sample and, after vortexing, the sample was kept at -80°C for one hour. The sample was then centrifuged for 20 min at 12,000 rpm at 4°C, the supernatant was aspirated, and 1 ml ice cold 75% ethanol was added. After dislodging the pellet by vortexing, the sample was centrifuged for 10 min at 12,000 rpm at 4°C, the supernatant was aspirated, and the sample was allowed to air dry at room temperature for five min. Distilled water (20 µl) was added to the DNA pellet and the DNA content was re-measured.

2.3 Genotyping

PCR of genomic DNA extracted from ear punches from mice as well as from cultured and freshly isolated MOSE cells and GCs were used to determine the genotype of mice. All PCRs were performed using primers and reagents from Invitrogen (Burlington, ON), unless stated otherwise, in an Eppendorf Mastercycler (Eppendorf, Mississauga, ON) and resulting samples were run in 1-1.5% agarose gels made with Tris acetate-EDTA (TAE) buffer along with a 100 bp ladder. Digital images of each gel were taken with the EpiChemi II Darkroom system (UVP, Upland, CA, USA).

2.3.1 *Brca1*$^{loxP/loxP}$

The *Brca1* gene was genotyped to determine whether introns 4 and 13 were wildtype or floxed. Genotyping was performed using primers for intron 4 forward (5' TAT CAC CAC TGA ATC TCT ACC G 3') and intron 4 reverse (5' GAC CTC AAA CTC TGA GAT CCA C 3'), which yielded a 391 bp product if wildtype and a 461 bp product if floxed, as well as intron 13 forward (5' TAT TCT TAC TTC GTG GCA CAT C 3') and intron 13 reverse (5' TCC ATA GCA TCT CCT TCT AAA C 3'), which yielded a 492 bp product if wildtype and a 562 bp product if floxed (**Figure 6**). The PCR reaction contained 1 µl genomic DNA, 1X PCR buffer (10X stock), 2.5 mM $MgCl_2$ (50 mM stock), 0.1 mM dNTPs (10 mM stock), 0.5 µM of each primer (100 µM stock), and 0.05 U/µl Taq DNA polymerase (5 U/µl stock) up to 20 µl with distilled water. The PCR conditions were 94°C for 5 min, 30 cycles of 94°C for 30 sec, 60°C for 30 sec, and 72°C for 60 sec, and then 72°C for 10 min.

2.3.2 *Cre*

The presence or absence of the *Cre* gene was confirmed by genotyping. Amplification using forward (5'GCC CGG TCT GGC AGT AAA AAC 3') and reverse

(5’ CAG ATG GCG CGG CAA CAC 3’) primers (Sigma-Aldrich, St. Louis, MO, USA) resulted in a 500 bp product or no product if *Cre* was (referred to as *Amhr2*$^{Cre/+}$, *Amhr2*$^{Cre/Cre}$, or *Amhr2-Cre* positive) or was not (referred to as *Amhr2*$^{+/+}$ or *Amhr2-Cre* negative) present in the genomic DNA respectively (**Figure 6 and 7**). The PCR reaction contained a final volume of 1 µl genomic DNA, 1X PCR buffer, 5% dimethylsulfoxide (DMSO; Fisher Scientific, Ottawa, ON), 1.5 mM $MgCl_2$, 1.2 mM dNTPs, 0.4 µM of each primer (10 µM stocks), and 0.08 U/µl Taq DNA polymerase up to 12.5 µl with distilled water. The PCR conditions were 94°C for 5 min, 34 cycles of 94°C, 65°C, and 72°C for 30 sec each, and then 72°C for 10 min.

2.3.3 *Amhr2-Cre*

Mice were also confirmed to be Cre negative or Cre positive by genotyping the *Amhr2-Cre* transgene. Forward (5’ GGT CCA GCA CCT TCT A 3’) and reverse (5’ TCA ACT TGC ACC ATG CCG 3’) primers yielded a 536 bp product or no product if *Amhr2-Cre* was (referred to as *Amhr2*$^{Cre/+}$ or *Amhr2-Cre* positive) or was not (referred to as *Amhr2*$^{+/+}$ or *Amhr2-Cre* negative) present in the genomic DNA respectively (**Figure 7**). The PCR reaction components and conditions were the same as for detection of the *Cre* gene described in section 2.3.2.

2.4 Detection of Recombination at loxP Sites

PCR was used to confirm the excision of exons 5-13 of the *Brca1* gene (henceforth referred to as recombined *Brca1*) caused by Cre recombinase in cultured and freshly isolated MOSE cells and GCs, tissues from mice, and MOSE cells isolated by LCM. The presence of recombined *Brca1* resulted in a 600 bp product when genomic DNA was amplified using primers for *Brca1* intron 4 forward and *Brca1* intron 13

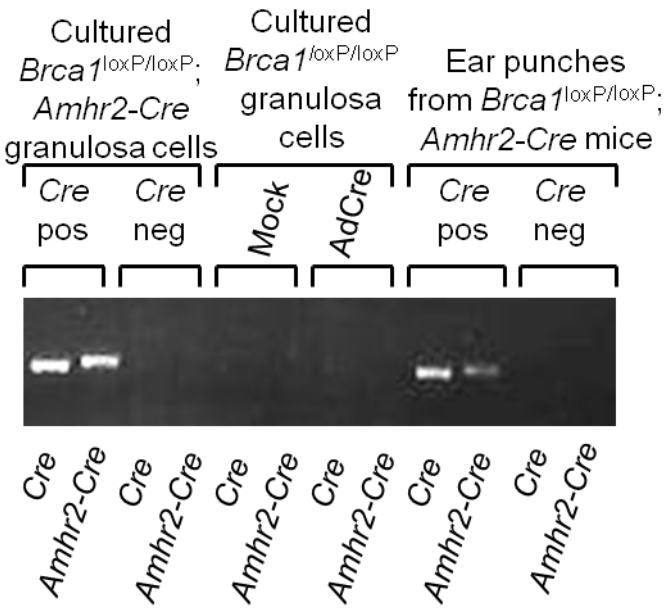

Figure 7. Genotyping of the *Amhr2-Cre* gene. PCR of genomic DNA extracted from cultured *Brca1*$^{loxP/loxP}$*;Amhr2-Cre* granulosa cells, cultured *Brca1*$^{loxP/loxP}$ granulosa cells, and ear punches from *Brca1*$^{loxP/loxP}$; *Amhr2-Cre* mice was performed with two separate sets of primers designed to amplify the *Cre* gene. The genotype of mice originally determined as carrying the *Cre* transgene or not carrying the *Cre* transgene (*Cre* = 500 bp) was confirmed (*Amhr2-Cre* = 536 bp). Cultured *Brca1*$^{loxP/loxP}$ granulosa cells infected with mock or AdCre served as a negative control.

reverse (sequences provided in section 2.3.1). The same primer set produced no product for intact wildtype *Brca1*, as the primers bind the genomic DNA too far away from each other to allow amplification. The proportion of cells containing wildtype *Brca1* after Cre-mediated recombination was detected in a separate PCR reaction using either *Brca1* exon 11 forward (5' ATC AGT AGT AGA AAT CCA AGC CCA CC 3') and *Brca1* exon 11 reverse (5' TGC CAC TCC CAG CAT TGT TAG 3') to yield a 592 bp product or *Brca1* intron 4 forward and *Brca1* intron 4 reverse to yield a 461 bp product (sequences provided in 2.3.1). The same primer sets produced no product for recombined *Brca1*. The PCR reaction contained 1 µl genomic DNA, 1X CoralLoad PCR buffer (10X stock; contains 15 mM $MgCl_2$; Qiagen, Mississauga, ON), 0.2 mM dNTPs, 0.5 µM of each primer (10 µM stock), and 0.025 U/µl Taq DNA polymerase (5 U/µl stock; Qiagen) up to 20 µl with distilled water. The PCR conditions were the same as described in section 2.3.1 and samples were run in 0.9-1.0% agarose gels and imaged in the same manner as described in section 2.3.

2.5 *In Vivo* Intrabursal Adenovirus Infection

At six to eight weeks of age, virgin female floxed *Brca1* mice were anaesthetized by intraperitoneal injection of avertin (2.5% v/v in saline, 0.015-0.017 ml/g body weight; Sigma-Aldrich). A single dorsal incision was made through the skin followed by an incision in the peritoneal membrane over the left ovarian fat pad. The ovary within the fat pad was exposed and, under a dissecting microscope, the bursal membrane was pulled taut and about 10 µl AdCre [Ad5CMVCre; 4 X 10^7 plaque forming units (pfu)/µl in phosphate buffered saline (PBS); Vector Development Laboratory, Houston, TX, USA] was injected in the bursal space using a 1 ml syringe and a 30-gauge needle (Terumo,

Somerset, NJ, USA; **Figure 8A**). The same procedure was performed to deliver AdCre to the right ovary.

2.6 Delivery of Exogenous Estradiol

During the surgery for *in vivo* delivery of AdCre to the MOSE, a slow-release hormone pellet designed to release 0.05 mg or 0.25 mg 17β-estradiol (placebo as control) over a sixty day time period (Innovative Research of America, Sarasota, FL, USA) was implanted subcutaneously in the neck region of each mouse (**Figure 8B)**. The low and high dose estradiol experiments were performed independently. In each case, mice were randomly assigned to scheduled euthanization time points of 60, 180, and 365 days after surgery. For the low dose pellet, 15 mice received a placebo pellet and 15 mice received an estradiol pellet, with five mice per treatment planned for each time point. For the high dose pellet, 16 mice received a placebo pellet and 15 received a high dose pellet, with three mice per treatment for the 60 day time point, five mice per treatment for the 180 day time point, and seven mice per treatment for the 365 day time point.

2.7 Tissue Collection

Mice were euthanized by CO_2 asphyxiation at scheduled time points or ages. Mice were euthanized before their intended time point if they reached a loss-of-wellness endpoint, which was defined as anorexia, dehydration that persisted after fluid therapy, respiratory distress, abdominal distension, and rapid weight loss or gain greater than five grams. Immediately after euthanization of mice that received a 0.05 mg estradiol pellet or its placebo control, a blood sample was obtained by inserting a 26½ gauge needle attached to a 1 ml syringe in the exposed abdominal aorta at close to 180º and drawing back until at least 0.5 ml blood was collected. After the necropsy was complete, blood

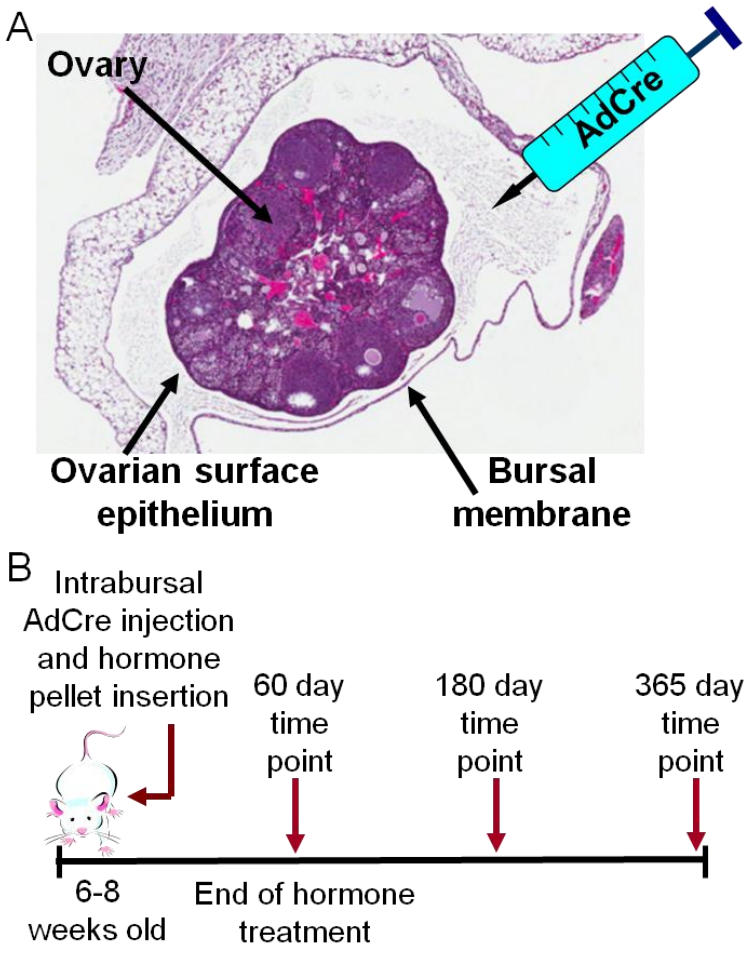

Figure 8. Schematic diagram of intrabursal injection of AdCre to inactivate *Brca1* in mouse ovarian surface epithelial cells *in vivo* and time course of the experiment. (A) Inactivation of *Brca1* in the ovarian surface epithelial cells of *Brca1*$^{loxP/loxP}$ mice was mediated by the intrabursal delivery of AdCre. (B) To study the effects of estradiol, a 60-day slow-release pellet containing estradiol (0.05 mg or 0.25 mg/pellet) or placebo was implanted subcutaneously at the same time as AdCre delivery. Mice were euthanized at various time points to examine the occurrence of preneoplastic morphologic changes in the ovarian surface epithelium.

samples were centrifuged for 10 min at 6,000 rpm and the supernatant, consisting of serum, was pipetted off and frozen in 120 µl aliquots at -20ºC. During necropsy, the abdominal cavity and organs therein were carefully examined for any abnormalities or signs of disease, with anything of interest noted. Both ovaries, along with the bursal membrane, oviduct, and a portion of the fat pad and uterine horn, were extracted, fixed in formalin for 24-72 hours, transferred to 70% ethanol for 24-72 hours, and then paraffin embedded. During some necropsies, only one ovary was paraffin embedded for future histological examination of preneoplastic lesions of the OSE and the other one as well as the oviduct and part of the uterine horns were individually snap frozen in Cryoware™ Cryovials (Nalge Nunc International Corp., Rochester, NY, USA) in liquid nitrogen and stored at -80ºC for future accessibility to DNA and RNA from these tissues to check *Brca1* recombination and Cre recombinase expression respectively.

2.8 Histological Examination

Three to eight non-consecutive 3 µm sections of paraffin embedded ovaries were taken from the middle of each ovary, allowed to dry overnight at room temperature, stained with Harris Modified Haematoxylin (Fisher Scientific) and eosin (Surgipath, Richmond, IL, USA) (H&E), scanned with an Aperio Scanscope CS system (Aperio Technologies Inc., Vista, CA, USA), and examined at high power magnification using Aperio ImageScope software (Aperio Technologies Inc.).

Each ovarian section was examined for MOSE that had undergone preneoplastic morphological changes. Lesions quantified included (1) columnar MOSE cells, which are longer than they are wide, (2) hyperplastic MOSE cells, which have lost apical/basal polarity and are no longer in a single layer, (3) invaginations, which are defined as the

MOSE cells invaginating at least 10 μm into the stroma of the ovary at close to a right angle to the normal MOSE with stroma on either side of the structure (**Figure 9**), and (4) number of inclusion cysts, which are spherical structures within the ovary and lined by MOSE cells.

Quantitative measurements were taken for the occurrence of each of these preneoplastic lesions. For columnar and hyperplastic MOSE, within each individual ovarian section, a line was traced along MOSE cells with these characteristics and a measurement in micrometers was provided by the ImageScope program. This value was then expressed as a percentage of the perimeter of the same ovarian section to give an indication of the extent of MOSE exhibiting columnar and hyperplastic morphology within that section. A percentage for both columnar and hyperplastic MOSE was obtained for each of the three to eight sections for a particular ovary and the mean of those measurements was calculated to obtain a representative mean for that ovary. Each ovary was considered as an independent unit and the means of each ovary within a treatment group were averaged to obtain an overall mean (± standard error of the mean (SEM)) for each treatment group. For invaginations and inclusion cysts, the number of each of these structures was counted for each ovarian section and an average per section for each ovary and then for each treatment group (± SEM) was determined. The sections were blinded prior to examination.

To investigate the possibility that particular structures within the ovary or estradiol-induced changes in those structures promote the formation of preneoplastic lesions in the MOSE, ovarian structures underlying MOSE cells exhibiting preneoplastic morphological changes were recorded in a minimum of two sections per ovary in the 60

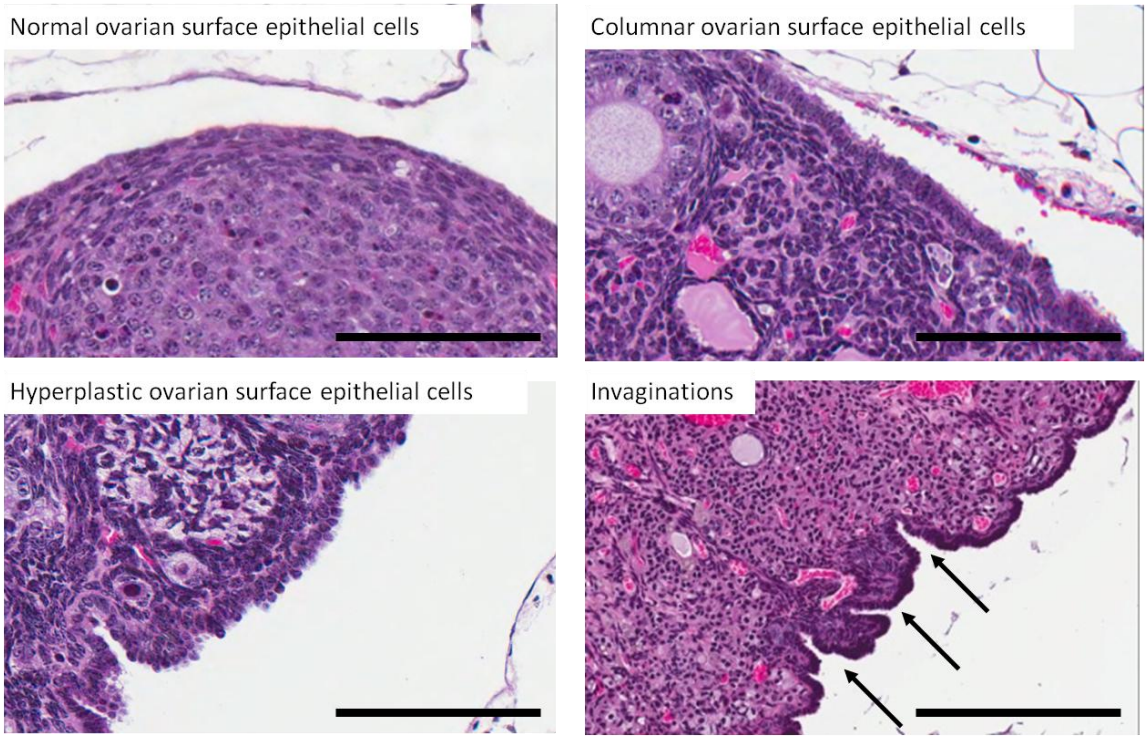

Figure 9. Representative images of preneoplastic morphological changes of the mouse ovarian surface epithelium. Ovarian sections from *Brca1*$^{loxP/loxP}$ mice following intrabursal injection of AdCre and implantation of a 60-day slow-release pellet containing 0.05 mg or 0.25 mg estradiol or placebo stained with H&E showing representative preneoplastic morphological changes of the ovarian surface epithelium, the occurrence of which were quantified with ImageScope software. Scale bar, 100 µm.

day time point ovaries for the high dose estradiol group and the 60, 180, and 365 day time point ovaries for the low dose estradiol group. For each section examined, each area of MOSE that was columnar, hyperplastic, or invaginating into the stroma of the ovary was marked as overlying stroma, primordial, primary, secondary, antral, or atretic follicles, corpus luteum, or any combination of these structures. For the 365 day time point only, ovarian structures underlying patches of normal MOSE were also recorded. Definitions of follicular stages were as follows: primordial follicles consist of a small oocyte surrounded by flattened GCs, primary follicles consist of an oocyte surrounded by a single layer of cuboidal GCs, secondary follicles consist of an oocyte surrounded by multiple layers of GCs, antral follicles consist of an oocyte in a fluid-filled cavity surrounded by GCs.

2.9 Immunohistochemistry

Ki-67 and E-cadherin expression in MOSE cells were assessed by immunohistochemistry of ovarian sections. For both procedures, paraffin embedded ovaries sectioned at 3 μm and allowed to dry overnight were deparaffinized and rehydrated in a series of xylenes and graded ethanol respectively according to standard protocol. Heat initiated epitope retrieval was performed by heating slides for 10 min in pH 6 sodium citrate buffer (Antigen Unmasking Solution; Vector Laboratories, Burlingame, CA, USA) in a pressure cooker. Once slides were cool, endogenous peroxidase activity was blocked by placing slides in a 3% solution of hydrogen peroxide in distilled water for 10 min.

For Ki-67 staining, slides were then incubated in Protein Block, Serum-Free (DAKO, Carpinteria, CA, USA; all reagents from DAKO unless specified otherwise) for

10 min immediately followed by blocking with an avidin/biotin blocking kit. Slides were incubated overnight at room temperature in Ki-67 primary antibody diluted 1:20 in Antibody Diluent with Background Reducing Components. Staining for Ki-67 was performed on three to five sections of three to four ovaries from mice given AdCre along with a pellet releasing either 0.05 mg and 0.25 mg 17β-estradiol or placebo and euthanized at the 60 day time point. An ovarian tumour from a nude mouse was used a positive control and sections of the same tumour incubated in diluent with primary antibody omitted served as a negative control. Furthermore, positively staining GCs served as an internal positive control in each ovarian section and sections showing no GC staining were excluded. The next morning, slides were washed three times for three min in Stockholm PBS (S-PBS), incubated in Biotinylated Rabbit anti-Rat Immunoglobulins diluted 1:200 in diluent, washed again, incubated in strepavidin/horseradish peroxidase diluted 1:200 in diluent, and underwent three final washes in PBS. The slides were then immersed for five min in diaminobenzidine (DAB) chromogen solution (Sigma-Aldrich) with 50 µl of 30% hydrogen peroxide before rinsing in water, counterstaining with haematoxylin, dehydrating, and mounting with Permount (Fisher Scientific) and cover slips.

The E-cadherin primary antibody (BD Transduction Laboratories, Mississauga, ON) was raised in mouse and therefore the Vector® Mouse on Mouse™ Immunodetection Kit (Vector Laboratories) was used. After blocking endogenous peroxidase activity, the avidin/biotin kit and the M.O.M Mouse Ig Blocking Reagent were used for blocking sequentially. Slides were then washed twice for five min with S-PBS and incubated with E-cadherin primary antibody diluted 1:400 in M.O.M Diluent for

1 hour and 30 min. E-cadherin staining was performed on one section of an ovary from mice given AdCre along with a pellet releasing either 0.05 mg and 0.25 mg 17β-estradiol or placebo and euthanized at the 60, 180, and 365 day time points. Oviduct and uterine horn included within the sections and ovarian sections incubated in diluent with primary antibody omitted served as a positive and negative control, respectively. After two washes for five min each in S-PBS, slides were incubated in M.O.M Biotinylated Anti-Mouse IgG Reagent for 10 min and then VECTASTAIN® Elite ABC Reagents for five min with three five min S-PBS washes after each incubation. Immersion in DAB and subsequent steps were performed in the same manner as for Ki-67 staining.

2.10 Radioimmunoassay to Measure Serum Estradiol

Serum samples from floxed *Brca1* mice given intrabursal AdCre and a pellet releasing 0.05 mg estradiol were assayed for their 17β-estradiol content using a Count-A-Count® Estradiol radioimmunoassay (RIA) kit (Diagnostic Products Corporation, Los Angeles, CA, USA). 100 µl of nine calibrators (0-3,600 pg/ml) and each sample were pipetted into Estradiol Ab-Coated Tubes. One ml of ^{125}iodine-labelled estradiol was added to each tube and after vortexing, samples were incubated at room temperature for three hours. Each tube was decanted thoroughly and struck sharply on absorbent paper to separate bound from non-bound estradiol before being read for one min in a Wizard 1470 Automatic Gamma Counter (Wallac, now PerkinElmer, Waltham, MA, USA). All calibrators and three out of nine serum samples were measured in duplicate and all samples were measured in the same run to avoid inter-assay variability. Estradiol content in samples was determined by comparison with measured calibrator values.

2.11 LCM of MOSE

Paraffin embedded ovaries sectioned at 5 µm were deparaffinised, rehydrated, and then dehydrated again in a series of xylenes and graded ethanol in coplin jars. After air drying for 5 min, slides were placed in 50 ml Falcon conical tubes (BD Biosciences, Mississauga, ON) containing desiccant to ensure they remained dehydrated. The ArcturusXT^{TM} LCM instrument and software (Applied Biosystems, Carlsbad, CA, USA) were used to isolate MOSE from ovarian sections. With the slide on the stage of the microscope, an overview image was taken and a CapSure® Macro LCM Cap (Applied Biosystems) was placed over an ovarian section. A path was traced along the MOSE and then an infrared laser pulsed along the path, melting the film on the cap to the MOSE but allowing the film rather than the cells to absorb the laser radiation. The cap was then lifted, with MOSE attached, removing the MOSE from the ovarian section. Once this procedure had been repeated to isolate MOSE from 32-100 ovarian sections, the film from each cap was peeled off and placed into a single microcentrifuge tube (**Figure 10**). Genomic DNA extraction was performed as described in Section 2.2.

MOSE cells were isolated from ovaries from floxed *Brca1* mice injected under the bursal membrane with AdCre to confirm that *Brca1* recombination had occurred. Ovaries chosen for this analysis included the right ovary of mouse 6564, a low dose placebo-treated mouse euthanized at 40 days after surgery, the left ovaries of mouse 7435 and mouse 7441, both high dose placebo-treated mice euthanized 180 days after surgery. The approximate number of sections used for MOSE isolation from these ovaries was 57, 32, and 58, respectively. MOSE cells were also isolated from 100 pooled ovarian sections from high dose estradiol-treated mice euthanized at 60 days after AdCre injection and pellet insertion.

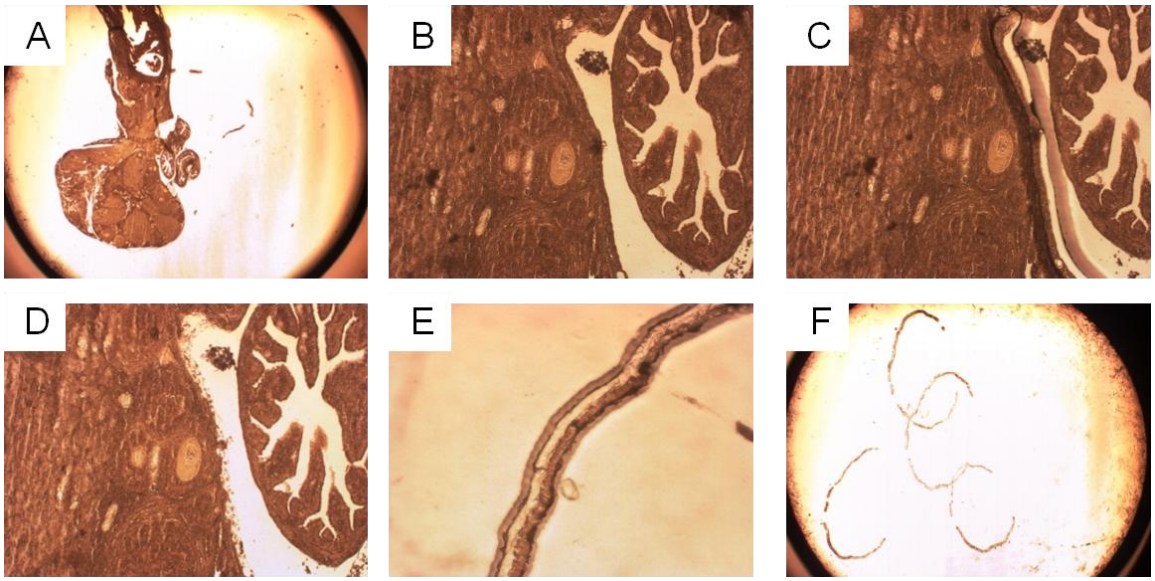

Figure 10. Procedure for isolating mouse ovarian surface epithelial cells from paraffin embedded ovaries using laser capture microdissection (LCM). Using the ArcturusXT^{TM} LCM instrument and software, an overview image of each slide was taken and (A) a CapSure® Macro LCM Cap was placed over one ovarian section. (B) Increased magnification allowed visualization and tracing of the ovarian surface epithelium. (C) An infrared laser pulsed along the traced path on the ovarian surface epithelium, melting the film on the cap to the ovarian surface epithelium. (D) The cap was lifted, removing the ovarian surface epithelium from the ovarian section and leaving internal ovarian cells and structures intact. (E) Strips of isolated ovarian surface epithelial cells remain attached to the cap. (F) Ovarian surface epithelial cells from numerous ovarian sections were isolated on a single cap. The entire procedure was repeated until the ovarian surface epithelium was isolated from 32-100 ovarian sections.

2.12 Tissue Culture

2.12.1 Charcoal-filtering of Serum

Fetal bovine serum (FBS; Hyclone) was treated with 10% dextran (Pharmacia)-treated charcoal (50 mg/ml; Sigma-Aldrich) and stirred overnight at 4°C. The solution was then centrifuged for 30 min at 1,800 x g and the supernatant was poured into two ultracentrifuge tubes for centrifugation for 60 min at 27,000 x g. The serum was then sterilized by filtration through a filter with 0.2 μm pores, aliquoted, and stored at -20°C. Thawed aliquots were not re-frozen. This dextran-treated charcoal-treated serum is henceforth called steroid-free serum.

2.12.2 Isolation of MOSE Cells

Ovaries extracted from euthanized mice were placed in Dulbecco's Modified Eagle's Medium Nutrient Mixture F-12 Ham (DMEM/F12) phenol red-free media (Sigma-Aldrich) that contained 5 U/ml penicillin/0.005 mg/ml streptomycin solution (Sigma-Aldrich), 0.1 μg/ml gentamicin (Invitrogen), and 1μg/ml insulin-transferrin-sodium-selenite solution (ITSS; Roche) (this media will henceforth be referred to as MOSE media) + 2% serum until all ovaries had been collected. After two washes with PBS, ovaries were incubated in 0.25% trypsin/PBS (Invitrogen) for 30 min in a 37°C water bath. The tube containing the ovaries was gently agitated to remove MOSE cells from the ovary and the MOSE-containing trypsin was decanted into a new 15ml Falcon tube which was then centrifuged to pellet the MOSE cells. The trypsin was aspirated and MOSE media + 5% serum was added to inactivate any remaining trypsin. The MOSE cells were then pelleted, washed with PBS, and pelleted again. These freshly isolated MOSE cells were used for RNA or genomic DNA extraction.

2.12.3 Isolation and Culturing of Primary Granulosa Cells

Prepubertal (19-21 days old) *Brca1*$^{loxP/loxP}$ and *Brca1*$^{loxP/loxP}$*; Amhr2-Cre* negative and positive mice were injected subcutaneously with 1 mg/day diethylstilbestrol (DES; Sigma-Aldrich) for three days to stimulate GC proliferation. Ovaries extracted from euthanized mice were placed in MOSE media + 10% serum on a 37°C heating block until all ovaries had been collected. Each ovary was then held with tweezers, poked with a 27 gauge needle to allow GCs to be released into the media, and then discarded. The cell-containing media was centrifuged to pellet the cells, which were then resuspended in MOSE media + 2% serum and the number of cells was counted with a Vi-CELL counter. GCs were plated at 300,000 cells per well of a twelve-well plate in 1 ml MOSE media + 2% serum. The remaining GCs were pelleted and immediately frozen at -80°C (freshly isolated GCs). GCs were kept in culture for 4-6 days during experiments.

2.12.4 Cell Maintenance

Cultured cells were maintained in MOSE media at 37°C in 5% CO_2. MOSE cells originally isolated by enzymatic digestion from floxed *Brca1* mouse ovaries and previously cultured for at least nine passages were thawed at 37°C and plated in 25 cm^2 flasks (Corning Inc., Corning, NY, USA) with 5 ml of MOSE media + 10% serum until nearing confluence. MOSE were then transferred to 75 cm^2 flasks where they were maintained. Each time the MOSE cells reached confluence they were passaged by washing with PBS (Hyclone, Logan, UT, USA) and then trypsin (Hyclone), incubating for 5-10 min at 37°C, resuspending in MOSE media + 10% serum, removing the majority of the media + MOSE cells, and adding fresh media + 10% serum back to the remaining MOSE cells in the flask. MOSE cells were periodically frozen by resuspending pelleted

MOSE cells in freezing media (90% serum + 10% DMSO), aliquoting resuspended cells into Cryoware™ Cryovials and storing at -80°C. For *in vitro* experiments, MOSE cells from 75 cm^2 flasks were counted with a Vi-CELL and plated at 300,000 cells per well of a twelve-well plate in 1 ml MOSE media + 2% serum.

2.12.5 *In Vitro* Adenovirus Infection

Twenty-four hours after plating MOSE cells or GCs in a twelve-well plate, cells from a single well were counted using a Vi-CELL counter and the total number of viable cells was used to calculate the volume of adenovirus required to infect cells with a multiplicity of infection of 200 pfu/cell. All other wells of cells were washed with PBS, covered with 0.5 ml serum-free MOSE media containing the appropriate concentration of virus, either AdCre, adenovirus expressing green fluorescent protein (AdGFP; Ad5CMVeGFP; Vector Development Laboratory), or a mock infection (serum-free MOSE media containing no virus), and incubated at 37ºC for 2 hours. Each well of cells was then washed twice with PBS and replenished with 1 ml fresh MOSE media + 2% serum. Any further treatment of the cells or extraction of genomic DNA to detect recombination at *Brca1* loxP sites was performed 72 hours after adenovirus infection. Treatments were then applied for 48 hours, resulting in cells being collected five days after infection. In a single experiment performed by a separate lab member, MOSE cells infected with mock, AdGFP, or AdCre infection were maintained in culture for two, three, or four months before cell collection.

2.12.6 Treatment of Cells with FSH and Testosterone

Treatments were performed on *Brca1*$^{loxP/loxP}$ MOSE cells and GCs previously plated in twelve-well plates and infected with adenoviral vectors or mock infection and

Brca1$^{loxP/loxP}$; *Amhr2*$^{Cre/+}$ or *Brca1*$^{loxP/loxP}$; *Amhr2*$^{Cre/Cre}$ and *Brca1*$^{loxP/loxP}$; *Amhr2*$^{+/+}$ GCs plated in twelve-well plates. In all cases, cells were washed once with PBS and then 1 ml MOSE media + 2% steroid-free serum containing the appropriate concentration of treatment was added. Treatments included ethanol control, FSH (50 ng/ml; Sigma-Aldrich), testosterone (10^{-6} M; Sigma-Aldrich), and FSH and testosterone (F+T) in combination. After 48 hours in treatment media, 1 ml of media was collected from each well of cells and stored at -20ºC. Cells were trypsinized, pelleted, and frozen at -80ºC as described in 2.17.

2.12.7 Cell Collection

At the conclusion of *in vitro* experiments, cells were washed once with 2 ml PBS, 0.5 ml trypsin was added and quickly removed, and cells were incubated at 37ºC for 10-15 min until cells had begun to detach from the plastic. One ml MOSE media + 2% steroid-free serum was added and pipetted up and down five times to fully detach cells. Cells were pelleted, washed with PBS, and pelleted again. Cell pellets were immediately placed on dry ice and stored at -80ºC or processed directly for genomic DNA extraction as described in section 2.2.

2.13 RNA Analysis

2.13.1 RNA Extraction and Quantification

RNA was extracted from MOSE and GC cell pellets using the RNeasy Micro Kit (Qiagen) and from frozen tissue fragments using the RNeasy Mini Kit (Qiagen). Frozen cell pellets were placed on ice and, after each tube was flicked to loosen the pellet, 350 µl RLT Buffer containing 3.5 µl β-mercaptoethanol (Sigma-Aldrich) was added and each tube was vortexed. Homogenization was accomplished using QIAshredder spin columns

(Qiagen). Tissue fragments were immersed in 350 µl RLT Buffer containing 3.5 µl β-mercaptoethanol and finely chopped before being passed through a 20-gauge needle fitted to a 1ml syringe at least five times. For both sample types, the RNeasy protocol was followed precisely, taking samples through multiple wash and spin down cycles. Total RNA was eluted from the spin column in 12 µl or 30 µl RNase-free water for the RNeasy Micro and Mini Kit respectively. RNA was quantified with the NanoDrop ND-1000 Spectrophotometer and then stored at -80ºC.

2.13.2 Reverse Transcription

RNA (250 ng or 500 ng) was transcribed into complimentary DNA (cDNA) using reverse transcription (RT). One hundred pmol random decamers (Ambion, Austin, TX, USA) was added to the volume containing the desired amount of RNA and the final volume was brought up to 12 µl with RNase-free water. After a five min incubation at 70ºC, 1X reaction buffer (5X stock, Fermentas, Burlington, ON), 1 mM dNTPs (10 mM each, Fermentas), 20 U RNase Inhibitor (Ambion), 0.5 µl RNase-free water, and 200 U RevertAid^{TM} Reverse Transcriptase (Fermentas) were added to the tube held on ice. Each tube was gently mixed, briefly centrifuged, and then incubated for five min at 37ºC, 60 min at 42ºC, and 10 min at 70ºC.

For some samples, reverse transcription was performed using QuantiTect® Reverse Transcription (Qiagen). The volume containing the desired amount of RNA was added to 1X genomic DNA Wipeout Buffer (7X stock) and the final volume was brought up to 14 µl with RNase-free water. Each tube was incubated at 42ºC for two min and placed immediately on ice. One µl Quantiscript Reverse Transcriptase (containing RNase inhibitor), 1X Quantiscript RT Buffer (5X stock; containing Mg^{2+} and dNTPs), and 1 µl

RT Primer Mix was added to the tube containing the RNA. Each tube was gently mixed, briefly centrifuged, and then incubated for 30 min at 42ºC and 3 min at 95ºC.

For both protocols, at least one negative control that did not receive reverse transcriptase was included in each reverse transcription reaction run. cDNA samples were stored at -20ºC.

2.13.3 Real-time PCR

Real-time PCR reactions were carried out in triplicate in a 96-well plate (Applied Biosystems; all reagents from Applied Biosystems unless specified otherwise) in the 7500 FAST Real-Time PCR System. A TaqMan® Gene Expression Assay for Mus musculus Cyp19a1 (74 bp) was used to measure aromatase expression in MOSE and GC samples in a duplex reaction with TaqMan® Ribosomal RNA Control Reagent designed to detect the 18S ribosomal RNA gene (187 bp) as an endogenous control. For GCs, reactions occurred in a total volume of 20 µl consisting of 7 µl RNase-free water, 1X TaqMan® Gene Expression Master Mix (2X stock), 1µl TaqMan® Gene Expression Assay for Cyp19a1, 1 µl TaqMan® Gene Expression Assay for 18S, and 1 µl cDNA. For OSE cells, reactions occurred in a total volume of 10 µl consisting of 3µl RNase-free water, 1X TaqMan® Gene Expression Master Mix, 0.5 µl TaqMan® Gene Expression Assay for Cyp19a1, 0.5 µl TaqMan® Gene Expression Assay for 18S, and 1 µl cDNA. The real-time PCR reaction was carried out using the following conditions: 50ºC for 20 sec, 95ºC for 10 min, and 40 cycles of 95ºC for 15 sec (denaturation) and 60ºC for 1 min (annealing), with fluorescence detected during the annealing stage of each cycle.

The expression of Cre recombinase and ERα were also determined using real-time PCR, with the endogenous control gene Ppia (primers: 5’ AGG GTG GTG ACT TTA

CAC GC 3' and 5' GAT GCC AGG ACC TGT ATG CT 3'; 133 bp; Invitrogen) amplified in a separate reaction for each sample as a reference for relative mRNA quantification. Cre amplification was accomplished by the primers 5' CAA TAC CGG AGA TCA TGC AA 3' and 5' CAC TAT CCA GGT TAC GGA TAT AGT TCA 3' (77 bp; Invitrogen) in a 10 µl reaction consisting of 3 µl RNase-free water, 5 µl RT^2 SYBR® Green with ROX (SA Biosciences, Frederick, MD, USA), 1 µM forward and reverse primers (10 µM stock), and 1 µl cDNA. Primers (5' TCT GCA GCA GCA GCA TCG CC 3' and 5' GGC ATG AAG GCG GTG GGC AT 3'; 166 bp; Invitrogen) were used to determine ERα expression in a 20 µl reaction consisting of 6 µl RNase-free water, 10 µl RT^2 FAST SYBR® Green with ROX (SA Biosciences), 0.5 µM forward and reverse primers (5 µM stock), and 2 µl cDNA. For both Cre and ERα, real-time PCR reaction conditions were: polymerase activation (95ºC for 10 min), 40 cycles of denaturation (95ºC for 15 sec for Cre and 10 sec for ERα) and annealing (60ºC for 1 min for Cre and 30 sec for ERα; fluorescence detected during this stage of each cycle), and dissociation (95ºC for 15 sec, 60ºC for one min, 95ºC for 15 sec, 60ºC 15 sec). The melt curves generated during the dissociation step helped to confirm that the C_T values used for analysis represented amplification of only the specific amplicon of interest.

Representative samples from real-time PCR reactions were run on a 2% agarose gel to confirm correct product size. No detectable C_T value or band was observed in the no template or no reverse transcriptase controls, excluding the possibility of contamination with genomic DNA.

Analysis of data from real-time PCR reactions was performed by 7500 Software V2.0.1 using the comparative C_T ($\Delta\Delta C_T$) real-time PCR method for relative quantitation

of mRNA expression. For each sample, C_T values for the endogenous control were subtracted from the C_T value of the gene of interest to obtain ΔC_T values. The ΔC_T value of the control sample was then subtracted from the ΔC_T value of each experimental sample to obtain $\Delta\Delta C_T$ values. The relative quantity (RQ) was calculated for each experimental sample using the formula $2^{-\Delta\Delta CT}$, resulting in a RQ value of 1 for the control sample and the fold difference in expression of each experimental sample compared to the control (Applied Biosystems, 2008).

2.14 ELISA to Measure Media Estradiol

Estradiol content in the media in which MOSE cells and GCs were grown was assayed using the Estradiol EIA Kit (96-well solid plate; Cayman Chemical Company, Ann Arbor, MI, USA). Fifty µl of eight standards (6.6-4,000 pg/ml) and each sample (in triplicate), undiluted and diluted 1:5 in EIA buffer, were pipetted into wells pre-coated with mouse monoclonal anti-rabbit IgG. Fifty µl estradiol-acetylcholinesterase conjugate (AchE Tracer) was added to each well followed by 50 µl Estradiol EIA Antiserum. The plate was then incubated for one hour at room temperature on an orbital shaker, during which time estradiol from samples competed with AchE Tracer for binding to estradiol antiserum and the antiserum-estradiol complex became bound to the mouse monoclonal anti-rabbit IgG attached to the well. After washing each well five times with Wash Buffer to remove unbound reagents, 200 µl Ellman's Reagent was added to each well and the plate developed in the dark for 60 min. During this time, AchE reacted with its substrate (provided in the Ellman's Reagent) to generate a product with a yellow colour that absorbs at 412 nm. The intensity of the colour of each well was read spectrophotometrically at 405 nm by a MRX microplate reader (Dynex Technologies,

Chantilly, VA, USA), with the absorbance measured proportional to bound AchE and inversely proportional to the amount of estradiol in the sample. Estradiol content in samples was determined by comparison with measured standard values, with a detection limit of 20 pg/ml as indicated in the kit manual.

2.15 Statistical Analyses

Data are represented as averages of independent samples ± SEM, with the number of samples per group indicated in each figure or its legend. Statistical significance was inferred when $p < 0.05$. T-tests and Fisher's exact tests were performed using GraphPad Prism software (version 3.02; GraphPad Software, San Diego, CA, USA). Analysis of variance (ANOVA) was performed by Rhea Ferguson using SAS software (version 9.2; SAS Institute Inc., Carry, NC, USA).

For the examination of preneoplastic morphological changes of the MOSE, an ANOVA with Tukey's Studentized Range Test identified differences between placebo and estradiol-treated ovaries at each time point and between time points within the same treatment group.

In the investigation of ovarian structures underlying areas of preneoplastic morphological changes, for each ovarian section, the type of ovarian structure (primordial, primary, secondary, antral, and atretic follicles, stroma, or corpus luteum) underlying each patch of hyperplastic MOSE cells was recorded. The total number of times a particular structure was recorded within a single section was then expressed as a percentage of the total number of ovarian structures recorded for that section. Percentages of each structure for each section were then averaged to obtain the mean incidence (by percentage) that each structure was associated with hyperplastic cells in each ovary. Each

of these averages from ovaries of the same treatment and time point were then averaged to obtain an overall mean for each group. It is these means (± SEM) that are represented in Figures 14-17. The same procedure was followed to obtain the incidence of specific ovarian structures underlying columnar MOSE and invaginations. This data, averaged per ovary, was not analyzed statistically. For statistical analysis, each ovarian section was considered independent and the total number of times each ovarian structure was recorded as underlying an area of hyperplasia was summed. This value was used in a Fisher's exact test to compare the occurrence of a particular ovarian structure in ovaries exposed to placebo versus estradiol. The same test was used for comparisons between placebo and estradiol for each ovarian structure underlying areas of hyperplasia as well as columnar MOSE and invaginations.

The *in vitro* experiment involving infection with adenoviral vectors and treatment with ethanol, FSH, testosterone, or FSH and testosterone combined was performed four and five times independently for MOSE cells and GCs respectively. Each treatment was not included in each independent replicate, but each treatment was performed in at least three independent experiments and appropriate controls for each treatment condition were always performed. Independent RNA extractions and RT reactions were performed following each experiment and each cDNA sample was run in triplicate on real-time PCR plates to determine relative aromatase expression. Because of the large number of samples, each independent experiment was run on a separate plate for real-time PCR; the threshold determining C_T values was set to the same value for all plates and repeat measurements of a particular sample on each plate showed that inter-plate variability was negligible. Mock-infected ethanol-treated cells from the first experiment performed were

chosen to have an RQ value set at 1 and values for aromatase expression in every other sample were compared to this control. The number of experimental samples, each run in triplicate, also required multiple plates to be used for ELISAs measuring media estradiol content and, once again, repeat measurements of a particular sample on each plate showed that inter-assay variability was negligible. Statistical analysis of real-time PCR and ELISA measurements for these *in vitro* experiments consisted of an ANOVA with Tukey's Studentized Range Test used to determine significance between infections within each treatment group and between treatments within each infection type.

GCs isolated from *Brca1*$^{loxP/loxP}$; *Amhr2-Cre* negative and positive mice were put into culture and treated with ethanol, FSH, testosterone, or FSH and testosterone combined three independent times, but estradiol secretion measured by ELISA was only performed on media collected from the first experiment. Each sample was measured in triplicate. An ANOVA with Tukey's Studentized Range Test showed differences between *Cre* negative and *Cre* positive samples within each treatment condition as well as differences induced by treatments.

An unpaired t-test was used to compare RIA measurements of serum estradiol from placebo and 0.05 mg estradiol-treated mice euthanized 60 days after surgery and to compare the number of Ki-67 positive MOSE cells per ovarian section in placebo versus estradiol-treated mice. For Ki-67 analysis, counts from a minimum of three non-consecutive sections per ovary were averaged to give a representative value for each ovary. At least three ovaries per treatment group were analyzed and their average number of Ki-67-positive MOSE cells per section was averaged to give an overall mean (± SEM) for each treatment group.

CHAPTER 3: RESULTS

3.1 Increased estradiol levels contribute to the formation of preneoplastic morphological changes of putatively Brca1-deficient MOSE cells.

3.1.1 Combined loss of Brca1 and treatment with exogenous estradiol promotes preneoplastic morphological changes in MOSE cells over time.

Evidence from the literature strongly suggests that *Brca1* inactivation increases estradiol production; this relationship is only clinically relevant to cancer if increased estradiol promotes preneoplastic lesions and tumourigenesis in Brca1-deficient cells. The effect of increased estradiol on MOSE cells with inactivated *Brca1* was therefore investigated *in vivo*. *Brca1*$^{loxP/loxP}$ mice were injected with AdCre under the bursal membrane with the intention of inactivating *Brca1* in the MOSE and at the same time administered a 60-day slow-release pellet delivering either low (0.05 mg) or high (0.25 mg) dose estradiol or placebo. Mice were euthanized at time points of 60, 180, and 365 days after surgery, at which time ovarian tumourigenesis was assessed and ovaries were examined histologically for the presence of preneoplastic morphological changes of the MOSE.

During necropsy, careful assessment of the abdominal cavity and organs therein did not reveal any abnormalities or signs of disease. Ovaries were fixed in formalin, sectioned, stained in haematoxylin and eosin, and thoroughly examined histologically. Although not quantified, it was consistently noted that ovaries from estradiol-treated mice had more atretic follicles and less CLs compared to placebo controls (**Figure 11**).

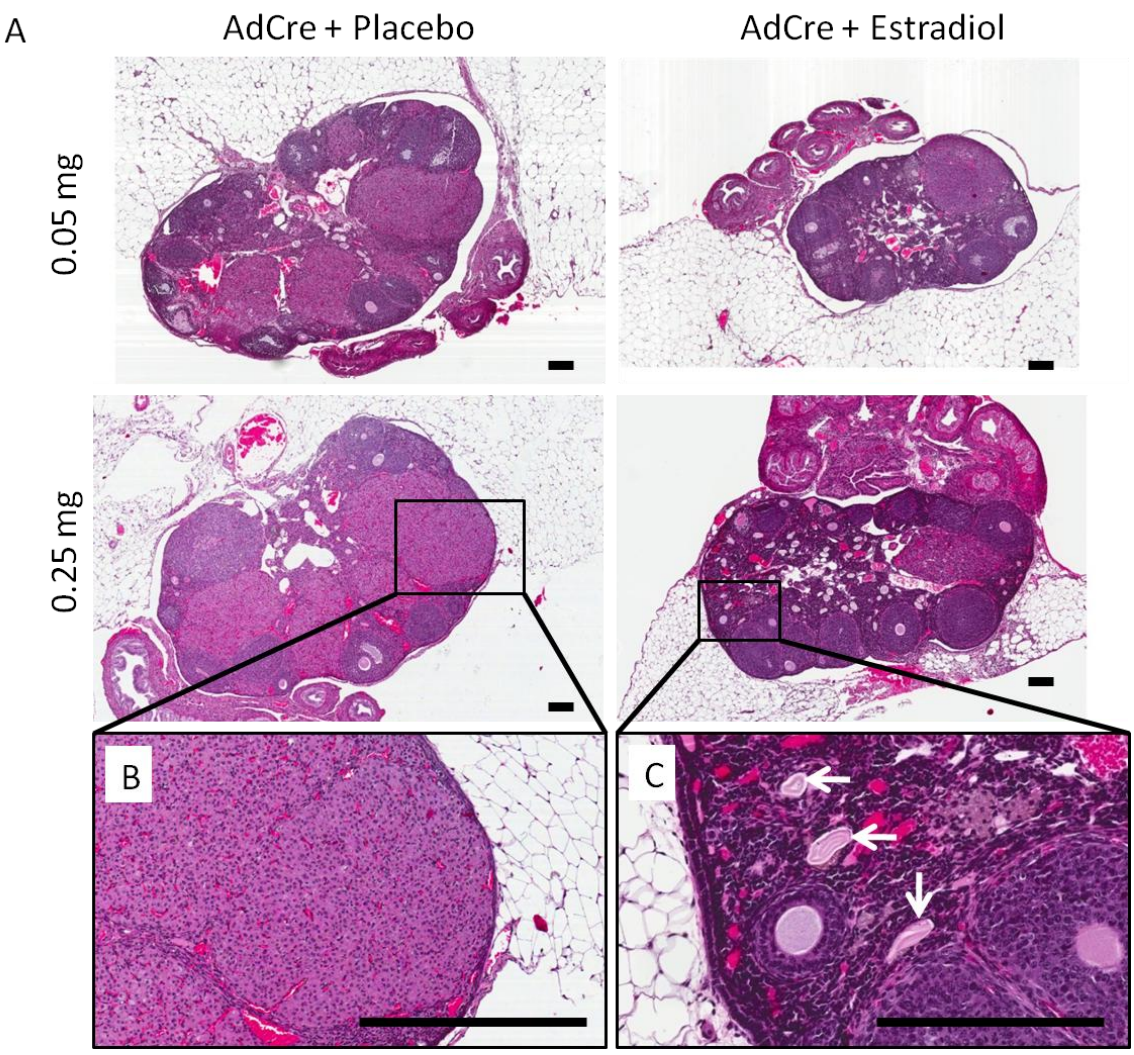

Figure 11. Representative images of ovarian sections from *Brca1*$^{loxP/loxP}$ mice following intrabursal injection of AdCre and implantation of a 60-day slow-release pellet containing 0.05 mg or 0.25 mg estradiol or placebo. (A) Representative ovarian sections from low and high dose estradiol-treated mice (placebo as control) euthanized 60 days after surgery stained with H&E. Exposure to exogenous estradiol tended to reduce the occurrence of corpora lutea (B) and increase the occurrence of atretic follicles (arrows, C). Scale bar, 100 µm.

Quantitative assessment of the prevalence of preneoplastic morphological changes in Brca1-deficient MOSE was performed on ovarian sections from estradiol and placebo-treated mice at each time point. Lesions observed included columnar MOSE, hyperplastic MOSE, and MOSE invaginating into the stroma of the ovary, representative images of which are shown in **Figure 9**.

Although determining the ability of estradiol to promote preneoplastic lesions in the MOSE was the main goal of the *in vivo* studies, documentation of preneoplastic changes in ovaries from placebo-treated mice, presumably due to the loss of Brca1 alone, showed that these lesions accumulate significantly over time. In mice given pellets that serve as placebo to the low estradiol dose, changes in MOSE morphology from flat-to-cuboidal to columnar and hyperplastic occurred within 180 days after surgery, with no further changes occurring between the 180 and 365 day time point. Specifically, 6.7 ± 1.4 % and 5.7 ± 1.0 % of the ovarian surface was columnar and hyperplastic respectively at the 180 day time point and 7.5 ± 1.2 % and 6.3 ± 1.0 % respectively at the 365 day time point compared to 2.3 ± 0.25 % and 2.4 ± 0.40 % respectively at the 60 day time point (60 versus 180 and 60 versus 365: $p < 0.05$ for both columnar and hyperplasia; **Figure 12A, B**). Invaginations accumulated more slowly, with a similar amount found in 60 (1.1 ±0.23) and 180 (0.85 ± 0.21) day time point mice, but a 2.8-fold increase observed between 180 and 365 days ($p < 0.05$; **Figure 12C**).

For mice given pellets that serve as placebo to the high estradiol dose, there were similar age-related increases in the morphological changes seen, but the timing of MOSE undergoing such changes was slightly different. The percent of the ovarian surface exhibiting columnar morphology was fairly consistent at the 60 (2.6 ± 0.60 %) and 180

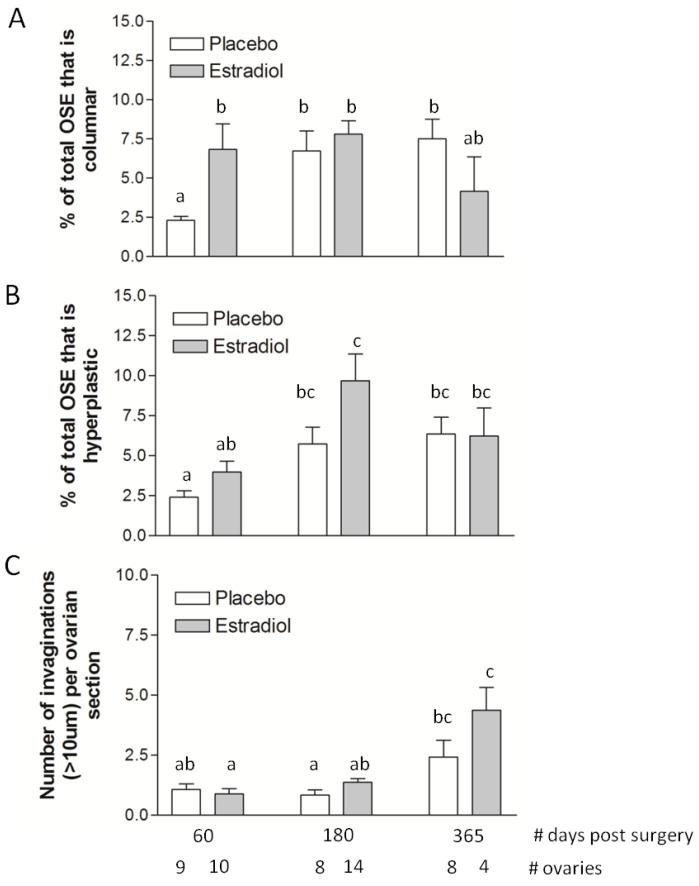

Figure 12. Time and estradiol treatment (0.05 mg) affect the occurrence of preneoplastic morphological changes in putatively Brca1-deficient mouse ovarian surface epithelial cells. Maximal change in ovarian surface epithelial cell morphology from flat-to-cuboidal to columnar and hyperplastic occurs within 180 days after pellet insertion and intrabursal injection of AdCre into *Brca1*$^{loxP/loxP}$ mice (A, B) while invaginations accumulate more slowly, with a significant increase observed between 180 and 365 days after surgery (C, $p < 0.05$, ANOVA). Estradiol-treated mice exhibit a higher percentage of ovarian surface epithelium with columnar morphology at 60 days compared to placebo-treated mice (A, $p < 0.05$, ANOVA). Different letters denote statistically significant differences ($p < 0.05$).

(3.6 ± 0.53 %) day time point, but a 3.4-fold increase occurred between 180 and 365 days ($p < 0.05$; **Figure 13A**). Hyperplastic MOSE and invaginations accumulated with increasing age. At 60 days, only 0.95 ± 0.44 % of the ovarian surface was hyperplastic and that increased 8-fold by 180 days ($p < 0.05$) and 15-fold by 365 days ($p < 0.05$; **Figure 13B**). At 60 days, only 0.25 ± 0.080 invaginations were found per ovarian section; this increased to 3.1 ± 0.55 by 180 days and then a significant increased occurred, resulting in 6.8 ± 1.2 invaginations per ovarian section by 365 days ($p < 0.05$; **Figure 13C**).

The age-related accumulation of preneoplastic lesions also occurred in Brca1-deficient MOSE cells treated with 0.05 mg estradiol. For hyperplastic MOSE, maximal occurrence was observed at the 180 day time point, with 9.7 ± 1.7 % of the ovarian surface exhibiting this morphological change. This was significantly higher than the 4.0 ± 0.7 % of hyperplastic ovarian surface observed at 60 days ($p < 0.05$). A significant difference in hyperplastic MOSE did not occur between 180 and 365 days, although there was a trend for a decrease (9.7 ± 1.7 % versus 6.2 ± 1.7 % respectively; **Figure 12B**). For invaginations, the number per ovarian section remained fairly steady between the 60 (0.90 ± 0.22) and 180 (1.4 ± 0.15) day time points, but then increased 4.5-fold between 180 and 365 days ($p < 0.05$; **Figure 12C**). The accumulation of columnar MOSE showed no significant changes over time, but with a trend towards a decrease between 180 (7.8 ± 0.85 %) and 365 days (4.2 ± 2.2 %; **Figure 12A**).

In putatively Brca1-deficient MOSE exposed to the high dose of estradiol, the time course of the age-related changes in accumulation of columnar cells was similar to placebo-treated mice. The percent of the ovarian surface exhibiting columnar

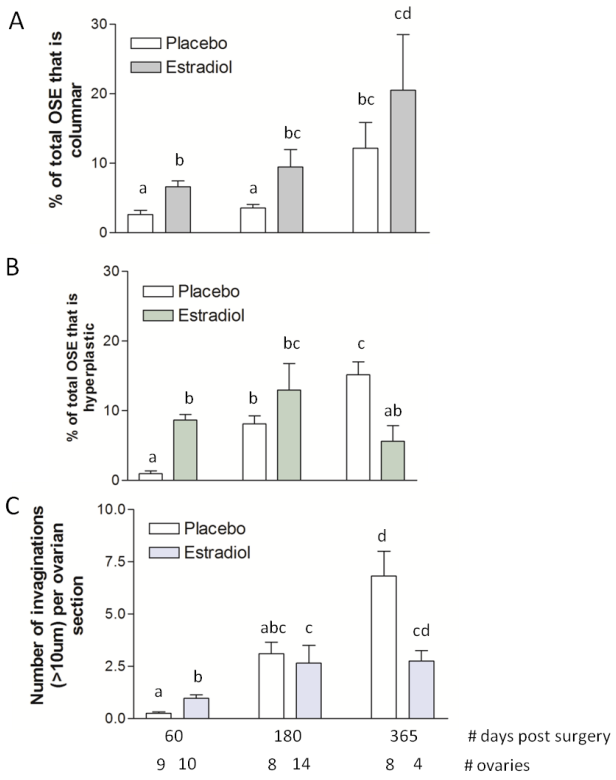

Figure 13. Time and estradiol treatment (0.25 mg) affect the occurrence of preneoplastic morphological changes in putatively Brca1-deficient mouse ovarian surface epithelial cells. Columnar and hyperplastic ovarian surface epithelial cells and number of invaginations per ovarian section in placebo-treated ovaries as well as columnar cells in estradiol-treated ovaries accumulate over time after pellet insertion and intrabursal injection of AdCre into *Brca1*$^{loxP/loxP}$ mice (A-C, $p < 0.05$, ANOVA). The incidence of hyperplasia does not change significantly over time in estradiol-treated ovaries (B) while the maximal number of invaginations occurs by 180 days after surgery (C, $p < 0.05$, ANOVA). Estradiol treatment increases columnar and hyperplastic morphology as well as the number of invaginations 60 days after surgery (A-C, $p < 0.05$) and decreases the percentage of hyperplastic ovarian surface epithelium at 365 days (B, $p < 0.05$, ANOVA). Different letters denote statistically significant differences ($p < 0.05$).

morphology did not change significantly between 60 (6.6 ± 0.87 %) and 180 days (9.5 ± 2.5%), but had increased 3-fold by 365 days ($p < 0.05$; **Figure 13A**). Estradiol-treated mice developed hyperplastic MOSE and invaginations at different rates than their placebo-treated counterparts. The incidence of hyperplasia did not change significantly over time, although there was a trend towards a decrease between 180 (13.0 ± 3.8 %) and 365 days (5.6 ± 2.3 %; **Figure 13B**). The maximal number of invaginations observed per ovarian section occurred by 180 days, which was 2.7-fold more than had been observed at 60 days ($p < 0.05$) but was not significantly different than 365 days (**Figure 13C**). These results indicate an age-related increase in the accumulation of columnar and hyperplastic cells and invaginations in Brca1-deficient MOSE in both the presence and absence of exogenous estradiol.

3.1.2 Exogenous estradiol can promote ovarian preneoplastic morphological changes in the MOSE *in vivo*.

The effect of estradiol on putatively Brca1-deficient MOSE was variable depending on the preneoplastic lesion examined, estradiol dose, and length of time after surgery. Compared to placebo-treated control mice, mice treated with 0.05 mg estradiol developed 3-fold more MOSE exhibiting columnar morphology by 60 days after surgery ($p < 0.05$; **Figure 12A**). By 180 and 365 days after surgery, estradiol was no longer significantly promoting MOSE cells to become columnar in shape. Interestingly, columnar morphology had the largest estradiol-induced change at 60 days and a trend for estradiol protecting against this lesion was observed at 365 days (7.5 ± 1.2 % placebo versus 4.2 ± 2.2 % E2; **Figure 12A**). The occurrence of flat-to-cuboidal MOSE cells

becoming hyperplastic and MOSE cells invaginating into the ovarian stroma was not significantly affected by low dose estradiol at any time point, although there was a trend for more hyperplastic MOSE in estradiol-treated mice at 60 (2.4 ± 0.40 % placebo versus 4.0 ± 0.67 % E2, **Figure 12B**) and 180 days (5.7 ± 1.0 % placebo verses 9.7 ± 1.7 % E2; **Figure 12B**) and more invaginations in estradiol-treated mice at 365 days (2.4 ± 0.70 placebo versus 4.4 ± 0.94 E2; **Figure 12C**).

High-dose estradiol significantly increased the occurrence of all three preneoplastic lesions of MOSE cells quantified 60 days after surgery (**Figure 13**). Compared to placebo treatment, 0.25 mg estradiol treatment resulted in a 2.5- and 9.2-fold increase in the proportion of MOSE exhibiting columnar ($p < 0.05$; **Figure 13A**) and hyperplastic morphology respectively ($p < 0.05$; **Figure 13B**)) as well as a 3.9-fold increase in the number of invaginations ($p < 0.05$; **Figure 13C**) 60 days after surgery. As was observed with columnar MOSE with low dose estradiol, the ability of high-dose estradiol to significantly promote hyperplasia and invaginations at the 60 time point was countered by a decrease at the 365 day time point (hyperplasia: 15.2 ± 1.9 % placebo versus 5.6 ± 2.3 % E2, $p < 0.05$; invaginations: 6.8 ± 1.2 placebo versus 2.8 ± 0.51 E2, trend; **Figure 13B, C**). MOSE cells becoming columnar was affected by high dose estradiol at later time points, with an increase of 2.6-fold observed at 180 days ($p < 0.05$) and of 1.64-fold observed at 365 days (trend; **Figure 13A**). The effect of high dose estradiol on columnar MOSE morphology was the only significant increase caused by estradiol observed past the 60 day time point. Overall, these results indicate that continuous estradiol treatment for 60 days can have significant effects on promoting putatively Brca1-deficicient MOSE to undergo preneoplastic morphological changes in a

dose-dependent manner and that its action on the ovaries can affect MOSE morphology long after the estradiol treatment has ceased.

3.1.3 Preneoplastic morphological changes occur most frequently near ovarian stroma.

To investigate if the incidence of preneoplastic morphological changes of MOSE cells was associated with a particular underlying ovarian structure, the occurrence of these structures was identified in the same histological sections. Recording ovarian structures underlying MOSE exhibiting preneoplastic morphological changes showed that columnar and hyperplastic MOSE cells as well as invaginations occurred more frequently near ovarian stroma as compared to primordial, primary, secondary, antral, or atretic follicles or CLs. This association with stroma was evident in both placebo and estradiol-treated mice (both low and high dose) at all time points examined (**Figures 14-17**). Normal MOSE also occurred more commonly near ovarian stroma than any other ovarian structure (**Figure 16**), suggesting that no particular structure within the ovary or factors secreted by them promotes the formation of preneoplastic lesions in putatively Brca1-deficient MOSE.

The occurrence of each ovarian structure underlying areas of preneoplastic morphological changes was compared in ovaries exposed to placebo versus estradiol to determine if treatment with estradiol or potential estradiol-induced changes in ovarian structures affected the occurrence of preneoplastic morphological changes near ovarian structures of any type. There were no differences due to estradiol treatment in the occurrence of stroma or primordial, primary, secondary, or antral follicles underlying any

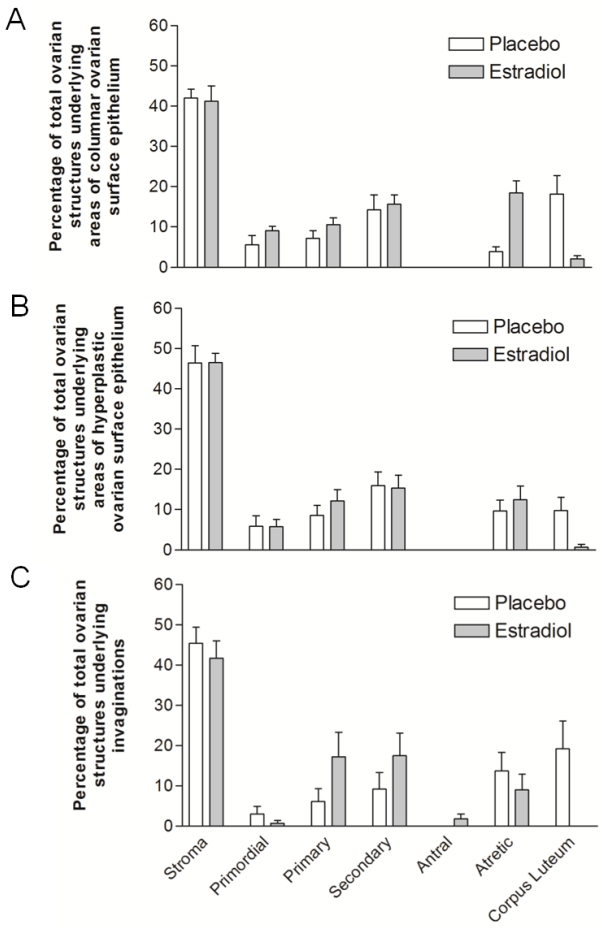

Figure 14. Preneoplastic morphological changes occur most frequently near ovarian stroma in ovaries from *Brca1*$^{loxP/loxP}$ mice treated with AdCre and given an estradiol (0.05 mg) or placebo pellet euthanized 60 days after surgery. (A) Areas of columnar ovarian surface epithelial cells, (B) areas of hyperplasia, and (C) epithelial invaginations are most commonly associated with ovarian stroma in ovarian sections from both placebo (n=8) and 0.05 mg estradiol (n=10) treated *Brca1*$^{loxP/loxP}$ mice 60 days after surgery. A decreased association of columnar and hyperplastic ovarian surface epithelium and invaginations with corpora lutea and an increased association of columnar ovarian surface epithelium with atretic follicles is found in estradiol versus placebo-treated mice (A-C, $p < 0.01$, Fisher's exact test).

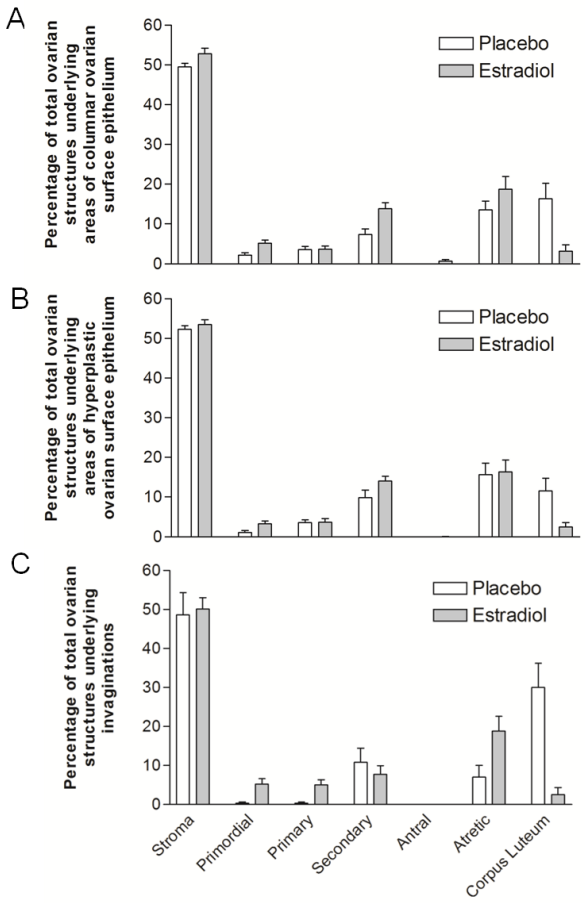

Figure 15. Preneoplastic morphological changes occur most frequently near ovarian stroma in ovaries from *Brca1*$^{loxP/loxP}$ mice treated with AdCre and given an estradiol (0.05 mg) or placebo pellet euthanized 180 days after surgery. (A) Areas of columnar ovarian surface epithelial cells, (B) areas of hyperplasia, and (C) epithelial invaginations are most commonly associated with ovarian stroma in ovarian sections from both placebo (n=8) and 0.05 mg estradiol (n=14) treated *Brca1*$^{loxP/loxP}$ mice 180 days after surgery. A decreased association of columnar and hyperplastic ovarian surface epithelium and invaginations with corpora lutea and an increased association of columnar ovarian surface epithelium and invaginations with atretic follicles is found in estradiol versus placebo-treated mice (A-C, $p < 0.0016$, Fisher's exact test).

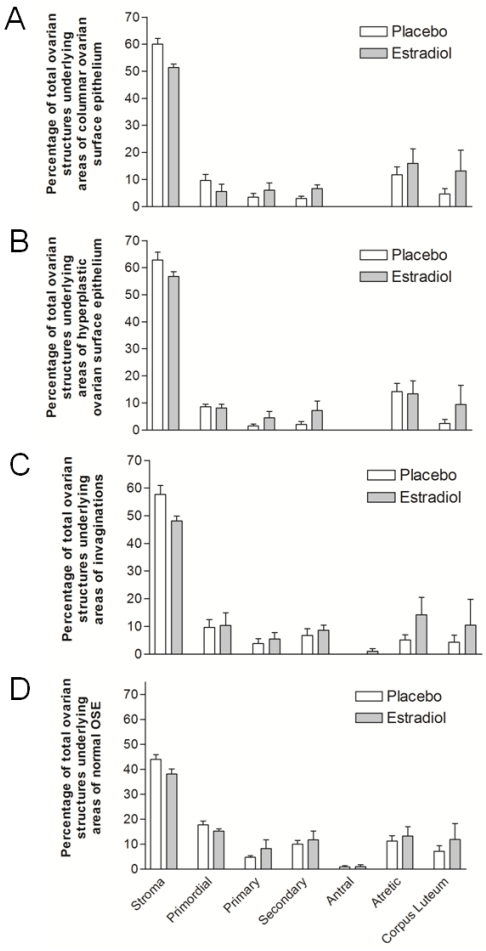

Figure 16. Preneoplastic morphological changes occur most frequently near ovarian stroma in ovaries from *Brca1*$^{loxP/loxP}$ mice treated with AdCre and given an estradiol (0.05 mg) or placebo pellet euthanized 365 days after surgery. (A) Areas of columnar ovarian surface epithelial cells, (B) areas of hyperplasia, (C) epithelial invaginations, and (D) normal ovarian surface epithelial cells are most commonly associated with ovarian stroma in ovarian sections from both placebo (n=8) and 0.05 mg estradiol (n=4) treated *Brca1*$^{loxP/loxP}$ mice 365 days after surgery. An increased association of columnar ovarian surface epithelium with atretic follicles is found in estradiol versus placebo-treated mice (A, $p = 0.028$, Fisher's exact test).

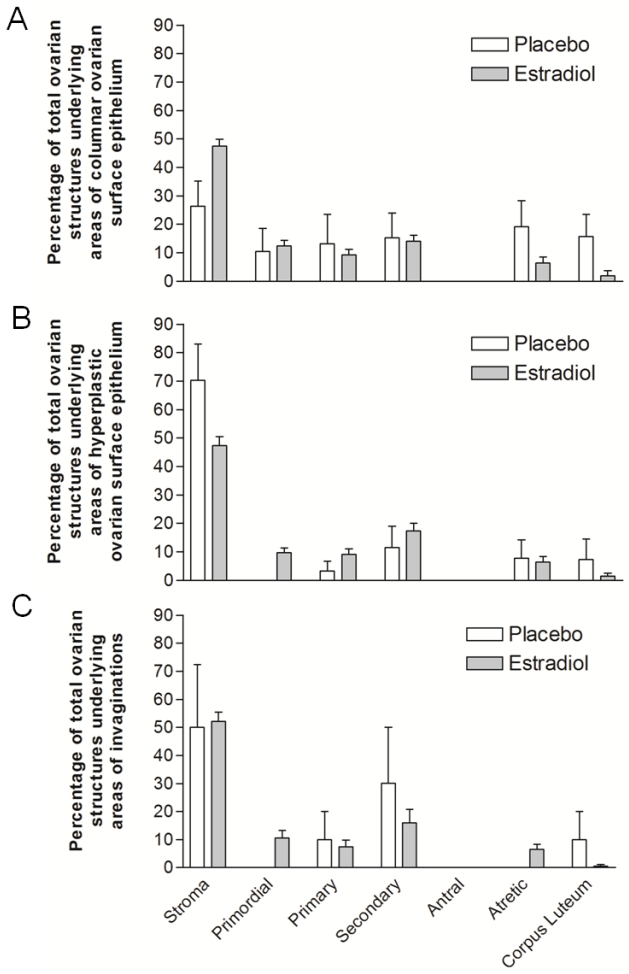

Figure 17. Preneoplastic morphological changes occur most frequently near ovarian stroma in ovaries from *Brca1*$^{loxP/loxP}$ mice treated with AdCre and given an estradiol (0.25 mg) or placebo pellet euthanized 60 days after surgery. (A) Areas of columnar ovarian surface epithelium, (B) areas of hyperplasia, and (C) epithelial invaginations are most commonly associated with ovarian stroma in ovarian sections from both placebo (n=6) and 0.25 mg estradiol (n=15) treated *Brca1*$^{loxP/loxP}$ mice 60 days after surgery. A decreased association of columnar and hyperplastic ovarian surface epithelium ($p < 0.019$) and invaginations (trend) with corpora lutea is found in estradiol versus placebo-treated mice (A-C, Fisher's exact test).

preneoplastic lesion or normal MOSE at any time point investigated (**Figure 14-17**). Estradiol-treated mice did exhibit fewer preneoplastic changes of all types near CLs than their placebo-treated counterparts. Low dose estradiol treatment at 60 days caused an 8.0-, 3.4-, and 7-fold decrease in the association of columnar MOSE ($p < 0.0001$), hyperplastic MOSE ($p = 0.001$), and invaginations ($p = 0.0002$) respectively with CLs (**Figure 14**). A similar decrease in association with CLs was observed at 180 days for regions of columnar cells (4-fold, $p < 0.0001$), hyperplasia (2.8-fold, $p < 0.0001$) and the incidence of invaginations (3.1-fold, $p < 0.0001$; **Figure 15**). High dose estradiol also reduced association between MOSE preneoplastic morphological changes and CLs, with a 4.5- ($p = 0.010$), 6.7- ($p = 0.019$), and 5.7-fold (trend) decrease observed for columnar cells, hyperplasia, and invaginations respectively at 60 days (**Figure 17**). A significant decline in frequency of CLs underlying areas of columnar and hyperplastic MOSE cells as well as invaginations and MOSE cells with normal morphology in estradiol versus placebo-treated mice was not observed at the 365 day time point (**Figure 16)**. Estradiol-treated mice also often exhibited more preneoplastic changes near atretic follicles than their placebo-treated counterparts, especially columnar MOSE cells. Significant increases were observed in low dose estradiol-treated mice euthanized at 60 (columnar: 5.9 % placebo versus 21.5 % E2, $p < 0.0001$; **Figure 14**), 180 (columnar: 15.0 % placebo versus 20.6 % estradiol, $p = 0.0012$; invaginations: 8.8 % placebo versus 20.9 % estradiol, $p = 0.0016$; **Figure 15**), and 365 days (columnar: 12.7 % placebo versus 18.4 % estradiol, $p = 0.028$; **Figure 16**). The pattern of increased frequency of associations with atretic follicles and decreased frequency of associations with CLs as underlying preneoplastic lesions in estradiol-treated mice is likely due to atretic follicles being more

common and CLs being less common in ovaries from estradiol-treated mice rather than a consequence of factors secreted from these structures.

3.1.4 Exogenous estradiol does not promote the proliferation of putatively Brca1-deficient MOSE *in vivo*.

The proliferation of AdCre-exposed MOSE cells with or without estradiol treatment was investigated by performing immunohistochemistry for Ki-67 expression on ovaries from mice treated with either low or high dose estradiol (placebo as control) for 60 days. A mouse ovarian tumour served as a positive control and consistently showed strong Ki-67 expression. Negative controls (primary antibody omitted) showed no staining, therefore excluding the possibility of staining in experimental samples being due to non-specific background (**Figure 18A, B**). The number of Ki-67-positive MOSE cells found in each ovarian section ranged from zero to seven and ovaries exposed to exogenous estradiol did not contain more Ki-67-positive MOSE cells compared to their placebo-treated counterparts. There was a trend for an increased number of MOSE cells positive for Ki-67 expression in 0.05 mg estradiol treated ovaries (2.7 ± 1.6) compared to control (1.8 ± 0.30), but very similar numbers observed for placebo and 0.25 mg estradiol treatments (1.7 ± 0.62 versus 1.4 ± 0.43 respectively; **Figure 19**). These findings suggest that estradiol-induced increases in the occurrence of preneoplastic morphological changes in putativelyBrca1-deficient MOSE are not due to increased proliferation. Additionally, Ki-67-positive MOSE cells were most commonly flat-to-cuboidal in shape, with very few positively staining cells found in MOSE exhibiting columnar or hyperplastic morphology (**Figure 18C, D)**. Ki-67-positive OSE cells were most commonly associated with stroma

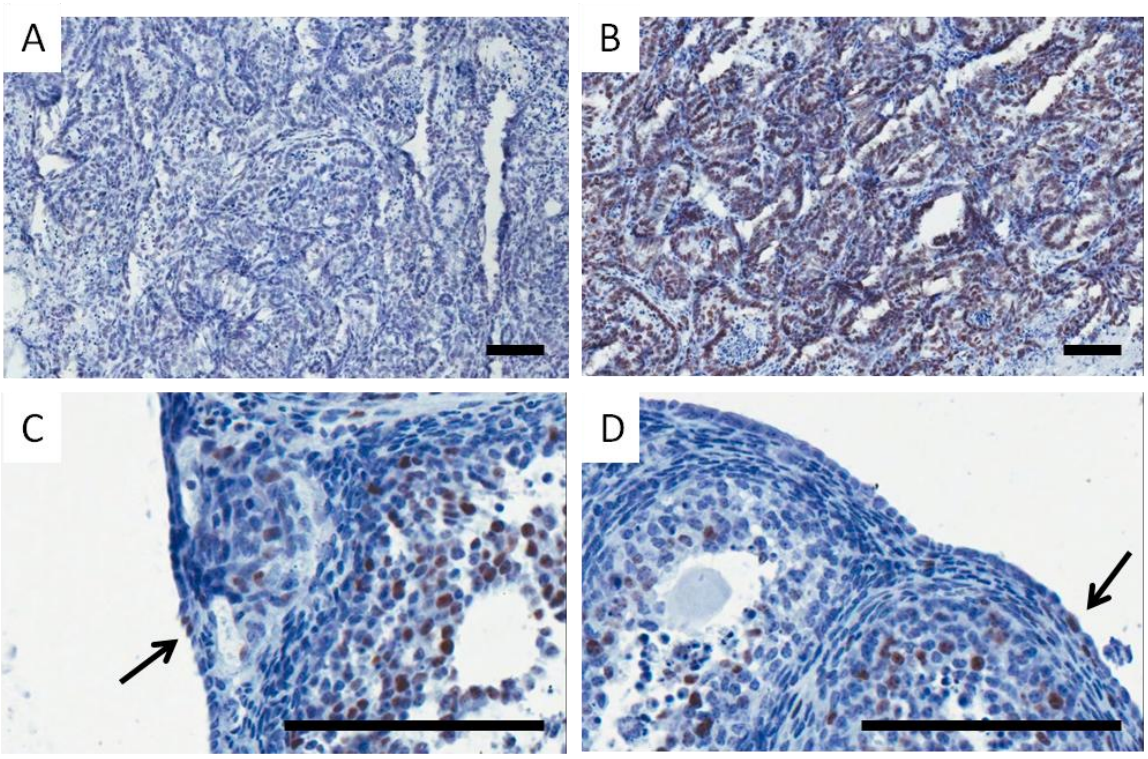

Figure 18. Representative images of immunohistochemical detection of Ki-67 expression within ovaries from *Brca1*$^{loxP/loxP}$ mice treated with AdCre and given an estradiol or placebo pellet. A mouse ovarian tumour section shows (A) no staining as a negative control (no primary antibody) and (B) strong staining as a positive control. An ovarian section from a placebo-treated (C) and an estradiol-treated (D) *Brca1*$^{loxP/loxP}$ mouse euthanized at 60 days after AdCre injection and pellet insertion shows Ki-67-positive ovarian surface epithelial cells (indicated by arrow) are scarce and most commonly flat-to-cuboidal in shape. Scale bar, 100 μm.

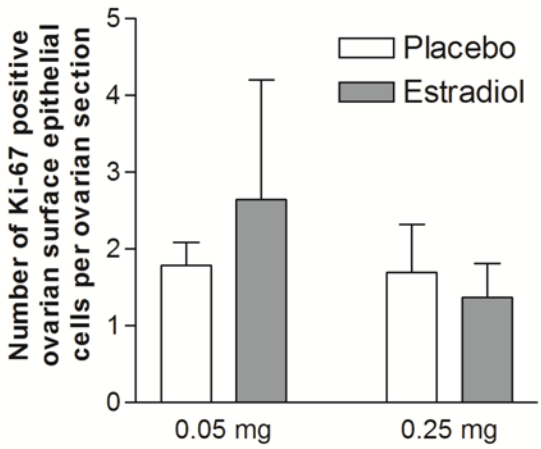

Figure 19. Exogenous estradiol does not promote the proliferation of putatively Brca1-deficient mouse ovarian surface epithelial cells *in vivo*. The proliferation of Brca1-deficient ovarian surface epithelial cells was assessed by immunohistochemical staining for Ki-67 in ovaries from 0.05 mg and 0.25 mg placebo (n = 3) and estradiol (n = 3 and 4 respectively)-treated mice euthanized 60 days after surgery. Ki-67-positive ovarian surface epithelial cells per ovarian section in three to five sections of each ovary were counted. Ovaries exposed to exogenous estradiol did not contain significantly more Ki-67-positive ovarian surface epithelial cells compared to those exposed to placebo ($p > 0.05$, t-test).

and large secondary follicles in both placebo and estradiol-treated mice as well as with corpus luteum in placebo but not estradiol-treated mice.

3.1.5 Exogenous estradiol does not affect the expression of E-cadherin in putatively Brca1-deficient MOSE *in vivo*.

E-cadherin expression in MOSE was examined as evidence for preneoplasia in AdCre-infected and therefore presumably Brca1-deficient OSE of mice treated with low and high dose estradiol (placebo as control). Although morphologically normal MOSE cells express E-cadherin, it was suspected that abnormal areas of MOSE may exhibit altered expression based on the published finding that E-cadherin is not expressed in morphologically normal human OSE, but is found in areas of preneoplastic changes and ovarian tumours (Maines-Bandiera and Auersperg, 1997; Sundfeldt et al., 1997). In other normal epithelia, loss of E-cadherin expression is a common occurrence during the early stages of transformation (Birchmeier and Behrens, 1994; Wijnhoven et al., 2000). Ovarian sections examined also contained oviduct or uterine horn, which served as internal positive controls. E-cadherin expression was consistently strong in the epithelial cells of these tissues, forming dark brown borders between cells (**Figure 20D**). Omitting the primary antibody served as negative controls; non-specific background staining was observed in CLs and fluid within the ovary, but epithelia cells including MOSE showed no staining (**Figure 20A, C, E**). Although not quantified, it was clear that E-cadherin was generally strongly expressed in flat-to-cuboidal and columnar MOSE (**Figure 20F**). E-cadherin expression in MOSE cells exhibiting hyperplastic morphology or invaginating into the stroma of the ovary was similar to or less than expression in MOSE with normal

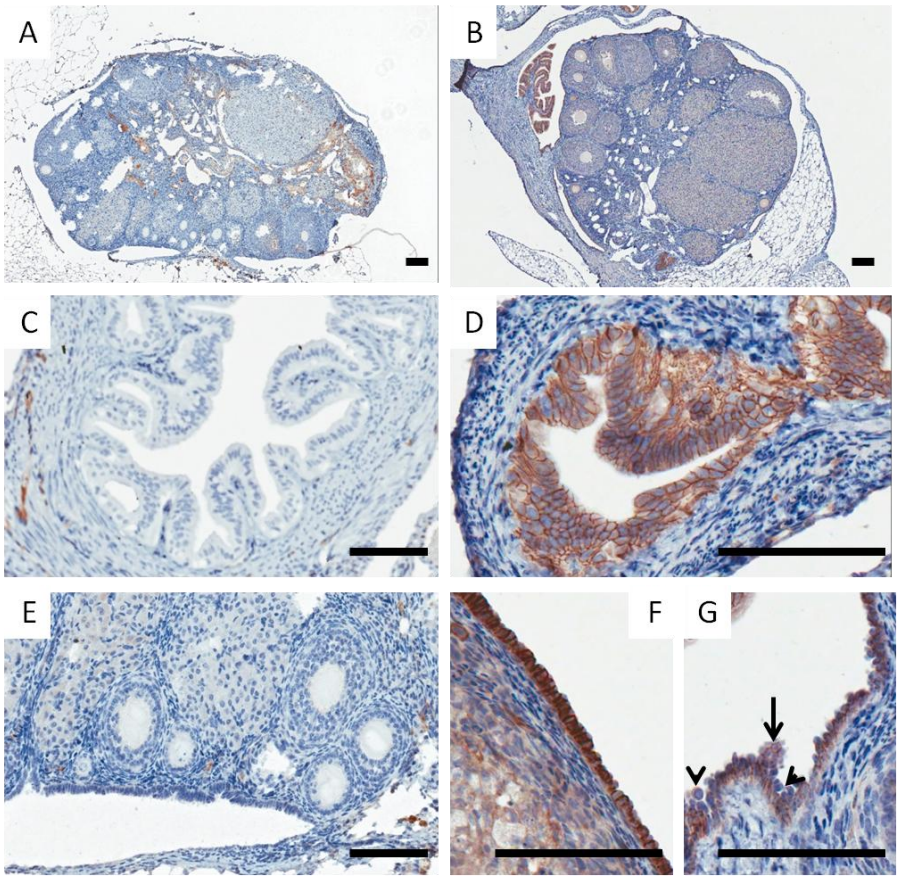

Figure 20. Representative images of immunohistochemical detection of E-cadherin expression within ovaries from *Brca1*$^{loxP/loxP}$ mice treated with AdCre and given an estradiol or placebo pellet. Mouse ovarian sections incubated without (A) and with (B) primary antibody specific to E-cadherin show non-specific staining within the stroma in open spaces and slight brown haze within corpus luteal cells. Oviductal epithelial cells (positive control) exhibit no staining without (C) and strong staining with (D) primary antibody. Mouse ovarian surface epithelial cells exhibit no staining without primary antibody (E). Mouse ovarian surface epithelial cells express variable levels of E-cadherin. Flat-to-cuboidal and columnar ovarian surface epithelial cells are strongly positive (F). Hyperplastic ovarian surface epithelial cells can maintain (arrow) or lose (arrowhead) their E-cadherin expression (G). Scale bar, 100 μm.

morphology (**Figure 20G**). No differences in E-cadherin expression were observed between different time points or between estradiol and placebo-treated mice. Although E-cadherin expression was sometimes lost in areas of hyperplasia, it was not a consistent marker of preneoplastic morphological changes in MOSE.

3.1.6 Exogenous estradiol does not cause ovarian tumourigenesis in mice with putatively Brca1-deficient MOSE.

Numerous studies have shown that loss of BRCA1 function increases aromatase expression and therefore presumably estradiol synthesis (Ghosh et al., 2007; Hu et al., 2005; Lu et al., 2006), however whether or not elevated estradiol causes tumourigenesis in BRCA1-deficient cells is unknown. The effect of increased estradiol on MOSE cells with inactivated *Brca1* was therefore investigated *in vivo*. It was found that the doses of estradiol administered in this study did not cause tumourigenesis in AdCre-exposed OSE of *Brca1*$^{loxP/loxP}$ mice, as none of the mice developed tumours over the course of one year. Several discoveries made after the conclusion of these *in vivo* experiments provide information pertinent to this lack of transformation.

Circulating estradiol levels were measured in serum samples collected from mice that received a 0.05 mg estradiol pellet or its placebo control using RIA. No significant difference was found between serum estradiol levels of placebo (12.0 ± 3.2 pg/ml) versus estradiol (14.8 ± 1.3 pg/ml)-treated mice euthanized 60 days after surgery ($p = 0.41$; **Figure 21**). Since the pellets are designed to release estradiol for 60 days, measurements for 180 and 365 day time points were assumed to be equivalent or lower. The serum

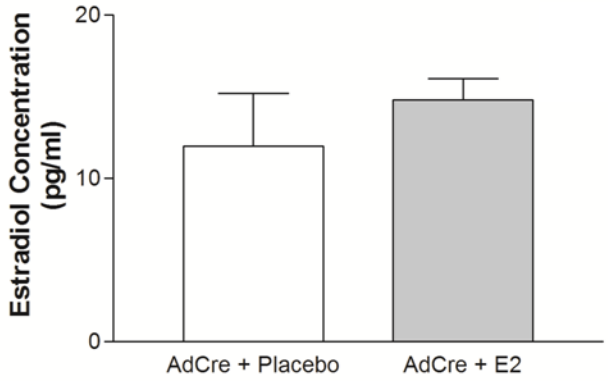

Figure 21. Basal serum levels of estradiol were not increased by a slow-release 0.05 mg estradiol pellet in *Brca1*$^{loxP/loxP}$ mice 60 days after pellet insertion. Estradiol treatment (0.05mg) (n=5) does not significantly increase estradiol levels in the serum of *Brca1*$^{loxP/loxP}$ mice 60 days after pellet insertion compared to placebo-treated mice (n=4), as measured with radioimmunoassay ($p = 0.41$, t-test).

estradiol measurements proved the insufficiency of the 0.05 mg estradiol pellet to significantly increase serum estradiol above basal levels, which may explain the lack of estradiol-induced tumourigenesis in the ovaries of the mice. However, with a significant increase in MOSE with columnar morphology observed at the 60 day time point (**Figure 12A**) and differences in the occurrence of atretic follicles and CLs (**Figure 11**), it is clear that low-dose estradiol treatment did have some physiological effects. Serum estradiol measurements were not taken for mice given the 0.25 mg dose of estradiol because this dose of estradiol has been used by other lab members, with RIA measurements showing 25-fold increases in serum estradiol detected 60 days after estradiol pellet insertion (Laviolette et al., 2010). Furthermore, although the 0.25 mg dose has been tolerated by other strains of mice, in this study many mice treated with this dose experienced abdominal distension caused by enlarged bladders by 60 days. Similar complications have been reported in estradiol-treated animals in previous studies (Elson et al., 2000; Shai et al., 2008). The required euthanization of many high dose estradiol mice in this study was unfortunate, but does indicate an increase in serum estradiol. Based on previous serum estradiol measurements for the 0.25 mg pellet and the bladder complications experienced by the mice, the high dose estradiol mice appear to have experienced increased circulating estradiol but the level did not cause tumourigenesis.

Although the bladder complications observed in mice that received high dose estradiol indicate increased levels of estradiol, they also resulted in unforeseen required mouse euthanizations and therefore reduced the number of mice in later time points dramatically, limiting the ability to interpret results and generate solid conclusions. Out of fifteen 0.25 mg estradiol-treated mice, seven experienced severe bladder complications

that resulted in a loss-of-wellness requiring euthanization long before intended time points (six required euthanization near 60 days post-surgery and one near 180 days post-surgery and were therefore included in the appropriate time point group). Additionally, three mice died overnight or were euthanized by animal care staff and therefore their ovaries could not be collected for further examination, leaving only five mice euthanized at their planned time point. Although none of the 0.25 mg estradiol-treated mice developed ovarian tumours, with only three surviving past 180 days, the possibility of cancer progression occurring in estrogen-treated Brca1-deficient mice as they continue to age cannot be excluded.

Another factor contributing to the lack of tumourigenesis observed in these *in vivo* studies is that the vast majority of MOSE cells contained fully functional Brca1 despite exposure to AdCre. MOSE cells from paraffin embedded ovarian sections were isolated using LCM and their genomic DNA was extracted to enable detection of recombination at *Brca1* loxP sites by PCR. A band for unrecombined but not recombined *Brca1* was found in three independent MOSE isolations, suggesting inactivation of *Brca1* did not occur or occurred at a very low level. The intensity of the band for intact *Brca1* increased with the number of ovarian section used for MOSE isolation, with the brightest band seen from MOSE cells collected from 100 sections from pooled ovaries of the same time point and treatment, less bright bands seen from about 60 sections, and no band detected when only 32 sections were used (**Figure 22**). Although not every ovary analyzed for preneoplastic morphological changes was subsequently tested for *Brca1* recombination within the MOSE, the ovaries examined are considered representative. Undetectable

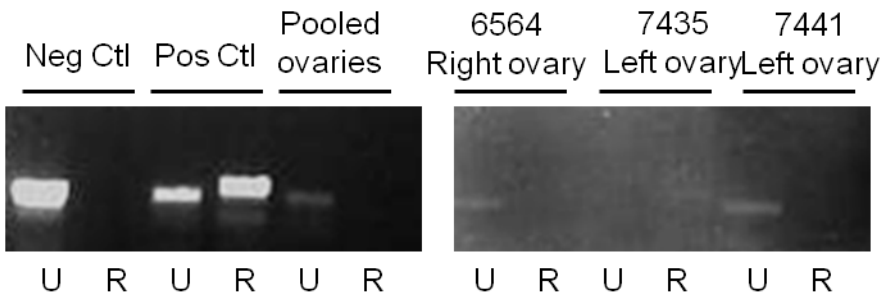

Figure 22. Assessment of recombination at *Brca1* loxP sites in ovarian surface epithelial cells from *Brca1*$^{loxP/loxP}$ mice following intrabursal adenoviral Cre recombinase infection. Laser capture microdissection was used to isolate ovarian surface epithelial cells from paraffin embedded ovaries from mice that underwent surgery for AdCre infection under the bursal membrane and placebo or estradiol pellet insertion. Samples include genomic DNA isolated from the mouse ovarian surface epithelial cells from 100 ovarian sections from pooled ovaries, from 57 ovarian sections from the right ovary of mouse 6564, from 32 ovarian sections from the left ovary of mouse 7435, and from 58 ovarian sections from the left ovary of mouse 7441. Negative and positive control samples are ovarian surface epithelial cells from *Brca1*$^{loxP/loxP}$ mice infected *in vitro* with mock and AdCre respectively and previously confirmed to show unrecombined and recombined *Brca1* as expected. PCR to detect recombination at *Brca1* loxP sites shows no recombined *Brca1* is detectable in any sample despite exposure to AdCre *in vivo* (R = recombined *Brca1*, intron 4 forward and intron 13 reverse, 600 bp; U = unrecombined *Brca1*, intron 4 forward and intron 4 reverse, 461 bp).

levels of recombined *Brca1* after *in vivo* infection of MOSE with AdCre may help to explain a lack of progression to neoplasia.

3.2 The loss of functional Brca1 does not significantly increase aromatase expression in or estradiol production from MOSE and primary GCs *in vitro.*

3.2.1 *In vitro* infection of MOSE and primary GCs with AdCre results in *Brca1* recombination.

BRCA1 repression of aromatase transcription has been reported in a human granulosa cell line (Hu et al., 2005), primary human breast adipose fibroblast, mature adipocyte, and human breast cancer cell lines (Ghosh et al., 2007; Lu et al., 2006), but not in primary GCs or MOSE cells. In the current study, *Brca1* inactivation in these cell types was accomplished by isolating the cells from *Brca1*$^{loxP/loxP}$ mice and infecting them with adenovirus expressing Cre recombinase (mock infection and AdGFP as control) *in vitro*. Both MOSE cells and primary GCs were successfully infected with adenoviral vectors, as confirmed by PCR for recombination at *Brca1* loxP sites. Genomic DNA extracted 72 hours after mock, AdGFP, and AdCre infection was subject to the same PCR conditions, with recombined *Brca1* only observed in cells exposed to Cre recombinase. Intact *Brca1* was always detected in all infection types, but consistently in less than 50% of AdCre-infected cells (**Figure 23**).

3.2.2 Aromatase expression is not affected by the inactivation of *Brca1* in MOSE cells and primary GCs.

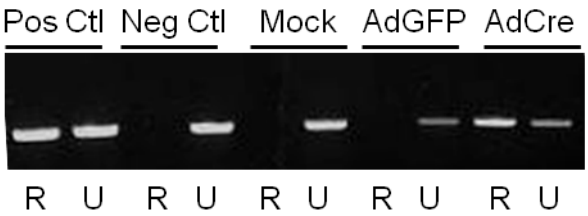

Figure 23. Assessment of recombination at *Brca1* loxP sites following adenoviral Cre recombinase infection *in vitro*. Representative PCR of genomic DNA extracted from cultured *Brca1*$^{loxP/loxP}$ mouse ovarian surface epithelial cells 72 hours after *in vitro* mock infection or infection with AdGFP or AdCre shows *Brca1* recombination is only detectable with exposure to AdCre (R = recombined *Brca1*, intron 4 forward and intron 13 reverse, 600 bp; U = unrecombined *Brca1*, intron 11 forward and intron 11 reverse, 592 bp).

With a consistent method for inactivating *Brca1* confirmed, effects of Brca1 loss on aromatase expression were evaluated. It was discovered that cultured MOSE do not express a detectable level of aromatase as measured with real-time PCR, regardless of treatment or *Brca1* status. In contrast, both freshly isolated and cultured GCs reliably express aromatase. Aromatase levels are strongly affected by time in culture, with levels about 40 times lower after six days in culture. Aromatase expression is not significantly induced in cultured GCs by FSH or testosterone treatment alone, although a trend toward increased expression is observed with exposure to testosterone. Expression does increase with FSH and testosterone treatment in combination in mock, AdGFP, and AdCre-infected cells compared to either ethanol (15.6-, 20.7-, and 6-fold respectively, $p < 0.05$), FSH (46.8-, 22-, and 10.6-fold respectively, $p < 0.05$), or testosterone treatment alone (3.7-, 3.4-, and 1.8-fold respectively, $p < 0.05$; **Figure 24A**). No significant difference in aromatase expression exists between mock, AdGFP, and AdCre-infected GCs within the same treatment condition, suggesting that the loss of functional Brca1 does not affect aromatase mRNA levels in primary GCs (**Figure 24A**).

3.2.3 Estradiol production is not affected by the inactivation of *Brca1* in MOSE cells and primary GCs.

Despite undetectable aromatase levels measured with real-time PCR, cultured MOSE cells do synthesize and secrete estradiol, although measured levels are 3.4-fold and 10-fold lower than unstimulated and FSH + testosterone-treated mock-infected GCs respectively. In both cell types and regardless of *Brca1* status, FSH treatment alone did not increase basal estradiol levels in the media (**Figure 24B, C)**.

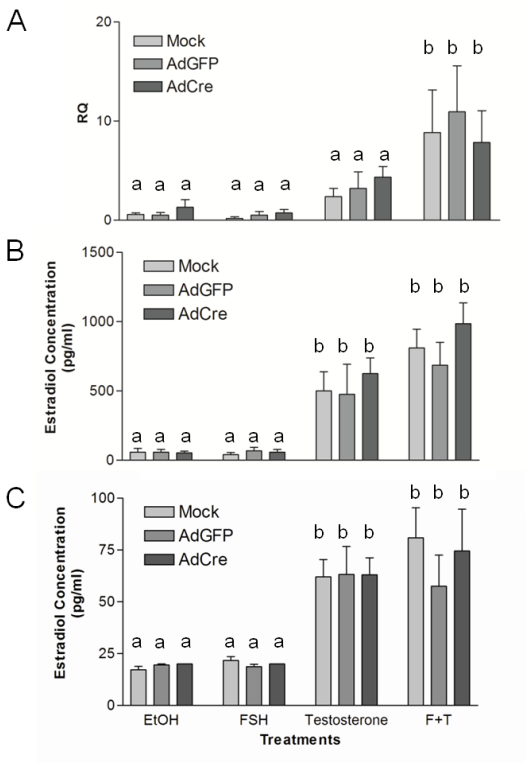

Figure 24. Cre-mediated inactivation of *Brca1 in vitro* does not increase aromatase expression in or estradiol production by primary granulosa cells or ovarian epithelial cells. Combined follicle stimulating hormone (FSH) and testosterone (F+T) treatment increases aromatase expression (A) and estradiol secretion (B, C) above basal, and FSH-stimulated levels in mock, AdGFP, and AdCre-infected primary granulosa cells (A, B) and ovarian epithelial cells (C) from *Brca1*$^{loxP/loxP}$ mice as well as aromatase expression above testosterone-stimulated levels in primary granulosa cells (A, $p < 0.05$, ANOVA). Granulosa cells (A, B) and ovarian surface epithelial cells (C) from *Brca1*$^{loxP/loxP}$ mice infected with AdCre to inactivate *Brca1* do not show Brca1-associated changes in aromatase expression, as measured with real-time PCR (A), or estradiol production as measured with ELISA (B,C), compared with mock or AdGFP infected cells (ANOVA, n = 3-5). Different letters denote statistically significant differences ($p < 0.05$).

Although combined treatment with FSH and testosterone did not significantly increase estradiol production from MOSE cells or GCs compared to testosterone treatment alone, both of these treatments did significantly increase estradiol secretion above basal and FSH-stimulated levels in all infection types (**Figure 24B, C)**. In MOSE cells, testosterone alone increased media estradiol levels by at least 2.8-fold compared to ethanol or FSH treatment ($p < 0.05$; **Figure 24C**). The effect of F+T treatment was similar, eliciting a 2.9- to 4.7-fold increase compared to ethanol or FSH treatment ($p < 0.05$; **Figure 24C**). In GCs, testosterone treatment alone increased media estradiol levels 8.5-fold ($p < 0.05$) in mock-infected cells, 8-fold ($p < 0.05$) in AdGFP-infected cells, and 11.5-fold ($p < 0.01$) in AdCre-infected cells compared to control levels. Testosterone treatment also increased estradiol production by GCs above FSH-stimulated levels in all infection types (mock: 12.3-fold, AdGFP: 6.9-fold, AdCre: 10.6-fold, $p < 0.05$; **Figure 24B**). The addition of FSH to testosterone treatment also significantly increase estradiol secretion above basal (mock: 13.8-fold, AdGFP; 11.6-fold, AdCre: 18.1-fold, $p < 0.05$) and FSH-stimulated levels (mock: 20-fold, AdGFP: 9.9-fold, AdCre: 16.7-fold, $p < 0.05$) regardless of Brca1 status (**Figure 24B**).

The inactivation of *Brca1* by AdCre infection did not significantly increase estradiol production under any treatment condition in either cell type studied, although there is a trend for increased estradiol secretion in AdCre -infected GCs (986.4 ±150.8 pg/ml) compared to mock (810.9 ± 136.1 pg/ml) or AdGFP (685.6 ± 165.5 pg/ml)-infected cells after combined treatment with FSH and testosterone (**Figure 24B, C**).

3.2.4 ERα expression is not affected by the inactivation of *Brca1* in MOSE cells and primary GCs.

Since Brca1 has been shown to be associated with ERα expression in breast tumours (Foulkes et al., 2004; Roldan et al., 2006) and cell lines (Hosey et al., 2007), the ability of Brca1 to influence ERα expression in mouse GCs and OSE cells was investigated, using mouse ovary as a positive control. Basal mRNA transcript levels of ERα, with mock infection and EtOH treatment, were almost two-fold higher in MOSE than GCs (0.20 ± 0.066 RQ versus 0.11 ± 0.060 RQ respectively) and were not affected by exposure to AdGFP or AdCre in either cell type (**Figure 25A, B**).

Cells in culture for a longer of period of time without functional Brca1 also exhibited no change in ERα expression. Although a trend for a decrease in AdCre-infected MOSE versus mock or AdGFP-infected MOSE was observed in cells analyzed two months after infection (0.083 RQ versus 0.18 RQ or 0.13 RQ respectively), this pattern was not sustained at later time points (**Figure 25C**). Only one independent replicate was completed for these extended time point experiments. Constant ERα expression despite mock, AdGFP, and AdCre-infection suggests the loss of functional Brca1 has no effect on ERα expression in either MOSE or primary GCs.

3.3 The consequence of Brca1 loss in both GC and MOSE cells *in vivo* simultaneously could not be evaluated because the mouse model was not successfully generated.

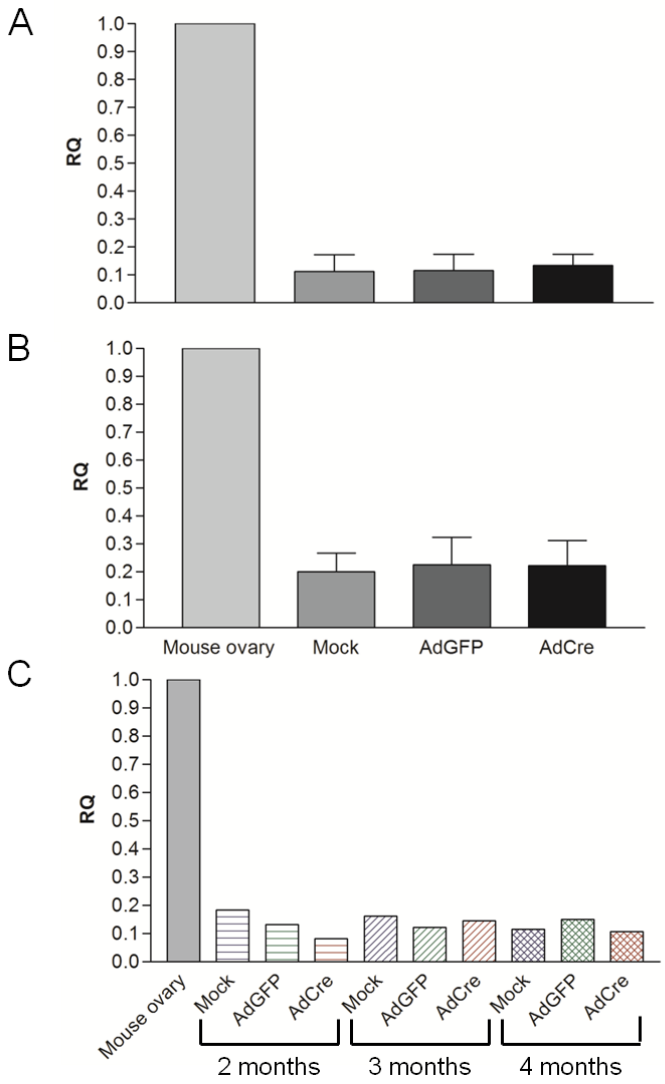

Figure 25. Cre-mediated inactivation of *Brca1 in vitro* does not affect estrogen receptor α expression in primary granulosa cells or mouse ovarian surface epithelial cells. Estrogen receptor α mRNA expression remained the same in (A) primary granulosa cells and (B, C) ovarian surface epithelial cells from *Brca1*$^{loxP/loxP}$ mice infected with AdCre to inactivate *Brca1* or AdGFP and mock infection as controls. Cells were collected either five days (A, B, n = 2 and 3 respectively) or 2, 3, or 4 months after infection (C, n = 1 for each time point).

3.3.1 Cre-mediated inactivation of *Brca1 in vivo* does not increase estradiol production from primary GCs *in vitro*.

In parallel with the *in vitro* experiments described in section 3.2, the effect of simultaneous inactivation of *Brca1* in GC and MOSE *in vivo* was investigated. *Brca1*$^{loxP/loxP}$ and *Amhr2*$^{Cre/Cre}$ mice were mated through several generations to generate *Brca1*$^{loxP/loxP}$*; Amhr2-Cre* animals that were "*Cre* negative" (*Amhr2*$^{+/+}$, not carrying the Cre transgene) or "Cre positive" (*Amhr2*$^{Cre/+}$ or *Amhr2*$^{Cre/Cre}$, heterozygous or homozygous for the Cre transgene respectively) (**Figure 6**). Mice were examined for the effects of simultaneous loss of Brca1 in MOSE and GCs on ovarian tumourigenesis. With the observation that the loss of Brca1 from *Brca1*$^{loxP/loxP}$ GCs *in vitro* by exposure to AdCre had no effect on aromatase expression or activity, it was suspected that the six days in culture for these experiments was too long, perhaps allowing GCs to spontaneously luteinize and therefore the full effects of treatments and *Brca1* status were not being captured. To address this potential problem, similar *in vitro* experiments were undertaken with GCs isolated from *Brca1*$^{loxP/loxP}$*; Amhr2-Cre* positive and negative mice. Since the exposure of GCs to Cre recombinase *in vivo* eliminated the need to infect GCs *in vitro* with adenoviral vectors, primary GCs only needed to be in culture for three days.

The first isolation of GCs from *Brca1*$^{loxP/loxP}$*; Amhr2-Cre* negative and positive mice revealed a very low level of recombined *Brca1* in Cre positive cells as detected by PCR (**Figure 26A**). Assaying estradiol in the media in which these cells were grown showed little induction of estradiol secretion with ethanol, FSH, and testosterone treatment. However, combined treatment with FSH and testosterone increased estradiol production by over 20-fold ($p < 0.05$) compared to ethanol or FSH treatment alone and by

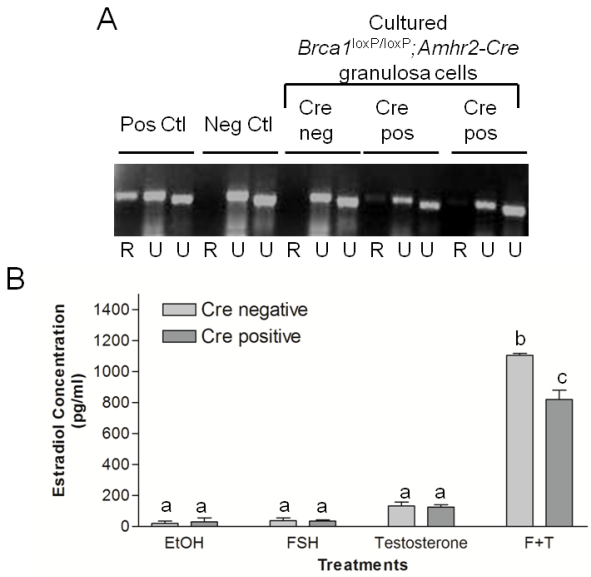

Figure 26. Cre-mediated inactivation of *Brca1 in vivo* does not increase estradiol production from primary granulosa cells *in vitro*. (A) PCR of genomic DNA extracted from the first isolation of granulosa cells from *Brca1*$^{loxP/loxP}$*; Amhr2-Cre* positive and negative mice shows only unrecombined *Brca1* in cells from *Cre* negative mice and slight *Brca1* recombination in cells from *Cre* positive mice (R = recombined *Brca1*, intron 4 forward and intron 13 reverse, 600 bp; U = unrecombined *Brca1*, two separate sets of primers: intron 11 forward and intron 11 reverse, 592 bp and intron 4 forward and intron 4 reverse, 461 bp). (B) Estradiol levels from the media of primary *Amhr2-Cre* positive and negative granulosa cells, as measured with ELISA, shows combined treatment with follicle stimulating hormone and testosterone (F+T) increases estradiol secretion above basal and individual treatment levels ($p < 0.05$, ANOVA) and the slight inactivation of *Brca1* in *Cre*-positive granulosa cells lowers media estradiol compared to granulosa cells with intact *Brca1* after treatment with F+T ($p < 0.05$, ANOVA, $n = 1$). Different letters denote statistically significant differences ($p < 0.05$).

over 6-fold ($p < 0.05$) compared to testosterone treatment alone in GCs that either did or did not express the *Cre* transgene. The slight inactivation of *Brca1* was sufficient to significantly lower the media estradiol level compared to GCs with fully intact *Brca1* after treatment with FSH and testosterone ($p < 0.05$, **Figure 26B**), however these results are based on triplicate measurements from a single experiment and therefore must be interpreted cautiously.

3.3.2 The presence of *Cre* in the genomic DNA does not cause inactivation of *Brca1* in GCs or MOSE cells or tissues of the female reproductive tract.

GCs were isolated from *Brca1*$^{loxP/loxP}$*; Amhr2-Cre* negative and positive mice four independent times and put into primary culture three of those times, but estradiol production was only measured from the first isolation because in subsequent isolations neither freshly isolated nor cultured GCs showed any amount of recombined *Brca1* detectable by PCR, despite consistently finding *Cre* in the genomic DNA of mice previously genotyped as *Cre*-positive (**Figure 27A**). Expected bands for positive and negative controls were identified and unrecombined *Brca1* in all GC samples validated the PCR method, but recombined *Brca1* remained undetectable (**Figure 26A, Figure 27A**). Recombined *Brca1* was also never observed in three independent isolations of MOSE from *Brca1*$^{loxP/loxP}$*; Amhr2-Cre* negative and positive mice (**Figure 27B**). The presence of only intact *Brca1* suggested that there would be no differences between experimental and control cells.

Tissues from the female reproductive tract had previously been collected and frozen from *Brca1*$^{loxP/loxP}$*; Amhr2-Cre* negative and positive mice euthanized at 60, 120,

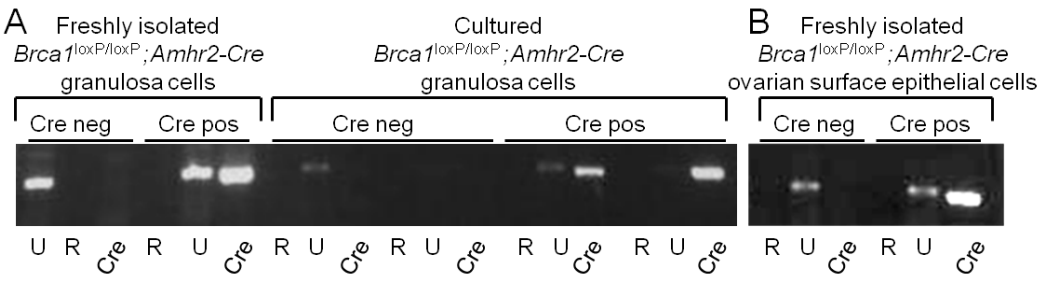

Figure 27. The presence of the *Cre* transgene in the genomic DNA does not cause inactivation of *Brca1* in granulosa cells or ovarian surface epithelial cells *in vivo*. PCR of genomic DNA extracted from freshly isolated mouse ovarian surface epithelial cells and granulosa cells (A, B) and cultured granulosa cells (A) from *Brca1*$^{loxP/loxP}$*; Amhr2-Cre* mice shows a strong band for unrecombined *Brca1* and no band for recombined *Brca1* in cells from both *Cre* negative and positive mice (R = recombined *Brca1*, intron 4 forward and intron 13 reverse, 600 bp; U = unrecombined *Brca1*, intron 4 forward and 4 reverse, 461 bp). Genotyping for *Amhr2-Cre* was performed concomitantly with the PCR for *Brca1* recombination and confirmed previously performed genotyping, with a band for *Cre* observed only in samples from *Amhr2-Cre* positive mice.

and 180 days of age. These samples presented the opportunity to check if *Brca1* recombination had ever occurred in *Amhr2-Cre* positive mice. Genomic DNA from ovaries, oviducts, and uterine horns of *Brca1*$^{loxP/loxP}$*; Amhr2-Cre* negative and positive mice at each age revealed *Brca1*recombination did not occur to an extent detectable by PCR in any tissue sample from any age. These results further indicate *Brca1* remained unrecombined and therefore presumably functional despite the presence of the *Cre* gene (**Figure 28**).

3.3.3 Repeated genotyping of a subset of *Brca1*$^{loxP/loxP}$*; Amhr2-Cre* mice confirmed previously determined *Brca1* and *Cre* status.

With the finding of intact *Brca1* in *Amhr2-Cre* positive mice indicating no difference between control and experimental mice and therefore potentially rendering the newly generated mouse model useless, the genotype of a subset of mice was reassessed. To confirm mice as *Cre* negative or positive, *Cre* genotyping of selected mice was repeated. In addition to re-analyzing genomic DNA extracted from ear punches in the PCR for genotyping *Cre*, genomic DNA from freshly isolated MOSE and GCs and cultured GCs was also analyzed. In all cases, the previously determined *Cre* status of each mouse or sample was confirmed as negative or positive (**Figure 7, Figure 27**). Additionally, a second set of primers for determining the presence of the *Amhr2-Cre* gene were used on a few DNA samples from *Brca1*$^{loxP/loxP}$*; Amhr2-Cre* mice, with cultured *Brca1*$^{loxP/loxP}$ GCs included as a negative control. PCR results with the new primers further re-confirmed whether mice were or were not carrying the *Cre* transgene (**Figure 7**) and ensured that the *Cre* primers used throughout the generation of the mouse model

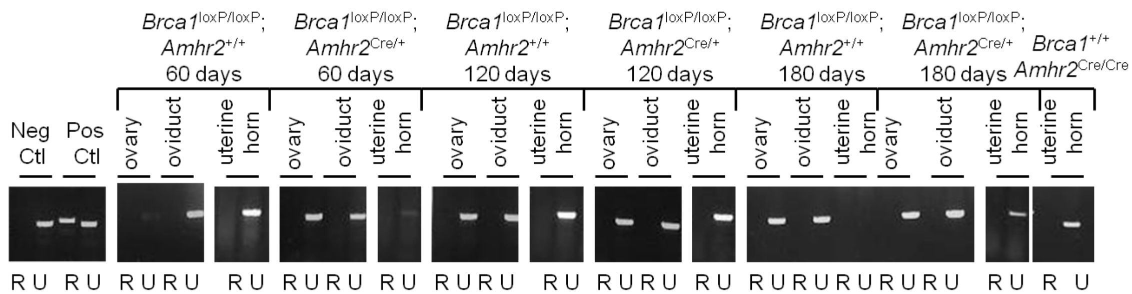

Figure 28. The presence of the *Cre* transgene in the genomic DNA does not cause inactivation of *Brca1* in tissues of the female reproductive tract *in vivo*. PCR of genomic DNA from tissues from *Brca1*$^{loxP/loxP}$*; Amhr2-Cre* negative and positive mice at 60, 120, and 180 days of age shows no *Brca1* recombination (R = recombined *Brca1*, intron 4 forward and intron 13 reverse, 600 bp; U = unrecombined *Brca1*, intron 4 forward and 4 reverse, 461 bp). The last two lanes are the results from PCR of genomic DNA from uterine horn tissue from a *Brca1*$^{+/+}$*; Amhr2-Cre* positive mouse, showing no *Brca1* recombination and unrecombined wild-type *Brca1* (391 bp).

were showing correct results.

Brca1 genotyping of a subset of *Brca1*$^{loxP/loxP}$*; Amhr2-Cre* mice was repeated to ensure all mice were indeed homozygous for floxed *Brca1*, as wildtype *Brca1* alleles would explain why the presence of the Cre gene was not causing *Brca1* to be recombined. Rather than re-testing genomic DNA extracted from ear punches of *Brca1*$^{loxP/loxP}$*; Amhr2-Cre* mice that had previously been determined, *Brca1* genotyping was performed on freshly isolated MOSE and GCs and cultured GCs from recent isolations. All samples analyzed were found to be homozygous for floxed *Brca1* (**Figure 29**). These results indicate that *Brca1* recombination was not occurring despite the presence of the *Cre* gene and loxP sites in the *Brca1* gene.

3.3.4 *Brca1*$^{loxP/loxP}$*; Amhr2-Cre* positive mice do not express detectable levels of Cre recombinase.

One possible explanation for the presence of the *Cre* gene in the genomic DNA without any effect on floxed *Brca1* is a lack of Cre recombinase expression. Using real-time PCR, strong Cre expression was found in *Brcal*$^{loxP/loxP}$ GCs that had been infected with AdCre *in vitro*. However, no Cre expression was detected in cells or tissues from *Brca1*$^{loxP/loxP}$*; Amhr2-Cre* negative or positive mice, including freshly isolated and cultured GCs and ovary, oviductal, and uterine horn tissue from mice euthanized at 60, 120, and 180 days of age. Additionally, *Amhr2*$^{Cre/Cre}$ mice from which generation of the *Brca1*$^{loxP/loxP}$*; Amhr2-Cre* mice originated were not found to express Cre. Tissues examined included freshly isolated GCs, oviductal, and uterine horn tissue from three week old mice and ovary, oviductal, uterine horn, and lung tissue from three month old

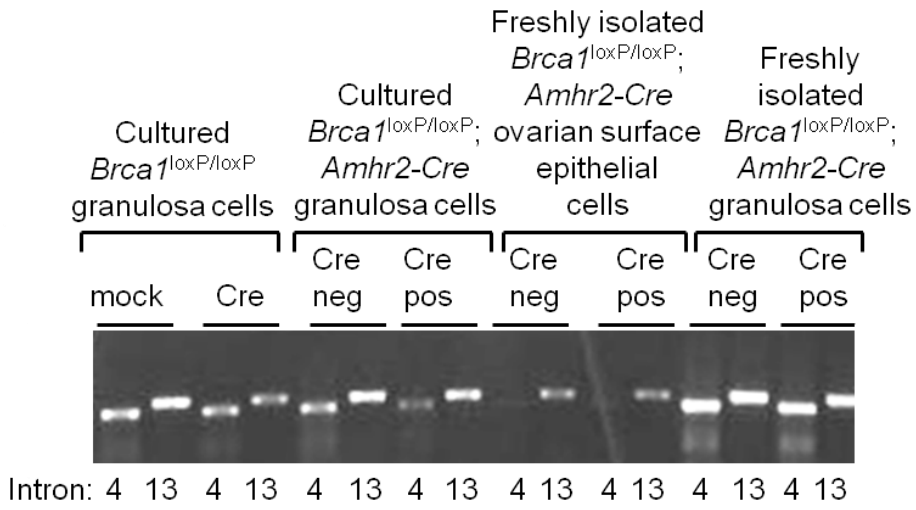

Figure 29. Repeated *Brca1* genotyping of a subset of *Brca1*$^{loxP/loxP}$*; Amhr2-Cre* mice confirmed all mice were indeed homozygous for floxed *Brca1*. PCR of genomic DNA from cultured *Brca1*$^{loxP/loxP}$ granulosa cells, cultured and freshly isolated *Brca1*$^{loxP/loxP}$*; Amhr2-Cre* granulosa cells, and freshly isolated *Brca1*$^{loxP/loxP}$*; Amhr2-Cre* mouse ovarian surface epithelial cells shows floxed *Brca1* alleles in both intron 4 (461 bp) and 13 (562 bp).

mice.

The *Amhr2*$^{Cre/Cre}$ mouse has been used in our lab previously in a cross with *SNF2L*$^{loxP/loxP}$ mice to cause recombination and inactivation of the *SNF2L* gene in tissues which express Amhr2. Recombination of the gene of interest was observed in the ovary as well as in non-target tissue, such as brain, kidney, spleen, and lung (**Figure 30**). With the same line of *Amhr2*$^{Cre/Cre}$ mice used in the current study for crosses with *Brca1*$^{loxP/loxP}$ mice, it is not known why Cre expression was not detectable is any tested tissues from *Brca1*$^{loxP/loxP}$ *Cre*-positive mice or the *Amhr2*$^{Cre/Cre}$ parental strain. However, the lack of Cre recombinase expression in mice containing the *Amhr2-Cre* gene does explain *Brca1* remaining unrecombined in *Cre* positive mice.

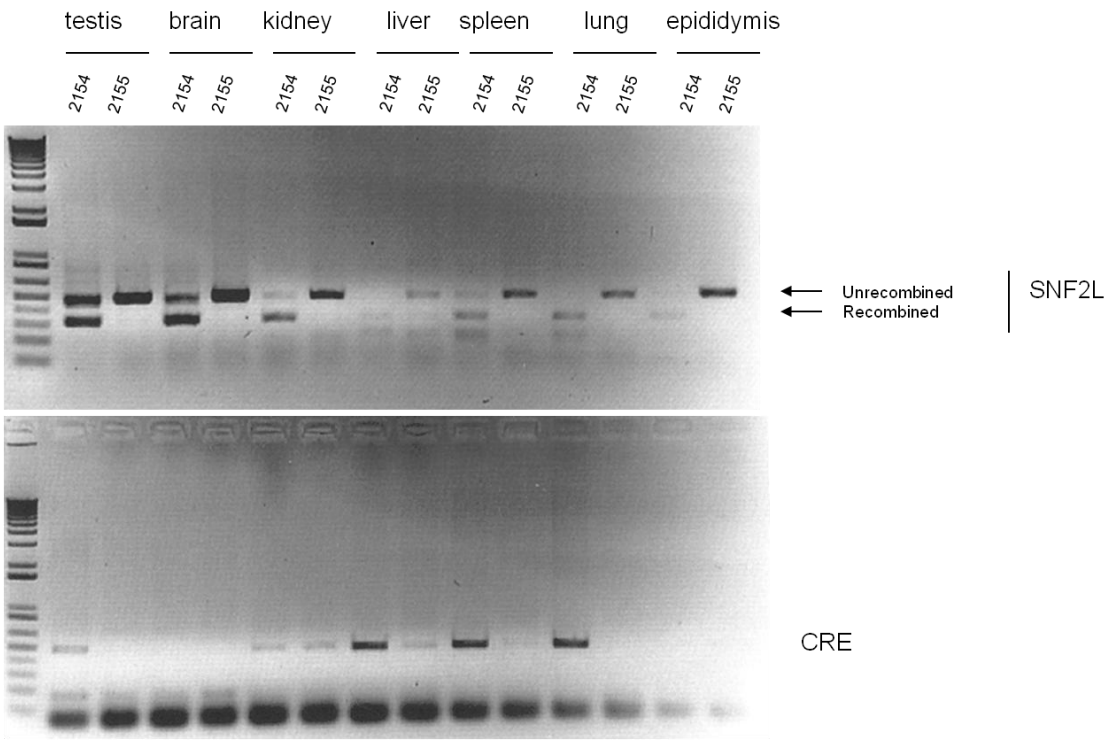

Figure 30. Cre-mediated *SNF2L* recombination in *SNF2L*$^{loxP/loxP}$; *Amhr2*$^{Cre/Cre}$ mice. Homozygous floxed *SNF2L Cre*-positive mice expressing Cre recombinase driven by the Amhr2 promoter in tissues outside of the female reproductive tract show recombination of *SNF2L* at the RNA level (Figure provided by David Pépin).

CHAPTER 5: DISCUSSION

Evidence from the literature strongly supports the hypothesis that loss of BRCA1 leads to increased aromatase expression and activity (Ghosh et al., 2007; Hu et al., 2005; Lu et al., 2006) as well as the ability of estradiol to promote preneoplastic changes and benign tumours of the ovary (Gotfredson and Murdoch, 2007; Laviolette et al., 2010; Silva et al., 1998). The possibility that increased estradiol synthesis induced by BRCA1 loss is sufficient to induce such changes in OSE has not been investigated, nor has the possibility that estradiol stimulation of BRCA1-deficient OSE would not only promote benign abnormalities, but also neoplastic changes through the combination of accumulating DNA damage and promotion of proliferation. The goal of the current study was to address these gaps in our knowledge using physiologically relevant models.

The purpose of the first objective of the study was to determine if high level estradiol acting on *Brca1*-deficient MOSE *in vivo* was capable of promoting preneoplastic changes and tumourigenesis. The interpretation of results from these *in vivo* studies, wherein $Brca1^{loxP/loxP}$ mice were injected with AdCre under the bursal membrane and concurrently administered a pellet delivering estradiol or placebo, is greatly limited by the inability to detect recombined *Brca1* in genomic DNA from LCM-isolated MOSE from ovaries of mice in this study. This finding suggests that any results observed were due to estradiol or placebo treatment of Brca1-intact rather than Brca1-deficient MOSE.

An explanation for the detection of only intact, fully functional Brca1 in MOSE exposed to AdCre via intrabursal injection is not evident. Injection of adenovirus under the bursal membrane to infect MOSE is a technique routinely used in our lab and surgeries for the current study were performed by two lab members, one of which was

highly experienced in intrabursal injection of adenoviruses, reducing the possibility of technical errors that may have prevented exposure of *Brca1*$^{loxP/loxP}$ MOSE to AdCre. The virus is also known to be active, as the same stocks used during surgeries of the *Brca1*$^{loxP/loxP}$ mice were and continue to be used to infect cells from *Brca1*$^{loxP/loxP}$ mice *in vitro*, with successful recombination observed. Intrabursal injection of AdCre yielding expected recombination was previously documented in two published models from our lab. AdCre injection under the bursa successfully induced ovarian tumours by activating the expression of simian virus 40 large and small T antigens (SV70 TAg) (Laviolette et al., 2010) and resulted in *Brca1* recombination within the same strain of *Brca1*$^{loxP/loxP}$ mice used in the current study (Clark-Knowles et al., 2007). It is possible that cells in which Brca1was inactivated by Cre recombinase stopped dividing or underwent apoptosis, as the loss of *Brca1* has previously been reported to decrease OSE cell proliferation due to increased apoptosis in cells with intact checkpoints (Clark-Knowles et al., 2007; Reedy et al., 2001), although this does not explain why successful recombination was observed by Clark-Knowles *et al.* (2007) and not in the current study,

Although it is possible that recombined, non-functional Brca1 is present in an undetectable minority of MOSE cells, observed results are most likely due to effects of time and exogenous estradiol on Brca1-competent cells. The accumulation of putative preneoplastic morphological changes, observed as a greater amount of the ovarian surface containing columnar and hyperplastic MOSE rather than flat-to-cuboidal MOSE as well as an increased number of invaginations, did occur over time in both placebo and estradiol-treated mice. This is consistent with previous findings showing that such preneoplastic morphological changes of OSE cells occur more frequently with age and

greater number of ovulations (Clark-Knowles et al., 2007; Clow et al., 2002; Nieto et al., 2001). The timing over which significant accumulation of preneoplastic morphological changes occurs is variable, as different patterns were observed in each treatment group, including between the two groups of placebo-treated mice from separate experiments. Patterns observed included gradual significant accumulation of morphological changes with age, significant accumulation within 60 or 180 days after surgery with no further increase occurring at later time points, and no significant accumulation until between 180 and 365 days after surgery. This variability demonstrates the uniqueness of each mouse during *in vivo* experiments and also potentially variable amounts MOSE with inactivated *Brca1*. Preneoplastic morphological changes would be expected to occur more frequently if *Brca1* had indeed been inactivated to any great extent, as such changes were previously observed to occur significantly earlier and more commonly in Brca1-deficient MOSE compared to Brca1-intact controls (Clark-Knowles et al., 2007).

Despite variable patterns, preneoplastic morphological increases always increased over time in placebo treated mice, however a trend for a decreased percentage of columnar and hyperplastic MOSE cells was found at the 365 day time point in the low and high dose estradiol group respectively. This finding suggests that waning estradiol levels were not able to sustain the promotion of morphological changes in the OSE and/or that estradiol-induced changes within the ovary at earlier time points prevented the formation of preneoplastic lesions at later time points. Additionally, it suggests that the lesions are either reversible or that the affected OSE can be replaced by cells with normal morphology. This property of the preneoplastic morphological changes in OSE cells has not been previously reported.

Estradiol significantly increased the occurrence of preneoplastic morphological changes of MOSE at certain doses and time points compared to placebo-treated mice. Although the pellet releasing 0.05 mg estradiol resulted in circulating estradiol levels equivalent to basal levels in serum collected 60 days after pellet insertion, it was sufficient to promote columnar morphology significantly more commonly compared to placebo controls at the 60 day time point. Circulating estradiol levels of mice implanted with the 0.25 mg estradiol pellet were not measured, but presumed to be significantly above basal levels based on the estrogen-related bladder problems experienced by mice (Elson et al., 2000; Shai et al., 2008) and previous measurements for the same pellets implanted in mice in our lab (Laviolette et al., 2010). This high dose of estradiol significantly promoted all three preneoplastic lesions of MOSE quantified at the 60 day time point and columnar morphology quantified at the 180 day time point, which was the only estradiol-induced increased observed past the 60 day time point. A study looking at the impact of a 0.25 mg estradiol-releasing pellet on MOSE morphology in normal mice at early time points up to 60 days found a very similar percentage of the ovarian surface covered with columnar and hyperplastic MOSE in both placebo and estradiol-treated mice as findings in the current study at the 60 day time point (Laviolette et al., 2010), This serves as further evidence that observed changes were due to the actions of estradiol on Brca1-intact rather than Brca1-deficient MOSE cells.

Although both low and high dose estradiol treatment were able to increase the occurrence of preneoplastic changes by 60 days after pellet insertion, low dose estradiol resulted in only significantly increased columnar MOSE and not also hyperplasia or invaginations as was accomplished by high dose estradiol. Although columnar MOSE are

considered a putative preneoplastic morphological change of OSE based on their occurrence in invaginations and inclusion cysts (Auersperg et al., 2001; Scully, 1995), evidence for hyperplastic OSE and invaginations as preneoplastic lesions of ovarian cancer is more strongly substantiated. Hyperplastic MOSE have been found to express CA-125 (Kabawat et al., 1983) and MOSE in invaginations have been found to express E-cadherin (Maines-Badniera and Auersperg, 1997; Sundfeldt et al., 1997) and c-KIT (Tonary et al., 2000), proteins found in epithelial ovarian tumours but not in OSE cells of normal morphology. Additionally, many studies have found MOSE hyperplasia and invaginations more often in ovaries at high risk of developing ovarian cancer compared to controls (Mittal et al., 1993; Plaxe et al., 1990; Resta et al., 1993; Salazar et al., 1996; Schlosshauer et al., 2003; Stewart et al., 2004). It appears that the higher dose of estradiol induced more aggressive morphological changes in MOSE cells than the lower dose.

Interestingly, the same preneoplastic changes highly induced by estradiol at the 60 day time point were commonly significantly decreased in estradiol-treated mice at the 365 day time point, suggesting some early effect of estradiol made the development of preneoplastic lesions at later time points less likely to occur. Although not quantified, it was noted that ovaries from estradiol-treated mice contained more atretic follicles and less CLs compared to their placebo-treated counterparts; perhaps greater atresia induced by high estradiol reduced the number of fully-grown follicles and/or ovulations and therefore protected against preneoplastic lesion formation at later time points. This idea is supported by literature showing that increased number of ovulations is associated with greater preneoplastic morphological changes (Clow et al., 2002; Nieto et al., 2001) and that, in addition to inducing follicular growth and development, estradiol can also cause

follicular atresia, particularly of the dominant follicle, in rats and rhesus monkeys (Dierschke et al., 1994).

It is currently not known how estradiol promotes both columnar and hyperplastic morphology of MOSE cells, but distinct mechanisms are likely responsible because these two phenotypes represent opposite ends of the epithelial-mesenchymal spectrum. Estradiol can promote epithelial and mesenchymal phenotypes in various cell types. The ability of estradiol to promote columnar MOSE cells is supported by oviductal epithelial cells of beagles, baboons, and rhesus macaques transitioning from cuboidal to columnar due to *in vivo* exposure to estradiol (Sawyer et al., 1984; Brenner et al., 1983; Verhage et al., 1997). The induction of hyperplastic MOSE due to estradiol is supported by evidence from *in vitro* studies of human ovarian cancer cell lines, human endometrial epithelial cells, and mouse mammary epithelial cells showing exposure to estradiol induced mesenchymal morphology, migration, multi-layered growth, and loss of tight junctions (Park et al., 2008; Fialka et al., 1996; Chen et al., 2010). These effects corresponded to upregulation of Snail and Slug, transcription factors known to promote epithelial to mesenchymal transition (Park et al., 2008; Chen et al., 2010). The acquired mesenchymal phenotype of MOSE cells may be due to decreased expression of Disabled-2 (Dab2), as Dab2 is required for epithelial cells to maintain polarity (Yang et al., 2007) and mice heterozygous for Dab2 develop preneoplastic lesions and benign cysts in their ovaries (Yang et al.. 2006), although there is currently no evidence for estradiol causing Dab2 downregulation. It is possible that certain stimuli and subsequent signalling cause flat or cuboidal OSE cells to transition into either a more or less epithelial-differentiated state, as OSE are known to be an uncommitted cell type, capable of becoming more mesenchymal

during ovulatory wound repair but more epithelial during malignant transformation (Auersperg et al., 2001). Alternatively, evidence of a putative progenitor cell population in the OSE (Szotek et al., 2008) allows for the possibility that the morphologic changes induced by estradiol exposure depends on the population of OSE cells on which estradiol acts. The mechanisms driving the formation of columnar and hyperplastic MOSE cells must be further investigated to gain a better understanding of the role of estradiol in promoting ovarian tumourigenesis.

With the overall hypothesis that estradiol promotes preneoplastic morphological changes of MOSE, it was suspected that the formation of these lesions may be influenced by structures within the ovary that produce estradiol, including large secondary and antral follicles (Nussey and Whitehead, 2001; Oktem and Oktay, 2008). All preneoplastic changes examined as well as normal MOSE were found to occur most frequently near ovarian stromal cells and this is attributed to stroma being more common than any other ovarian structure. Therefore, no particular structure within the ovary appears to secrete factors that promote the formation of preneoplastic lesions on the surface. The distribution of stroma and primordial, primary, secondary, and antral follicles underlying MOSE with preneoplastic morphological changes was similar in both placebo and estradiol-treated ovaries, suggesting no effect of estradiol or potential estradiol-induced changes in these ovarian structures. There was a pattern for estradiol-treated ovaries to contain more preneoplastic changes near atretic follicles and less near CLs than placebo-treated mice. This is thought to be another representation of the greater frequency of follicular atresia over CL formation and therefore decreased ovulation due to estradiol

treatment rather than effects of atretic follicles and CLs promoting the formation of preneoplastic lesions of OSE cells.

In the current study, quantification of Ki-67 staining was performed on ovaries from the 60 day time point only because the implanted pellets release hormone for 60 days and therefore direct effects of estradiol would be expected to be equivalent or lower at later time points. Ki-67 is expressed in the nucleus of all cells undergoing cell division and its overexpression in OSE cells is indicative of an abnormality (Schlosshauer et al., 2003). The very few proliferative MOSE cells found in ovaries from either treatment group in the current study is consistent with reports in the literature. A study by Davies *et al.* (1999) measuring the number of bromodeoxyuridine (BrdUrd) positive cells as a percent of the total number of epithelial cells per ovarian section found less than 1% of OSE are proliferative in sexually mature mice. In ovaries prophylactically removed from women with and without a family history of ovarian cancer and then sectioned and stained for Ki-67, one study found less than 1% of positive OSE cells (Piek et al., 2003) and another study showed very few ovaries with any OSE cells staining positively (Werness et al., 1999). No increase in MOSE proliferation due to exogenous estradiol has also been reported previously (Laviolette et al., 2010).

The stimulus for proliferation in the few MOSE cells found to express Ki-67 per section in the current study is unknown, but appears related to mechanical stress caused by the development of large structures, such as late-stage secondary follicles and CLs, within the ovary requiring greater ovarian surface area (Davies et al., 1999). Although Wright *et al.* (2008) did not find an association between such structures and OSE cell proliferation and in the current study stroma was found to underlie the majority of

proliferative MOSE cells, large secondary follicles were also commonly found as well as CLs specifically in placebo-treated mice.

MOSE found to express Ki-67 were most commonly flat-to-cuboidal in shape rather than columnar or in patches of hyperplasia, suggesting these premalignant phenotypes are not the result of increased proliferation. Ki-67-negative hyperplastic OSE cells were noted in a histological study of prophylactically removed ovaries of women, prompting the authors to challenge OSE hyperplasia as a valid preneoplastic lesion for ovarian cancer (Piek et al., 2003). With evidence from numerous studies implicating OSE hyperplasia as a preneoplastic change (Chêne et al., 2009; Nnene et al., 2004; Resta et al., 1993; Salazar et al., 1996; Stewart et al., 2004), including involvement of p53 mutations (Cai et al., 2009; Nnene et al., 2004), the finding that these cells lack Ki-67 expression does not seem sufficient to exclude them as putative premalignant lesions. Proliferation-independent mechanisms driving preneoplastic morphological changes of MOSE cells over time and with estradiol treatment remain unknown. However, evidence that estradiol prevents apoptosis (Choi et al., 2001; Murdoch and Van Kirk, 2002) suggests patches of hyperplastic OSE cells could form without proliferating. Furthermore, estradiol has been linked to the loss of polarity through epithelial to mesenchymal transition (Chen et al., 2010; Park et al., 2008).

Because of E-cadherin's function of maintaining cell-cell adhesions and epithelial cell polarity, its down-regulation is often observed in tumour progression and metastasis (Birchmeier and Behrens, 1994; Wijnhoven et al., 2000). However, in EOCs, which become more differentiated as they progress, E-cadherin is upregulated from non-detectable in human OSE cells to uniform expression in benign, borderline, and

metastatic tumours (Maines-Bandiera and Auersperg, 1997; Sundfeldt et al., 1997). In addition to being a marker of preneoplastic morphological changes in human OSE cells, E-cadherin expression in MOSE cells was investigated in the current study because numerous studies have found estradiol-induced epithelial to mesenchymal transition is associated with downregulation of E-cadherin (Chen et al., 2010; Park et al., 2008), although one study found *in vivo* estradiol treatment upregulated E-cadherin mRNA expression in the mouse ovary (MacCalman et al., 1994). No differences in E-cadherin expression were found in mouse OSE due to aging, estradiol treatment, columnar morphology, or invaginations in the current study. Because, unlike humans, morphologically normal mouse OSE do express E-cadherin (Auersperg et al., 2001; Clark-Knowles et al., 2007), increased expression in preneoplastic lesions is likely to be more subtle or the increased expression of E-cadherin associated with EOC progression may be unique to humans. E-cadherin expression was decreased in some patches of hyperplastic MOSE cells and this is consistent with its established role in maintaining epithelial polarity (Birchmeier and Behrens, 1994; Wijnhoven et al., 2000).

The first objective of the study, to determine the impact of exogenous estradiol on the occurrence of preneoplastic lesions and tumourigenesis in Brca1-deficient MOSE, was not fulfilled due to technical difficulties in inactivating *Brca1* in a significant proportion of OSE *in vivo*. However, estradiol did induce three distinct preneoplastic lesions in Brca1-intact MOSE cells. It is predicted that greater effects of estradiol would be observed with successful *Brca1* inactivation. In future experiments, this could potentially be demonstrated with greater numbers of mice living to later time points, the use of a dose of estradiol that raises serum estradiol but does not cause severe bladder

complications, and replacement of the estradiol-releasing pellet every 60 days to ensure circulating levels remain high. The possibility still remains that the combination of increased DNA damage due to concomitant Brca1 loss and elevated estradiol is a significant factor in promoting ovarian tumourigenesis in *BRCA1* mutation carriers.

The function of BRCA1 in regulating aromatase expression and therefore estradiol secretion was investigated in the second objective of the current study and was not substantiated in mouse OSE cells or primary GCs. This is the first reported *in vitro* study measuring estradiol secretion, which is important in assessing potential physiological effects of aromatase mRNA levels.

The contradiction between findings in the current study and published literature could be due to a number of factors. Although every effort was made to employ culture conditions that minimize spontaneous luteinisation of the primary cultures of GCs, the possibility exists that the experimental conditions used in the current study prevented the full effects of inactivated *Brca1* on aromatase expression and activity from being observed because of some degree of luteinisation taking place. The likelihood that enough functional Brca1 remained in GCs and MOSE cells to mask the effect of Brca1 loss is considered low because at least fifty percent *Brca1* recombination was confirmed in every experiment and a published study observed increased aromatase mRNA expression with BRCA1 knockdown of about fifty percent accomplished by siRNA (Lu et al., 2006).

Unfavourable treatment conditions may have impacted observed results. It is well documented that 48 hours of FSH treatment induces aromatase mRNA expression and estradiol production in cultured GCs, but serum prevents this effect (Fitzpatrick and

Richards, 1991; Orly et al., 1980). This may explain the similarity of aromatase expression and estradiol secretion in vehicle and FSH-treated primary GCs in the current study, as 2% serum was included in media during treatment. Consistent with the current study, it has been shown that concurrent testosterone treatment rescues FSH-stimulated aromatase expression when serum is present; this effect of testosterone is mediated through androgen receptor (Fitzpatrick and Richards, 1991). The effects of FSH and testosterone appear similar in OSE cultured with serum. With aromatase mRNA levels generally representative of corresponding estradiol production in GCs (Fitzpatrick and Richards, 1991) and the highly specific and sensitive TaqMan® Gene Expression Assay used to determine aromatase mRNA expression, it was surprising to find undetectable expression but detectable estradiol production from MOSE cells. Despite inhibition of FSH-induced aromatase expression and estradiol production by components of the serum, any significant effect of *Brca1* inactivation should have been observed, particularly because previous studies documented the relationship in GCs without any cAMP-stimulation used to increase aromatase expression (Hu et al., 2005; Lu et al., 2011).

The published Brca1 repression of aromatase in GCs could be an artefact of *in vitro* systems that are not physiologically relevant. Knockdown of BRCA1 causing aromatase upregulation has been previously reported in only one cell line of GCs (Hu et al., 2005) and, in terms of mechanistic investigation, the interaction between BRCA1 and transcription factor SF-1 was shown in the HEK 293 T cell line but could not be substantiated in the human GC cell line (Lu et al., 2011).

BRCA1 regulation of aromatase may also be more pronounced in breast tissue than in ovaries. Increased aromatase transcription caused by BRCA1 knockdown has

been observed in primary breast adipose cells (Ghosh et al., 2007; Hu et al., 2005; Lu et al., 2006) and the mechanism by which BRCA1 represses aromatase transcription has begun to be elucidated in similar systems (Lu et al., 2006; Lu et al., 2011; Subbaramaiah et al., 2008). Furthermore, a significant increase in aromatase mRNA transcript levels in women with germline BRCA1 mutations versus controls has been found, but was only statistically significant for breast and not ovarian tissue (Chand et al., 2009; Lu et al., 2006; Lu et al., 2011).

Finally, it is possible that transcriptional repression of aromatase by BRCA1 does not occur in mice, as all studies directly investigating this relationship have been performed on human cells (Ghosh et al., 2007; Ghosh et al., 2008; Hu et al., 2005; Subbaramaiah et al., 2008). Hong *et al.*'s paper (2010) is the only evidence for Brca1 regulation of estrogen in mice. Their study convincingly shows that loss of functional Brca1in GCs increases circulating estradiol and lengthens the proestrous phase of the estrous cycle, but perhaps this occurs independent of Brca1 regulation of aromatase. The authors suggest investigating the effect of Brca1 loss on gonadotropin surge attenuating factor, inhibin, and activin (Hong et al., 2010). *In vitro* measurements of aromatase expression in and estradiol secretion from GCs with and without functional Brca1 isolated from the mice used Hong *et al.*'s study would help to clarify Brca1's ability to regulate aromatase in mice. Overall, the hypothesis of a causal link between BRCA1 and aromatase is strongly supported in the literature, but remains invalidated in relation to ovarian cancer until it is observed in primary GCs and in an *in vivo* model.

The effect of Brca1 loss on ERα expression was investigated because of literature showing cross regulation between these two proteins. About 90% of BRCA1-associated

breast cancers are negative for ERα expression (Foulkes et al., 2004), ERα and BRCA1 expression are correlated in sporadic breast tumours (Roldan et al., 2006), and BRCA1 knockdown in human breast cancer cell lines is associated with decreased ERα mRNA and protein expression (Hosey et al., 2007). A correlation between Brca1 and ERα expression was not observed in the current study. It is possible that the propensity for BRCA1-associated breast cancers to be ERα negative is not due to BRCA1 regulation of ERα expression but rather the inability of BRCA1-null mammary stem/progenitor cells, which are ERα negative, to differentiate into ERα positive mammary epithelial cells. The accumulation of DNA damage in these stem/progenitor cells make them likely to later transform and from a breast tumour (Liu et al., 2008). Alternatively, it is possible BRCA1 regulation of ERα occurs in breast but not ovarian cell types. Further elucidating the regulation of ERα by BRCA1 in the context of ovarian cancer may increase understanding of tissue-specific cancer induction in *BRCA1* mutation carriers.

The aim of the third objective of the current study was to address the lack of i*n vivo* evidence of the relationship between BRCA1 and aromatase by concurrently inactivating *Brca1* in mouse GCs and OSE cells to determine if estradiol levels were elevated and, if so, to evaluate their impact on the occurrence of preneoplastic morphological changes and tumour initiation in OSE cells. Firm rationale supported the design of creating a mouse model in which to study Brca1 loss in both GCs and OSE cells. Amhr2 is a serine/threonine kinase receptor for anti-Müllerian hormone. It is expressed in somatic cells of the adult female reproductive tract, including GCs and OSE cells (Broekmans et al., 2008; Jamin et al., 2002). The *Amhr2*$^{Cre/Cre}$ mouse has been used previously in crosses with homozygous floxed mice to cause recombination and

inactivation of a gene of interest, including the *SNF2L* gene by a previous lab member and *Brca1* by a different group (Xing et al., 2009). It is currently not known why the same *Amhr2*$^{Cre/Cre}$ mice used previously in the lab are no longer expressing Cre recombinase. Although a small proportion of recombined *Brca1* was observed in a single isolation of GCs from *Brca1*$^{loxP/loxP}$ *Cre*-positive mice, intact Brca1 alone found in every other isolation of cells and tissues necessitated the conclusion of no functional difference between mice with or without the *Cre* transgene and subsequent abandonment of this mouse model for the study of the effects of inactivated *Brca1* on estradiol production.

The importance of investigating cellular processes in physiologically relevant settings is highlighted in the study of the relationship between BRCA1 and aromatase, as *in vivo* evidence is sorely lacking. Unfortunately, technical challenges impeded the current study in furthering our understanding of Brca1 regulation of aromatase in such relevant systems. Exogenous estradiol did not induce tumourigenesis of mouse OSE, but there was evidence of increased preneoplastic morphological changes and the possibility remains that estradiol may cause more severe effects on OSE lacking functional Brca1. Unfortunately conclusions about the consequences of Brca1 loss in both GCs and OSE cells *in vivo* simultaneously on aromatase expression and ovarian tumour initiation were not possible, as a mouse model exhibiting *Brca1* inactivation in both cell types was not successfully generated. One strong finding of the current study was that Brca1 loss did not upregulate aromatase expression or estradiol synthesis in MOSE cells or primary GCs, contrasting published studies performed in different cell systems. Despite this finding, evidence from the published reports remains strong enough to make the investigation of an *in vivo* model of this relationship a worthwhile endeavour. It is

important to confirm or invalidate the promotion of malignant transformation of BRCA1 deficient epithelial cells in breast and ovarian tissue by elevated estradiol from cells lacking BRCA1 in physiologically relevant systems; the findings have the potential to uncover pathways responsible for tumour initiation and early progression and provide evidence for aromatase inhibitors as a cancer prevention measure in women with a germline *Brca1* mutation. Many functions of BRCA1 likely contribute to its role as a tumour suppressor and their further investigation will improve understanding of the molecular events responsible for the enigma of tissue-specificity of BRCA1-associated cancers with the goal of improving the quality of life and survival of mutation carriers.

REFERENCES

Anonymous (1987). The reduction in risk of ovarian cancer associated with oral-contraceptive use. N Engl J Med *316,* 650-655.

Applied Biosystems. (2008). Guide to performing relative quantitation of gene expression using real-time quantitative PCR. 1-70.

Auersperg, N., Maines-Bandiera, S.L., and Dyck, H.G. (1997). Ovarian carcinogenesis and the biology of ovarian surface epithelium. J Cell Phys *173,* 261-265.

Auersperg, N., Wong, A.S.T., Choi, K., Kang, S.K., and Leung, P.C.K. (2001). Ovarian surface epithelium: biology, endocrinology, and pathology. Endocrine Reviews *22,* 255-288.

Bai, W., Oliveros-Saunders, B., Wang, Q., Acevedo-Duncan, M.E., and Nicosia, S.V. (2000). Estrogen stimulation of ovarian surface epithelial cell proliferation. In Vitro Cell Dev Biol Anim *36,* 657-666.

Bankhead, C.R., Collins, C., Stokes-Lampard, H., Rose, P., Wilson, S., Clements, A., Mant, D., Kehoe, S.T., and Austoker, J. (2008). Identifying symptoms of ovarian cancer: a qualitative and quantitative study. BJOG *115,* 1008-1014.

Barakat, R.R., Federici, M.G., Saigo, P.E., Robson, M.E., Offit, K., and Boyd, J. (2000). Absence of premalignant histologic, molecular, or cell biologic alterations in prophylactic oophorectomy specimens from BRCA1 heterozygotes. Cancer *89,* 383-390.

Bast, R.C., Hennessy, B., and Mills, G.B. (2009). The biology of ovarian cancer: new opportunities for translation. Nat Rev Cancer. *9,* 415-428.

Bell, D.A. (2005). Origins and molecular pathology of ovarian cancer. Mod Pathol *18,* S19-S32.

Bell, D.A., and Scully, R.E. (1994). Early de novo ovarian carcinoma: a study of fourteen cases. Cancer *73,* 1859-1864.

Berchuck, A., Heron, K., Carney, M.E., Lancaster, J.M., Fraser, E.G., Vinson, V.L., Deffenbaugh, A.M., Miron, A., Marks, J.R., Futreal, P.A., and Frank, T.S. (1998). Frequency of germline and somatic BRCA1 mutations in ovarian cancer. Clin Can Res *4,* 2433-2437.

Berstein, L.M. (2008). Endocrinology of the wild and mutant BRCA1 gene and types of hormonal carcinogenesis. Future Oncol *4,* 23-39.

Birchmeier, W., and Behrens, J. (1994). Cadherin expression in carcinomas: role in the formation of cell junctions and the prevention of invasiveness. BBA - Reviews on Cancer *1198,* 11-26.

Bjersing, L., and Cajander, S. (1975). Ovulation and the role of the ovarian surface epithelium. Experientia *31,* 605-608.

Blackshear, P.E., Goldsworthy, S.M., Foley, J.F., McAllister, K.A., Bennett, L.M., Collins, N.K., Bunch, D.O., Brown, P., Wiseman, R.W., and Davis, B.J. (1998). Brca1 and Brca2 expression patterns in mitotic and meiotic cells of mice. Oncogene *16,* 61-68.

Bosetti, C., Negri, E., Trichopoulos, D., Franceschi, S., Beral, V., Tzonou, A., Parazzini, F., Greggi, S., and La Vecchia, C. (2002). Long-term effects of oral contraceptives on ovarian cancer risk. Int J Cancer *102,* 262-265.

Brenner, R.M., Carlisle, K.S., Hess, D.L., Sandow, B.A., and West, N.B. (1983). Morphology of the oviducts and endometria of cynomolgus macaques during the menstrual cycel. Biol Reprod *29* 1289-1302.

Bowtell, D.D. (2010). The genesis and evolution of high-grade serous ovarian cancer. Nat Rev Cancer *10,* 803.

Broekmans, F.J., Visser, J.A., Laven, J.S.E., Broer, S.L., Themmen, A.P.N., and Fauser, B.C. (2008). Anti-Müllerian hormone and ovarian dysfunction. Trends Endocrinol Metab *19,* 340-347.

Bulun, S.E., Lin, Z., Imir, G., Amin, S., Demura, M., Yilmaz, B., Martin, R., Utsunomiya, H., Thung, S., Gurates, B., *et al.* (2005). Regulation of aromatase expression in estrogen-responsive breast and uterine disease: from bench to treatment. Pharmacol Rev *57,* 359-383.

Burdette, J.E., Kurley, S.J., Kilen, S.M., Mayo, K.E., and Woodruff, T.K. (2006). Gonadotropin-induced superovulation drives ovarian surface epithelia proliferation in CD1 mice. Endocrinology *147,* 2338-2345.

Cai, K.Q., Wu, H.S., Klein-Szanto, A.J., and Xu, X.X. (2009). Acquisition of a second mutation of the Tp53 alleles immediately precedes epithelial morphological transformation in ovarian tumorigenicity. Gynecol Oncol *114,* 18-25.

Calvert, H., and Azzariti, A. (2011). The clinical development of inhibitors of poly(ADP-ribose) polymerase. Ann Oncol *22,* i53-i59.

Canadian Cancer Society's Steering Committee. (2010). Canadian Cancer Statistics 2010.

Casey, M.J., Bewtra, C., Hoehne, L.L., Tatpati, A.D., Lynch, H.T., and Watson, P. (2000). Histology of prophylactically removed ovaries from BRCA1 and BRCA2

mutation carriers compared with noncarriers in hereditary breast ovarian cancer syndrome kindreds. Gynecol Oncol *78,* 278-287.

Chand, A.L., kConFab, Simpson, E.R., and Clyne, C.D. (2009). Aromatase expression is increased in BRCA1 mutation carriers. BMC Cancer *9,* 148.

Chen, S., and Parmigiani, G. (2007). Meta-analysis of BRCA1 and BRCA2 penetrance. J Clin Oncol *25,* 1329-1333.

Chen, Y., Li, H., Huang, C., Twu, N., Yen, M., Wang, P., Chou, T., Liu, Y., Chao, K., and Yang, M. (2010). Oestrogen-induced epithelial–mesenchymal transition of endometrial epithelial cells contributes to the development of adenomyosis. J Pathol *222,* 261-270.

Chêne, G., Penault-Llorca, F., Le Bouëdec, G., Mishellany, F., Dauplat, M.M., Jaffeux, P., Aublet-Cuvelier, B., Pouly, J.L., Déchelotte, P., and Dauplat, J. (2009). Ovarian epithelial dysplasia and prophylactic oophorectomy for genetic risk. Int J Gynecol Cancer *19,* 65-72.

Chodankar, R., Kwang, S., Sangiorgi, F., Hong, H., Yen, H.Y., Deng, C., Pike, M.C., Shuler, C.F., Maxson, R., and Dubeau, L. (2005). Cell-nonautonomous induction of ovarian and uterine serous cystadenomas in mice lacking a functional Brca1 in ovarian granulosa cells. Curr Biol *15,* 561-565.

Choi, K., Kang, S.K., Tai, C., Auersperg, N., and LEUNG, P.C.K. (2001). Estradiol up-regulates antiapoptotic Bcl-2 messenger ribonucleic acid and protein in tumorigenic ovarian surface epithelium cells. Endocrinology *142,* 2351-2360.

Clark-Knowles, K.V., Garson, K., Jonkers, J., and Vanderhyden, B.C. (2007). Conditional inactivation of Brca1 in the mouse ovarian surface epithelium results in an increase in preneoplastic changes. Experimental Cell Research *313,* 133-145.

Clark-Knowles, K.V., Senterman, M.K., Collins, O., and Vanderhyden, B.C. (2009). Conditional inactivation of Brca1, p53 and Rb in mouse ovaries results in the development of leiomyosarcomas. PLoS One *4,* e8534.

Clow, O.L., Hurst, P.R., and Fleming, J.S. (2002). Changes in the mouse ovarian surface epithelium with age and ovulation number. Mol Cell Endocrinol *191,* 105-111.

Coleman, K.A., and Greenberg, R.A. (2011). The BRCA1-RAP80 complex regulates DNA repair mechanism utilization by restricting end resection. J Biol Chem *Epub ahead of print.*

Davies, B.R., Finnigan D S., Smith S K., and Ponder B A J. (1999). Administration of gonadotropins stimulates proliferation of normal mouse ovarian surface epithelium. Gynecol Endocrinol *13,* 75-81.

Deng, C. (2006). BRCA1: cell cycle checkpoint, genetic instability, DNA damage response and cancer evolution. Nucleic Acids Research *34*, 1416-1426.

Dierschke, D.J., Chaffin, C.L., and Hutz, R.J. (1994). Role and site of estrogen action in follicular atresia. Trends Endocrinol Metab *5*, 215-219.

Dong, Y., Hakimi, M.A., Chen, X., Kumaraswamy, E., Cooch, N.S., Godwin, A.K., and Shiekhatter, R. (2003). Regulation of BRCC, a holoenzyme complex containing BRCA1 and BRCA2, by a signalosome-like subunit and its role in DNA repair. Mol Cell *12*, 1087-1099.

Elledge, S.J., and Amon, A. (2002). The BRCA1 suppressor hypothesis: an explanation for the tissue-specific tumor development in BRCA1 patients. Cancer Cell *1*, 129-132.

Elson, D.A., Riley, R.R., Lacey, A., Thordarson, G., Talamantes, F.J., and Arbeit, J.M. (2000). Sensitivity of the cervical transformation zone to estrogen-induced squamous carcinogenesis. Cancer Res *60*, 1267-1275.

Fan, S., Wang, J., Yuan, R., Ma, Y., Meng, Q., Erdos, M.R., Pestell, R.G., Yuan, F., Auborn, K.J., Goldberg, I.D., and Rosen, E.M. (1999). BRCA1 inhibition of estrogen receptor signaling in transfected cells. Science *284*, 1354-1356.

Fathalla, M.F. (1971). Incessant ovulation - a factor in ovarian neoplasia? Lancet *2*, 163.

Fearon, E.R., and Vogelstein, B. (1990). A genetic model for colorectal tumorigenesis. Cell *61*, 759-767.

Fialka, I., Schwarz, H., Reichmann, E., Oft, M., Busslinger, M., and Beug, H. (1996). The estrogen-dependent c-JunER protein causes a reversible loss of mammary epithelial cell polarity involving destabilization of adherens junctions. J Cell Biol *132*, 1115-1132.

Fitzpatrick, S.L., and Richards, J.S. (1991). Regulation of cytochrome P450 aromatase messenger ribonucleic acid and activity by steroids and gonadotropins in rat granulosa cells. Endocrinology *129*, 1452-1462.

Foulkes, W.D., Metcalfe, K., Sun, P., Hanna, W.M., Lynch, H.T., Ghadirian, P., Tung, N., Olopade, O.I., Weber, B.L., McLennan, J., *et al.* (2004). Estrogen receptor status in BRCA1- and BRCA2-related breast cancer. Clinical Cancer Research *10*, 2029-2034.

Geisler, J.P., Hatterman-Zogg, M.A., Rathe, J.A., and Buller, R.E. (2002). Frequency of BRCA1 dysfunction in ovarian cancer. Journal of the National Cancer Institute *94*, 60.

Ghosh, S., Lu, Y., and Hu, Y. (2008). A role of CREB in BRCA1 constitutive promoter activity and aromatase basal expression. Int J Biomed Sci *4*, 260-265.

Ghosh, S., Lu, Y., Katz, A., Hu, Y., and Li, R. (2007). Tumor suppressor BRCA1 inhibits a breast cancer-associated promoter of the aromatase gene (CYP19) in human adipose stromal cells. Am J Physiol Endocrinol Metab *292*, E246-E252.

Gotfredson, G.S., and Murdoch, W.J. (2007). Morphologic responses of the mouse ovarian surface epithelium to ovulation and steroid hormonal milieu. Exp Biol Med (Maywood) *232*, 277-280.

Gudmundsdottir, K., and Ashworth, A. (2006). The roles of BRCA1 and BRCA2 and associated proteins in the maintenance of genomic stability. Oncogene *25*, 5864-5874.

Hong, H., Yen, H.Y., Brockmeyer, A., Liu, Y., Chodankar, R., Pike, M.C., Stanczyk, F.Z., Maxson, R., and Dubeau, L. (2010). Changes in the mouse estrus cycle in response to BRCA1 inactivation suggest a potential link between risk factors for familial and sporadic ovarian cancer. Cancer Res *70*, 221-228.

Hong, Y., Li, H., Yuan, Y.C., and Chen, S. (2009). Molecular characterization of aromatase. Ann N Y Acad Sci *1155*, 112-120.

Hosey, A.M., Gorski, J.J., Murray, M.M., Quinn, J.E., Chung, W.Y., Stewart, G.E., James, C.R., Farragher, S.M., Mulligan, J.M., Scott, A.N., *et al.* (2007). Molecular basis for estrogen receptor alpha deficiency in BRCA1-linked breast cancer. J Natl Cancer Inst *99*, 1683-1694.

Hu, Y. (2009). BRCA1, hormone, and tissue-specific tumor suppression. Int J Biol Sci *5*, 20-27.

Hu, Y., Ghosh, S., Amleh, A., Yue, W., Lu, Y., Katz, A., and Li, R. (2005). Modulation of aromatase expression by BRCA1: a possible link to tissue-specific tumor suppression. Oncogene *24*, 8343-8348.

Jamin, S.P., Arango, N.A., Mishina, Y., Hanks, M.C., and Behringer, R.R. (2002). Requirement of Bmpr1a for Müllerian duct regression during male sexual development. Nat Genet *32*, 408-410.

Ji, J., Forsti, A., Sundquist, J., Lenner, P., and Hemminki, K. (2008). Survival in ovarian cancer patients by histology and family history. Acta Oncol *47*, 1133-1139.

Kabawat, S.E., Bast, R.C., Bhan, A.K., Welch, W.R., Knapp, R.C., and Colvin, R.B. (1983). Tissue distribution of a coelomic-epithelium-related antigen recognized by the monoclonal antibody OC125. Int J Gynecol Pathol *2*, 275-285.

Karlan, B.Y., Jones, J., Greenwald, M., and Lagasse, L.D. (1995). Steroid hormone effects on the proliferation of human ovarian surface epithelium in vitro. Am J Obstet Gynecol *173*, 97-104.

Kauff, N.D., Satagopan, J.M., Robson, M.E., Scheuer, L., Hensley, M., Hudis, A., Ellis, N.A., Boyd, J., Borgen, P.I., Barakat, R.R., *et al.* (2002). Risk-reducing salpingo-oophorectomy in women with a BRCA1 or BRCA2 mutation. N Engl J Med *346,* 1609-1615.

Kobel, M., Kalloger, S.E., Boyd, N., McKinney, S., Mehl, E., Palmer, C., Leung, S., Bowen, N.J., Ionescu, D.N., Rajput, A., *et al.* (2008). Ovarian carcinoma subtypes are different diseases: implications for biomarker studies. PLoS Med *5,* e232.

Kruk, P.A., Uitto, V., Firth, J.D., Dedhar, S., and Auersperg, N. (1994). Reciprocal interactions between human ovarian surface epithelial cells and adjacent extracellular matrix. Exp Cell Res *215,* 97-108.

Lacey, J.V.J., Brinton, L.A., Leitzmann, M.F., Mouw, T., Hollenbeck, A., Schatzkin, A., and Hartge, P. (2006). Menopausal hormone therapy and ovarian cancer risk in the National Institutes of Health-AARP Diet and Health Study Cohort. J Natl Cancer Inst *98,* 1397-1405.

Lane, T.F., Deng, C., Elson, A., Lyu, M.S., Kozak, C.A., and Leder, P. (1995). Expression of Brca1 is associated with terminal differentiation of ectodermally and mesodermally derived tissues in mice. Genes & Development *9,* 2712-2722.

Lau, K.M., Mok, S.C., and Ho, S.M. (1999). Expression of human estrogen receptor-alpha and -beta, progesterone receptor, and androgen receptor mRNA in normal and malignant ovarian epithelial cells. Proc Natl Acad Sci USA *96,* 5722-5727.

Laviolette, L.A., Garson, K., Macdonald, E.A., Senterman, M.K., Courville, K., Crane, C.A., and Vanderhyden, B.C. (2010). 17beta-estradiol accelerates tumor onset and decreases survival in a transgenic mouse model of ovarian cancer. Endocrinology *151,* 929-938.

Li, W., Xiao, C., Vonderhaar, B.K., and Deng, C. (2007). A role of estrogen/ERa signaling in BRCA1-associated tissue-specific tumor formation. Oncogene *26,* 7204-7212.

Li, Y.F., Hu, W., Fu, S.Q., Li, J.D., Liu, J.H., and Kavanagh, J.J. (2008). Aromatase inhibitors in ovarian cancer: is there a role? Int J Gynecol Cancer *18,* 600-614.

Liu, S., Ginestier, C., Charafe-Jauffret, E., Foco, H., Kleer, C.G., Merajver, S.D., Dontu, G., and Wicha, M.S. (2008). BRCA1 regulates human mammary stem/progenitor cell fate. Proc Natl Acad Sci USA *105,* 1680-1685.

Lu, M., Chen, D., Lin, Z., Reierstad, S., Trauernicht, A.M., Boyer, T.G., and Bulun, S.E. (2006). BRCA1 negatively regulates the cancer-associated aromatase promoters I.3 and II in breast adipose fibroblasts and malignant epithelial cells. J Clin Endocrinol Metab *91,* 4514-4519.

Lu, Y., Kang, T., and Hu, Y. (2011). BRCA1/BARD1 complex interacts with steroidogenic factor 1--A potential mechanism for regulation of aromatase expression by BRCA1. J Steroid Biochem Mol Biol *123*, 71-78.

MacCalman, C.D., Farookhi, R., and Blaschuk, O.W. (1994). Estradiol regulates E-cadherin mRNA levels in the surface epithelium of the mouse ovary. Clin Exp Metastasis *12*, 276-282.

Maines-Bandiera, S.L., and Auersperg, N. (1997). Increased E-cadherin expression in ovarian surface epithelium: an early step in metaplasia and dysplasia? Int J Gynecol Pathol *16*, 250-255.

Mehrad, M., Ning, G., Chen, E.Y., Mehra, K.K., and Crum, C.P. (2010). A pathologist's road map to benign, precancerous, and malignant intraepithelial proliferations in the fallopian tube. Adv Anat Pathol *17*, 293-302.

Merajver, S.D., Pham, T.M., Caduff, R.F., Chen, M., Poy, E.L., Cooney, K.A., Weber, B.L., Collins, F.S., Johnston, C., and Frank, T.S. (1995). Somatic mutations in the BRCA1 gene in sporadic ovarian tumours. Nat Genet *9*, 439-443.

Miki, Y., Swensen, J., Shattuck-Eidens, D., Futreal, P.A., Harshman, K., Tavtigian, S., Liu, Q., Cochran, C., Bennett, L.M., and Ding, W. (1994). A strong candidate for the breast and ovarian cancer susceptibility gene BRCA1. Science *266*, 66-71.

Mittal, K.R., Zeleniuch-Jacquotte, A., Cooper, J.L., and Demopoulos, R.I. (1993). Contralateral ovary in unilateral ovarian carcinoma: a search for preneoplastic lesions. Int J Gynecol Pathol *12*, 59-63.

Modugno, F., Ness, R.B., and Wheeler, J.E. (2001). Reproductive risk factors for epithelial ovarian cancer according to histologic type and invasiveness. Ann Epidemiol *11*, 568-574.

Monteiro, A.N. (2003). BRCA1: the enigma of tissue-specific tumor development. Trends Genet *19*, 312-315.

Mullan, P.B., Quinn, J.E., and Harkin, D.P. (2006). The role of BRCA1 in transcriptional regulation and cell cycle control. Oncogene *24*, 5854-5863.

Murdoch, W.J., and Van Kirk, E.A. (2002). Steroid hormonal regulation of proliferative, p53 tumor suppressor, and apoptotic responses of sheep ovarian surface epithelial cells. Mol Cell Endocrinol *186*, 67.

Murdoch, W.J., Van Kirk, E.A., and Shen, Y. (2008). Pathogenic reactions of the ovarian surface epithelium to ovulation, dimethylbenzanthracene, and estrogen are negated by vitamin E. Reprod Sci *15*, 839-845.

Murdoch, W.J., and McDonnel, A.C. (2002). Roles of the ovarian surface epithelium in ovulation and carcinogenesis. Reproduction *123,* 743-750.

Naora, H., Montz, F.J., Chai, C.Y., and Roden, R.B. (2001). Aberrant expression of homeobox gene HOXA7 is associated with müllerian-like differentiation of epithelial ovarian tumors and the generation of a specific autologous antibody response. Proc Natl Acad Sci USA *98,* 15209-15214.

Narod, S., Risch, H.A., Moslehi, R., Dorum, A., Neuhausen, S., Olsson, H., Provencher, D., Radice, P., Evans, G., Bishop, S., Brunet, J.S., and Ponder, B.A. (1998). Oral contraceptives and the risk of hereditary ovarian cancer. Hereditary Ovarian Cancer Clinical Study Group. N Engl J Med *339,* 424-428.

Ness, R.B., Ann Grisso, J., Klapper, J., Schlesselman, J.J., Silberzweig, S., Vergona, R., Morgan, M., Wheeler, J.E., and and the SHARE Study Group,. (2000). Risk of ovarian cancer in relation to estrogen and progestin dose and use characteristics of oral contraceptives. American Journal of Epidemiology *152,* 233-241.

Newbold, R.R., and Liehr, J.G. (2000). Induction of uterine adenocarcinoma in CD-1 mice by catechol estrogens. Cancer Res *60,* 235-237.

Nieto, J.J., Crow, J.C., Sundaresan, M., Constantinovici, N., Perrett, C.W., MacLean, A.B., and Hardiman, P. (2001). Ovarian epithelial dysplasia in relation to ovulation induction and nulliparity. Gynecol Oncol *82,* 344-349.

Nnene, I.O., Nieto, J.J., Crow, J.C., Sundaresan, M., MacLean, A.B., Perrett, C.W., and Hardiman, P. (2004). Cell cycle and apoptotic proteins in relation to ovarian epithelial morphology. Gynecol Oncol *92,* 247-251.

Nussey, S., and Whitehead, S. (2001). Endocrinology: An Integrated Approach (Oxford: BIOS Scientific Publishers Limited).

Oei, A.L., Massuger, L.F., Bulten, J., Ligtenberg, M.J., Hoogerbrugge, N., and de Hullu, J.A. (2006). Surveillance of women at high risk for hereditary ovarian cancer is inefficient. Br J Cancer *94,* 814-819.

Oketm, O., and Oktay, K. (2008). The ovary anatomy and function throughout human life. Ann N Y Acad Sci *1127,* 1-9.

Okubo, T., Mok, S.C., and Chen, S. (2000). Regulation of aromatase expression in human ovarian surface epithelial cells. J Clin Endocrinol Metab *85,* 4889-4899.

Olivier, R.L., Lubsen-Brandsma, M.A., Verhoef, S., and van Beurden, M. (2006). CA125 and transvaginal ultrasound monitoring in high-risk women cannot prevent the diagnosis of advanced ovarian cancer. Gynecol Oncol *100,* 20-26.

Orly, J., Sato, G., and Erickson, G.F. (1980). Serum suppresses the expression of hormonally induced functions in cultured granulosa cells. Cell *20,* 817-827.

Pal, T., Permuth-Wey, J., Betts, J.A., Krischer, J.P., Fiorica, J., Arango, H., LaPolla, J., Hoffman, M., Martino, M.A., Wakeley, K., *et al.* (2005). *BRCA1* and *BRCA2* mutations account for a large proportion of ovarian carcinoma cases. Cancer *104,* 2807.

Park, S., Cheung, L., W.T., Wong, A.S.T., and Leung, P.C.K. (2008). Estrogen regulates snail and slug in the down-regulation of E-cadherin and induces metastatic potential of ovarian cancer cells through estrogen receptor alpha. Mol Endocrinol *22,* 2085-2098.

Petrucelli, N., Daly, M.B., and Feldman, G.L. (2010). Hereditary breast and ovarian cancer due to mutations in *BRCA1* and *BRCA2*. Genet Med *12,* 245-259.

Phillips, K.W., Goldsworthy, S.M., Bennett, L.M., Brownlee, H.A., Wiseman, R.W., and Davis, B.J. (1997). Brca1 is expressed independently of hormonal stimulation in the mouse ovary. Lab Invest *76,* 419-425.

Piek, J.M., Verheijen, R.H., Menko, F.H., Jongsma, A.P., Weegenaar, J., Gille, J.J., Pals, G., Kenemans, P., and van Diest, P.J. (2003). Expression of differentiation and proliferation related proteins in epithelium of prophylactically removed ovaries from women with a hereditary female adnexal cancer predisposition. Histopathology *43,* 26-32.

Pignata, S., Cannella, L., Leopardo, D., Pisano, C., Salvatore Bruni, G., and Facchini, G. (2011). Chemotherapy in epithelial ovarian cancer. Cancer Lett *303,* 73-83.

Pinto, A.P., and Crum, C.P. (2000). Natural history of cervical neoplasia: defining progression and its consequence. Clin Obstet Gynecol *43,* 352-362.

Plaxe, S.C., Deligdisch, L., Dottino, P.R., and Cohen, C.J. (1990). Ovarian intraepithelial neoplasia demonstrated in patients with stage I ovarian carcinoma.. Gynecol Oncol *38,* 367-372.

Pruthi, S., Gostout, B.S., and Lindor, N.M. (2010). Identification and management of women with BRCA mutations or hereditary predisposition for breast and ovarian cancer. May Clin Proc *85,* 1111-1120.

Purdie, D.M., Bain, C.J., Siskind, V., Webb, P.M., and Green, A.C. (2003). Ovulation and risk of epithelial ovarian cancer. Int J Cancer *104,* 228-232.

Rebbeck, T.R., Lynch, H.T., Neuhausen, S.L., Narod, S.A., Van't Veer, L., Garber, J.E., Evans, G., Isaacs, C., Daly, M.B., Matloff, E., *et al.* (2002). Prophylactic oophorectomy in carriers of BRCA1 or BRCA2 mutations. N Engl J Med *346,* 1616-1622.

Reedy, M.B., Hang, T., Gallion, H., Arnold, S., and Smith, S.A. (2001). Antisense inhibition of BRCA1 expression and molecular analysis of hereditary tumors indicate that functional inactivation of the p53 DNA damage response pathway is required for BRCA-associated tumorigenesis. Gynecol Oncol *81,* 441-446.

Resta, L., Russo, S., Colucci, G.A., and Prat, J. (1993). Morphologic precursors of ovarian epithelial tumors. Obstet Gynecol *82,* 181-186.

Richards, J.S., Hickey, G.J., Chen, S.A., Shively, J.E., Hall, P.F., Gaddy-Kurten, D., and Kurten, R. (1987). Hormonal regulation of estradiol biosynthesis, aromatase activity, and aromatase mRNA in rat ovarian follicles and corpora lutea. Steroids *50,* 393-409.

Risch, H.A. (1998). Hormonal etiology of epithelial ovarian cancer, with a hypothesis concerning the role of androgens and progesterone. J Natl Cancer Inst *90,* 1774-1786.

Risch, H.A., McLaughlin, J.R., Cole, D.E., Rosen, B., Bradley, L., Kwan, E., Jack, E., Vesprini, D.J., Kuperstein, G., Abrahamson, J.L., *et al.* (2001). Prevalence and penetrance of germline BRCA1 and BRCA2 mutations in a population series of 649 women with ovarian cancer.. Am J Hum Genet *68,* 700-710.

Roldan, G., Delgado, L., and Muse, I.M. (2006). Tumoral expression of BRCA1, estrogen receptor alpha and ID4 protein in patients with sporadic breast cancer. Cancer Biol Ther *5,* 505-510.

Rosen, E.M., Fan, S., and Ma, Y. (2006). BRCA1 regulation of transcription. Cancer Lett *236,* 175-185.

Roy, D., Cai, Q., Felty, Q., and Narayan, S. (2007). Estrogen-induced generation of reactive oxygen and nitrogen species, gene damage, and estrogen-dependent cancers. J Toxicol Environ Health B Crit Rev *10,* 235-257.

Salazar, H., Godwin, A.K., Daly, M.B., Laub, P.B., Hogan, W.M., Rosenblum, N., Boente, M.P., Lynch, H.T., and Hamilton, T.C. (1996). Microscopic benign and invasive malignant neoplasms and a cancer-prone phenotype in prophylactic oophorectomies. J Natl Cancer Inst *88,* 1790.

Sawyer, H.R., Olson, P.N., and Gorell, T.A. (1984). Effects of progesterone on the oviductal epithelium in estrogen-primed perpubertal beagles: light and electron microscopic observations. Am J Anat *169,* 75-87.

Schildkraut, J.M., Schwingl, P.J., Bastos, E., Evanoff, A., and Hughes, C. (1996). Epithelial ovarian cancer risk among women with polycystic ovary syndrome. Obstet Gynecol *88,* 554-559.

Schlosshauer, P.W., Cohen, C.J., Penault-Llorca, F., Miranda, C.R., Bignon, Y., Dauplat, J., and Deligdisch, L. (2003). Prophylactic oophorectomy a morphologic and immunohistochemical study. Cancer *98*, 2599.

Schrock, E., Badger, P., Larson, D., Erdos, M., Wynshaw-Boris, A., Ried, T., and Brody, L. (1996). The murine homolog of the human breast and ovarian cancer susceptibility gene Brca1 maps to mouse chromosome 11D. Hum Genet *97*, 256-259.

Scully, R.E. (1995). Pathology of Ovarian Cancer Precursors. J Cell Biochem *Supplemental 23*, 208-218.

Seidman, J.D., Horkayne-Szakaly, I., Cosin, J.A., Ryu, H.S., Haiba, M., Boice, C.R., and Yemelyanova, A.V. (2006). Testing of two binary grading systems for FIGO stage III serous carcinoma of the ovary and peritoneum. Gynecol Oncol *103*, 703-708.

Senturk, E., Cohen, S., Dottino, P.R., and Martignetti, J.A. (2010). A critical re-appraisal of BRCA1 methylation studies in ovarian cancer. Gynecol Oncol *119*, 376-383.

Shai, A., Pitot, H.C., and Lambert, P.F. (2008). p53 loss synergizes with estrogen and papillomaviral oncogenes to induce cervical and breast cancers. Cancer Res *68*, 2622-2631.

Sharan, S.K., Wims, M., and Bradley, A. (1995). Murine Brca1: sequence and significance for human missense mutations. Hum Mol Genet *4*, 2275-2278.

Sherman, M.E., Lee, J.S., Burks, R.T., Struewing, J.P., Kurman, R.J., and Hartage, P. (1999). Histopathologic features of ovaries at increased risk for carcinoma. A case-control analysis. Int J Gynecol Pathol *18*, 151.

Shih, l., and Kurman, R.J. (2004). Ovarian tumorigenesis: a proposed model based on morphological and molecular genetic analysis.. Am J Pathol *164*, 1511-1518.

Silva, E.G., Tornos, C., Deavers, M., Kaisman, K., Gray, K., and Gershenson, D. (1998). Induction of epithelial neoplasms in the ovaries of guinea pigs by estrogenic stimulation. Gynecol Oncol *71*, 240-246.

Simpson, E.R., Clyne, C., Rubin, G., Boon, W.C., Robertson, K., Britt, K., Speed, C., and Jones, M. (2002). Aromatase--a brief overview. Annu Rev Physiol *64*, 93-127.

Stewart, S.L., Querec, T.D., Ochman, A.R., Gruver, B.N., Bao, R., Babb, J.S., Wong, T.S., Koutroukides, T., Pinnola, A.D., Klein-Szanto, A., Hamilton, T.C., and Patriotis, C. (2004). Characterization of a carcinogenesis rat model of ovarian preneoplasia and neoplasia.. Cancer Res *64*, 8177-8183.

Stocco, C. (2008). Aromatase expression in the ovary: hormonal and molecular regulation. Steroids *73*, 473-487.

Stratton, J.F., Buckley, C.H., Lowe, D., and Ponder, B.A. (1999). Comparison of prophylactic oophorectomy specimens from carriers and noncarriers of a BRCA1 or BRCA2 gene mutation. United Kingdom Coordinating Committee on Cancer Research (UKCCCR) Familial Ovarian Cancer Study Group. J Natl Cancer Inst *91,* 626-628.

Subbaramaiah, K., Hudis, C., Change, S.H., Hla, T., and Dannenberg, A.J. (2008). EP2 and EP4 receptors regulate aromatase expression in human adipocytes and breast cancer cells. Evidence of a BRCA1 and p300 exchange. J Biol Chem *283,* 3433-3444.

Sundfeldt, K., Piontkewitz, Y., Ivarsson, K., Nilsson, O., Hellberg, P., Brannstrom, M., Janson, P.O., Enerback, S., and Hedin, L. (1997). E-cadherin expression in human epithelial ovarian cancer and normal ovary. Int J Cancer *74,* 275-280.

Symonds, D.A., Merchenthaler, I., and Flaws, J.A. (2008). Methoxychlor and estradiol induce oxidative stress DNA damage in the mouse ovarian surface epithelium. Toxicol Sci *105,* 182-187.

Szotek, P.P., Chang, H.L., Brennand, K., Fujino, A., Pleretti-Vanmarcke, R., Lo Celso, C., Dombkowski, D., Preffer, F., Cohen, K.S., Teixeira, J., and Donahoe, P.K. (2008). Normal ovarian surface epithelial label-retaining cells exhibit stem/progenitor cell characteristics. PNAS *105,* 12469-12473.

Thompson, D., Easton, D.F., and Breast Cancer Linkage Consortium. (2002). Cancer incidence in BRCA1 mutation carriers. J Natl Cancer Inst *94,* 1358-1365.

Thrall, M., Gallion, H.H., Kryscio, R., Kapali, M., Armstrong, D.K., and DeLoia, J.A. (2006). BRCA1 expression in a large series of sporadic ovarian carcinomas: a gynecologic oncology group study. Int J Gynecol Cancer *16,* 166-171.

Tonary, A.M., Macdonald, E.A., Faught, W., Senterman, M.K., and Vanderhyden, B.C. (2000). Lack of expression of c-KIT in ovarian cancers is associated with poor prognosis. Int J Cancer *89,* 242-250.

Tsuchiya, Y., Nakajima, M., and Yokoi, T. (2005). Cytochrome P450-mediated metabolism of estrogens and its regulation in human. Cancer Lett *227,* 115-124.

Tsutsui, T., Taquchi, S., Tanaka, Y., and Barrett, J.C. (1997). 17beta-estradiol, diethylstilbestrol, tamoxifen, toremifene and ICI 164,384 induce morphological transformation and aneuploidy in cultured Syrian hamster embryo cells. Int J Cancer *70,* 188-193.

Tung, K., Goodman, M.T., Wu, A.H., McDuffie, K., Wilkens, L.R., Kolonel, L.N., Nomura, A.M.Y., Terada, K.Y., Carney, M.E., and Sobin, L.H. (2003). Reproductive factors and epithelial ovarian cancer risk by histologic type: a multiethnic case-control study. American Journal of Epidemiology *158,* 629-638.

Vang, R., Shih, I., and Kurman, R.J. (2009). Ovarian low-grade and high-grade serous carcinoma: pathogenesis, clinicopathologic and molecular biologic features, and diagnostic problems. Adv Anat Pathol *16,* 267-282.

Venkitaraman, A.R. (2009). Linking the cellular functions of BRCA genes to cancer pathogenesis and treatment. Am J Pathol *4,* 461-487.

Verhage, H.G., Fazleabas, A.T., Mavrogianis, P.A., O'Day-Bowman, M.B., Donnelly, K.M., Arias, E.B., and Jaffe, R.C. (1997). The baboon oviduct: characteristic of an oestradiol-dependent oviduct-specific glycoprotein. Hum Reprod Update. *3,* 541-552.

Weberpals, J.I., Clark-Knowles, K.V., and Vanderhyden, B.C. (2008). Sporadic epithelial ovarian cancer: clinical relevance of BRCA1 inhibition in the DNA damage and repair pathway. J Clin Oncol. *26,* 3259-3267.

Werness, B.A., Afify, A.M., Bielat, K.L., Eltabbakh, G.H., Piver, M.S., and Paterson, J.M. (1999). Altered surface and cyst epithelium of ovaries removed prophylactically from women with a family history of ovarian cancer. Hum Pathol *30,* 151-157.

Werness, B.A., Afify, A.M., Eltabbakh, G.H., Huelsman, K., Piver, M.S., and Paterson, J.M. (1999). p53, c-erbB, and Ki-67 expression in ovaries removed prophylactically from women with a family history of ovarian cancer.. Int J Gynecol Pathol *18,* 338-343.

Whittemore, A.S., Balise, R.R., Pharoah, P.D., Dicioccio, R.A., Oakley-Girvan, I., Ramus, S.J., Daly, M., Usinowicz, M.B., Garlinghouse-Jones, K., Ponder, B.A., *et al.* (2004). Oral contraceptive use and ovarian cancer risk among carriers of BRCA1 or BRCA2 mutations. Br J Cancer *91,* 1911-1915.

Wijnhoven, B.P., Dinjens, W.N., and Pignatelli, M. (2000). E-cadherin-catenin cell-cell adhesion complex and human cancer. Br J Surg *87,* 992-1005.

Wright, J.W., Pejovic, T., Fanton, J., and Stouffer, R.L. (2008). Induction of proliferation in the primate ovarian surface epithelium in vivo. Hum Reprod *23,* 129-138.

Xing, D., Scangas, G., Nitta, M., He, L., Xu, X., Ioffe, Y.J., Aspuria, P.J., Hedvat, C.Y., Anderson, M.L., Olivia, E., *et al.* (2009). A role for BRCA1 in uterine leiomyosarcoma. Cancer Res *69,* 8231-8235.

Yang, D., Fazili, Z., Smith, E.R., Cai, K.Q., Klein-Szanto, A., Cohen, C., Horowitz, I., and Xu, X. (2006). Disabled-2 heterozygous mice are predisposed to endometrial and ovarian tumourigenesis and exhibit sex-based embryonic lethality in a p53-null background. Am J Pathol *169,* 258-267.

Yang, D., Cai, K.Q., Roland, I.H., Smith, E.R., and Xu, X. (2007). Disabled-2 is an epithelial surface positioning gene. J Biol Chem *282,* 13114-13122.

Zheng, W., Magid, M.S., Kramer, E.E., and Chen, Y. (1996). Follicle-stimulating hormone receptor is expressed in human ovarian surface epithelium and fallopian tube. Am J Pathol *148,* 47-53.

Zhou, B., Sun, Q., Cong, R., Gu, H., Tang, N., Yang, L., and Wang, B. (2008). Hormone replacement therapy and ovarian cancer risk: a meta-analysis. Gynecol Oncol *108,* 641-651.